Subduction V
Multi-scale models and joint constraints

Thorsten W Becker

University of Southern California

Short course at
Universita di Roma
TRE

April 18 – 20, 2011

Plate boundary forcing

- Can we use plate velocities to infer plate boundary strength?

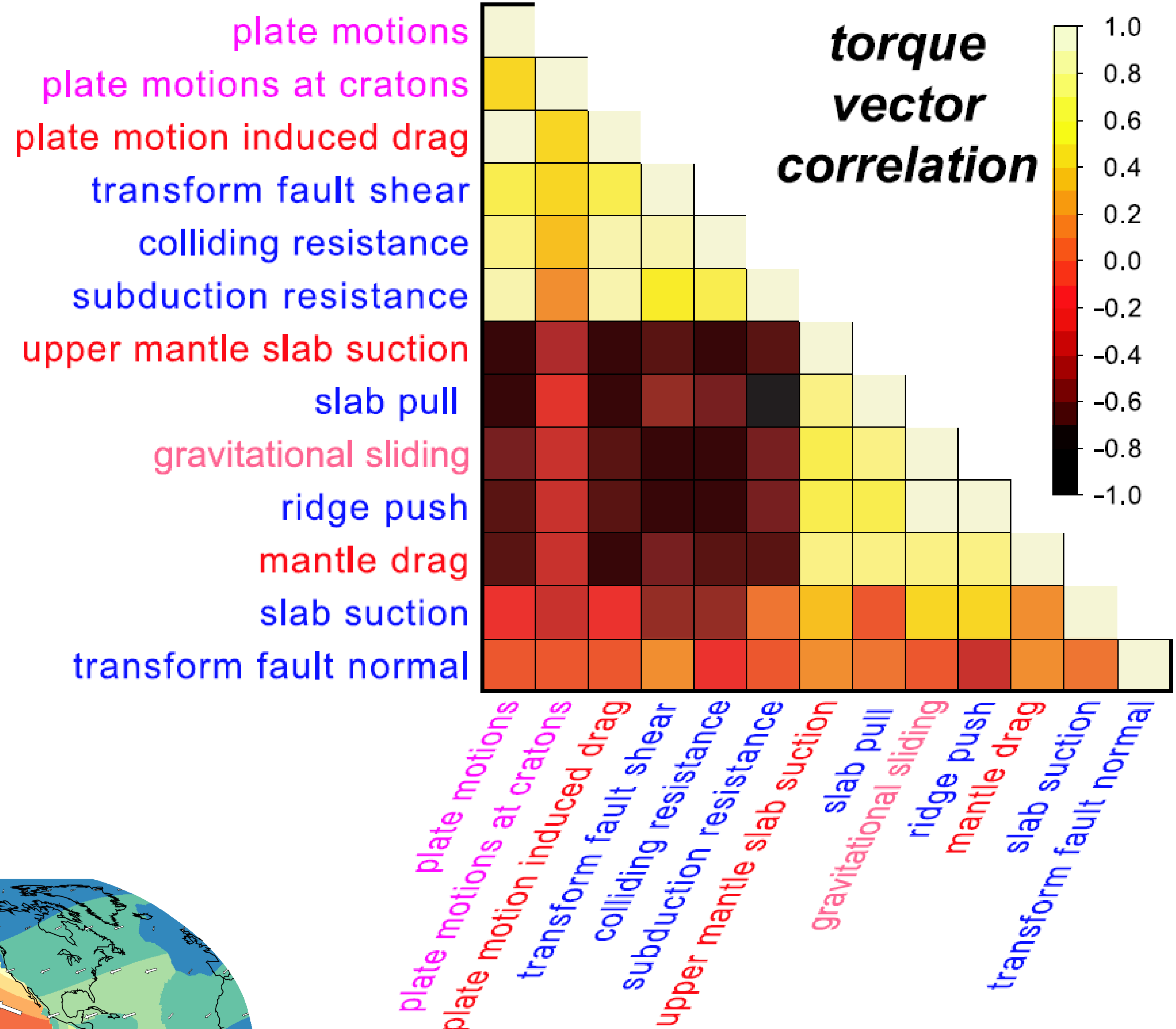

Becker & O'Connell (2001)

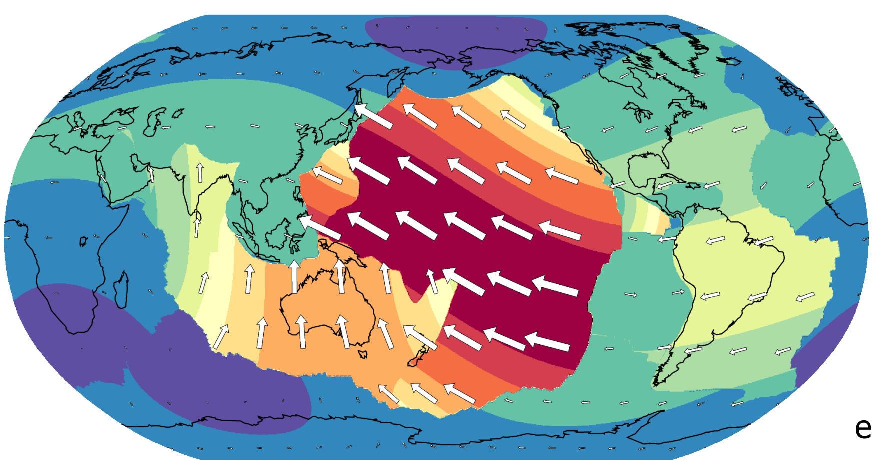

e.g. Becker & O'Connell (2001); Conrad & Lithgow-Bertelloni (2002); Becker (2006)

Correlations are ambiguous what else can we use?

- Need to understand rheological properties of slabs and plates
  - Use absolute motion information (and not just correlations)
  - Use deformation, rather than rigid plate motion
- Better treatment of plate boundaries

Plate motions and reference frames
(slab pull contributes ~ 70% of driving force)

rigid plate model in HS2 frame

HS2

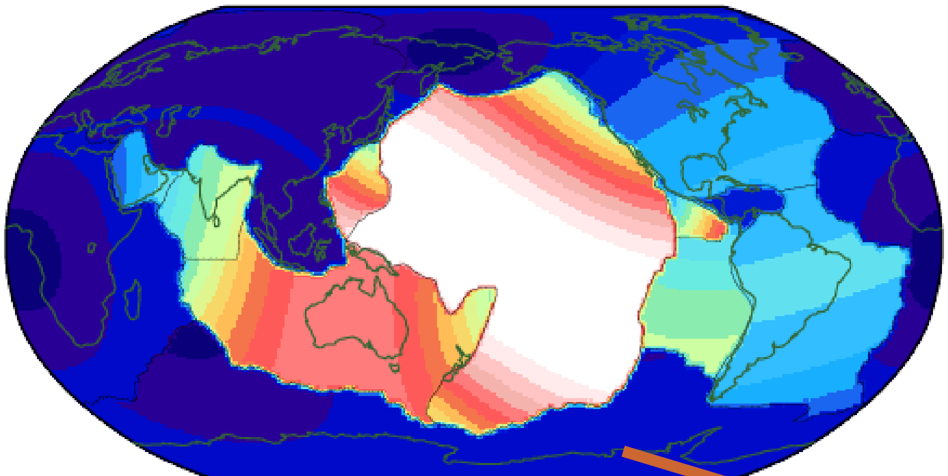

Gripp & Gordon (1990)

deforming model in NNR frame

GSRM

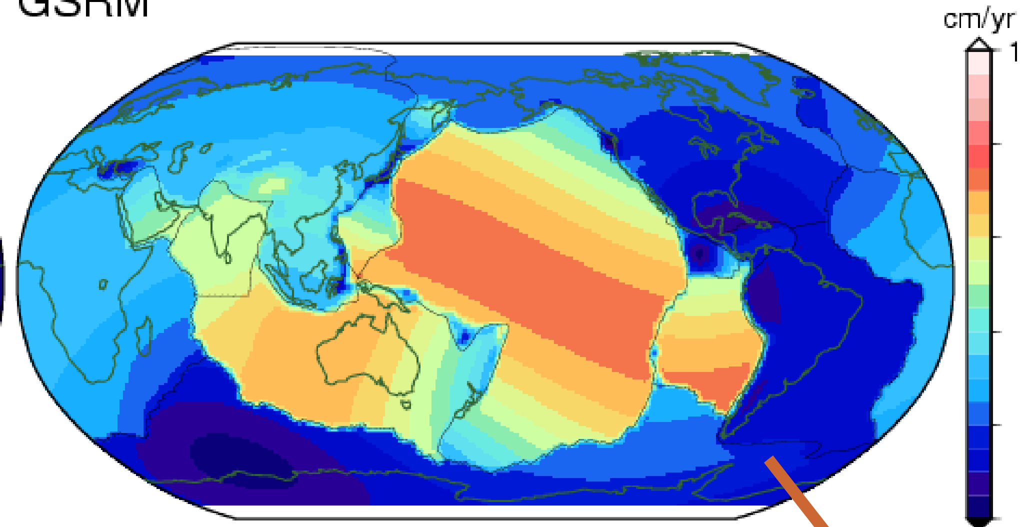

Kreemer *et al.* (2003)

	HS2	NNR-GSRM
ocean/continent RMS	**2.9**	**1.55**
plateness	**1**	**0.9**
toroidal/poloidal power (l > 2)	**0.5**	**0.6**
net rotation	**3 cm/yr**	**0**

Plate Mantle Coupling: Viscosity Structure

How do slabs drive plate motions?

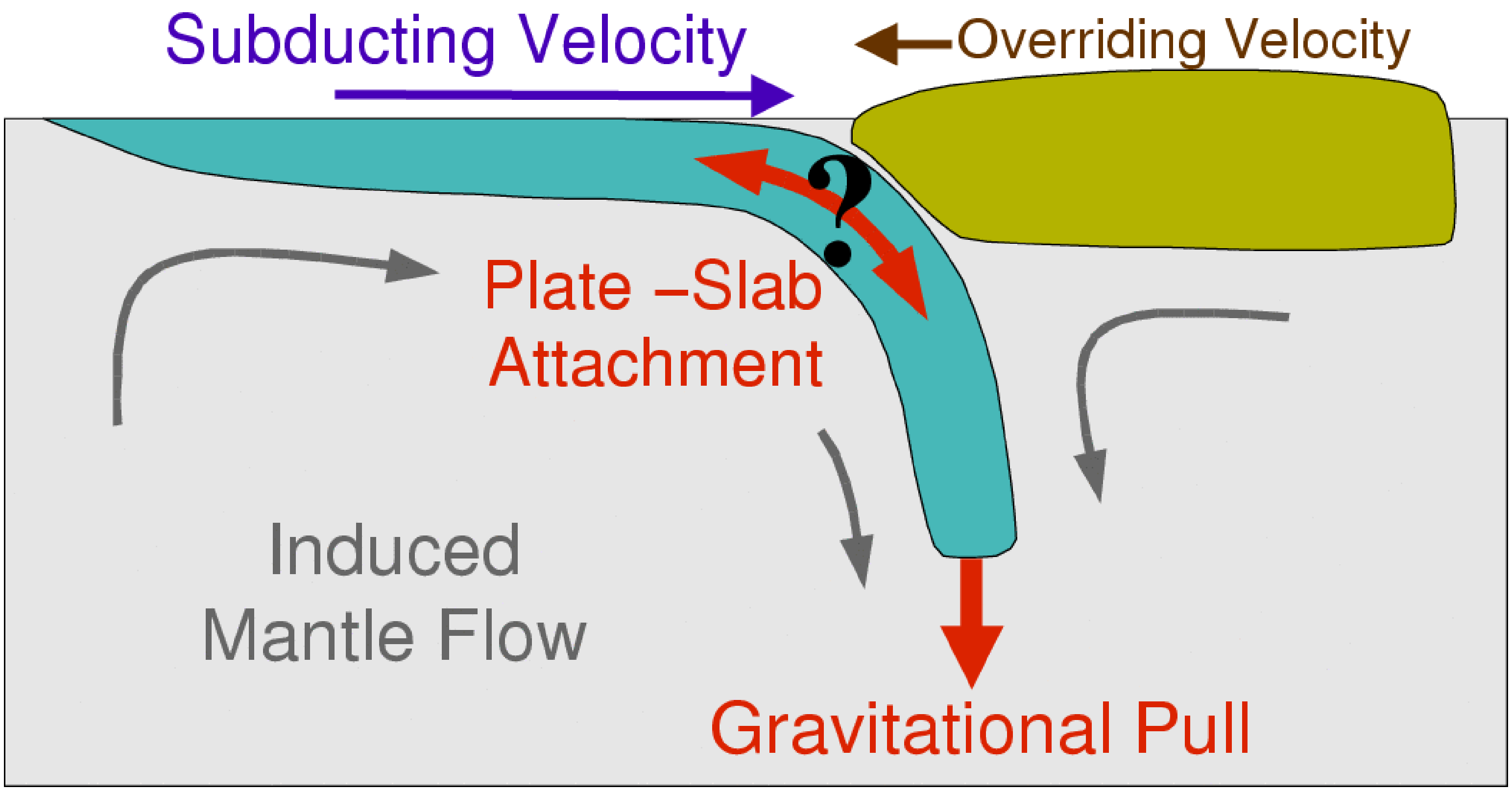

Slide courtesy of C. Lithgow-Bertelloni

[*Conrad and Lithgow-Bertelloni*, 2004]

Plate Driving Forces

The Slab Pull Force:
Calculate excess weight of upper mantle slabs

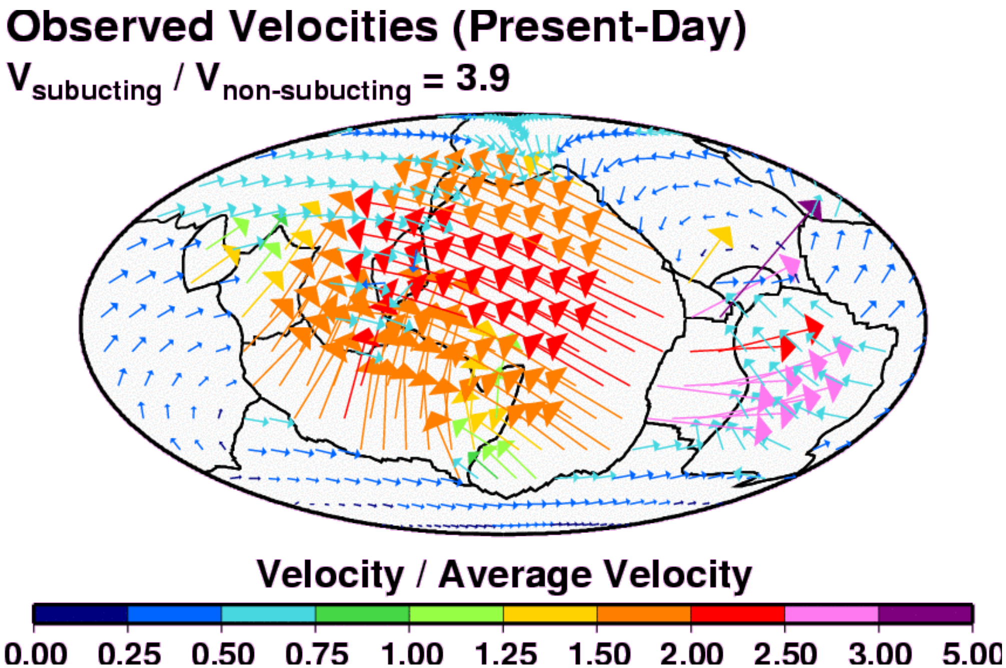

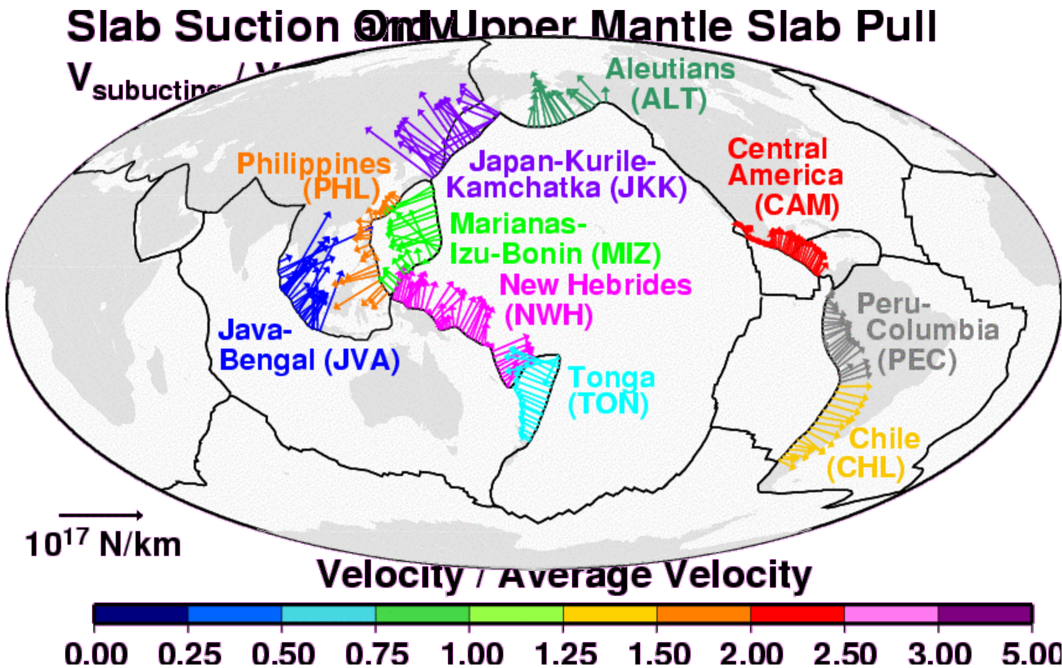

Slab Pull from Upper Mantle Slabs
Slab Suction from Lower Mantle Slabs

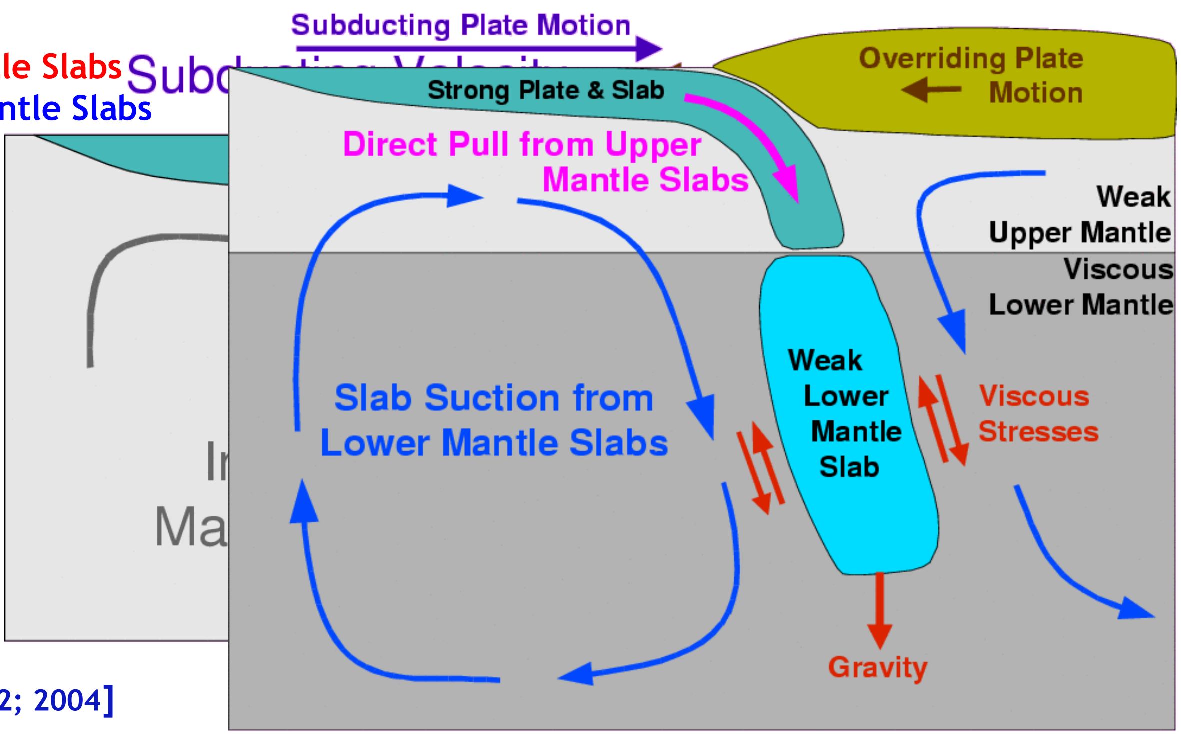

Slide courtesy of C. Lithgow-Bertelloni

[*Conrad and Lithgow-Bertelloni*, 2002; 2004]

Plate-Slab Coupling

Detached Slabs?

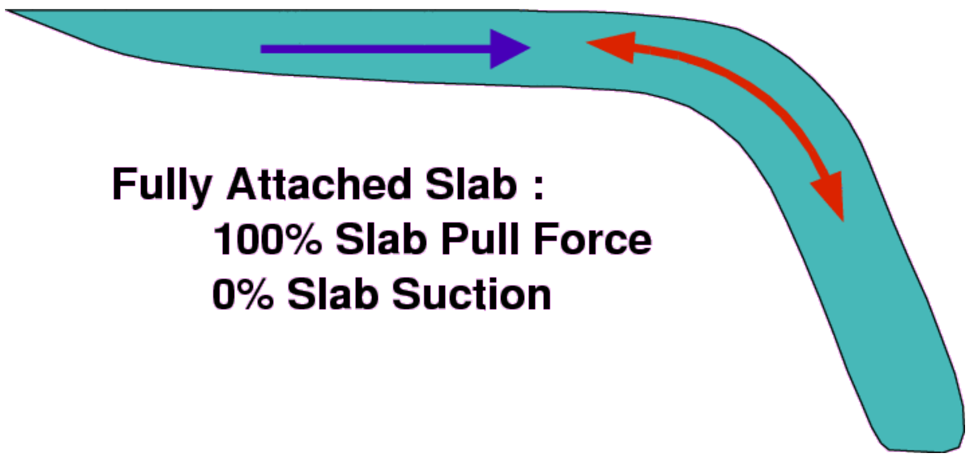

Fully Attached Slab :
100% Slab Pull Force
0% Slab Suction

Which slabs must be detached to produce the best fit to plate motions?

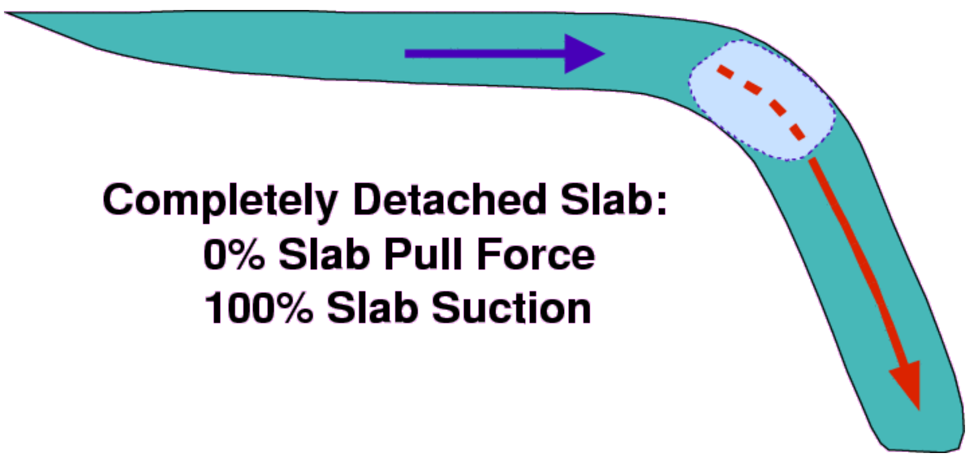

Completely Detached Slab:
0% Slab Pull Force
100% Slab Suction

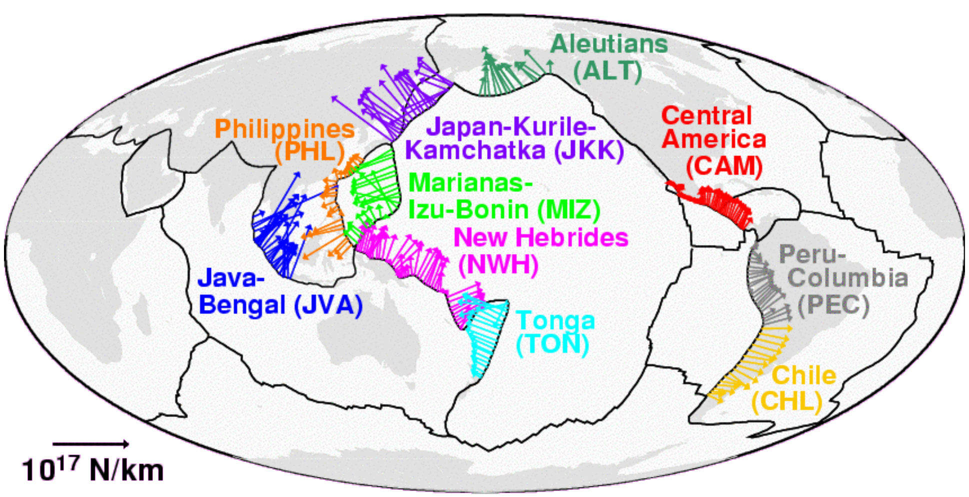

Slide courtesy of C. Lithgow-Bertelloni

Deep Seismicity (300-670 km)

Sum moments using the Harvard CMT Catalog (1977-2002)

Slide courtesy of C. Lithgow-Bertelloni

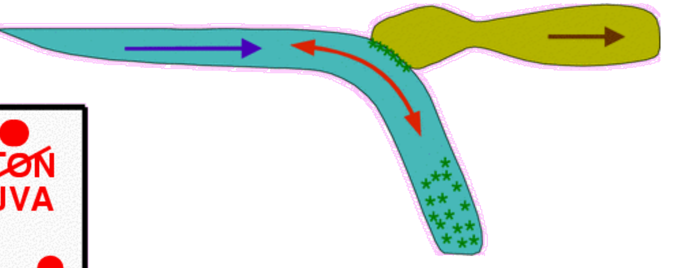

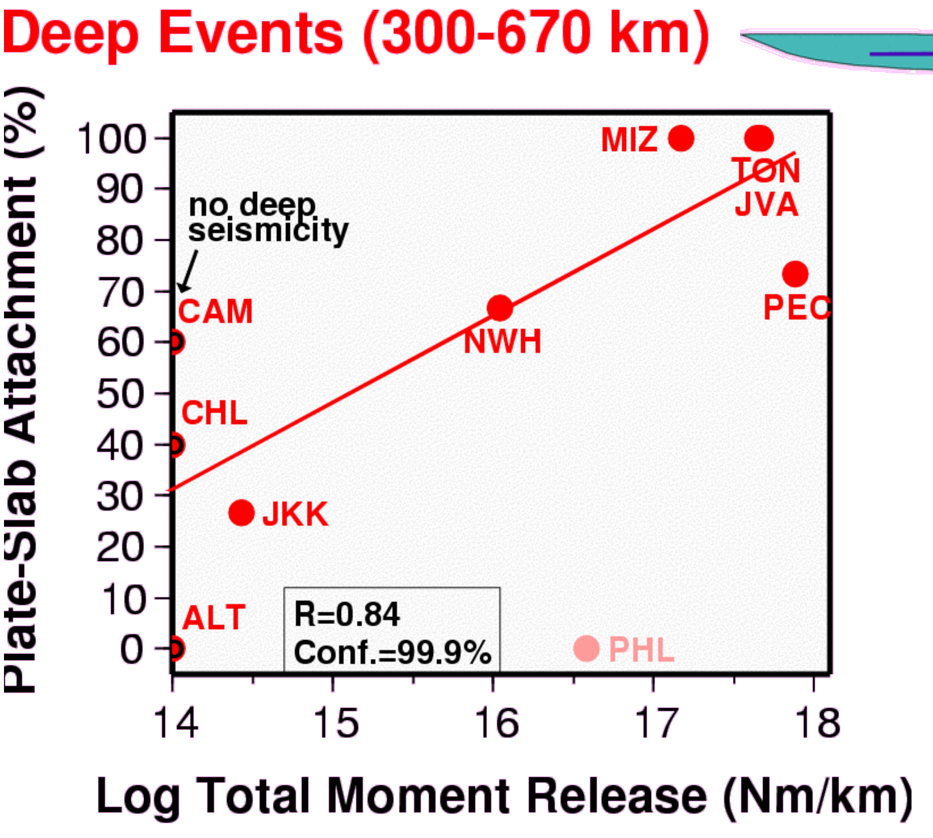

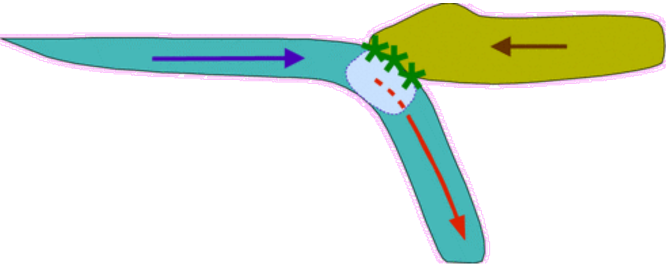

Strong plate-slab attachment allows for more seismicity at depth.

[*Bilek et al.*, 2005]

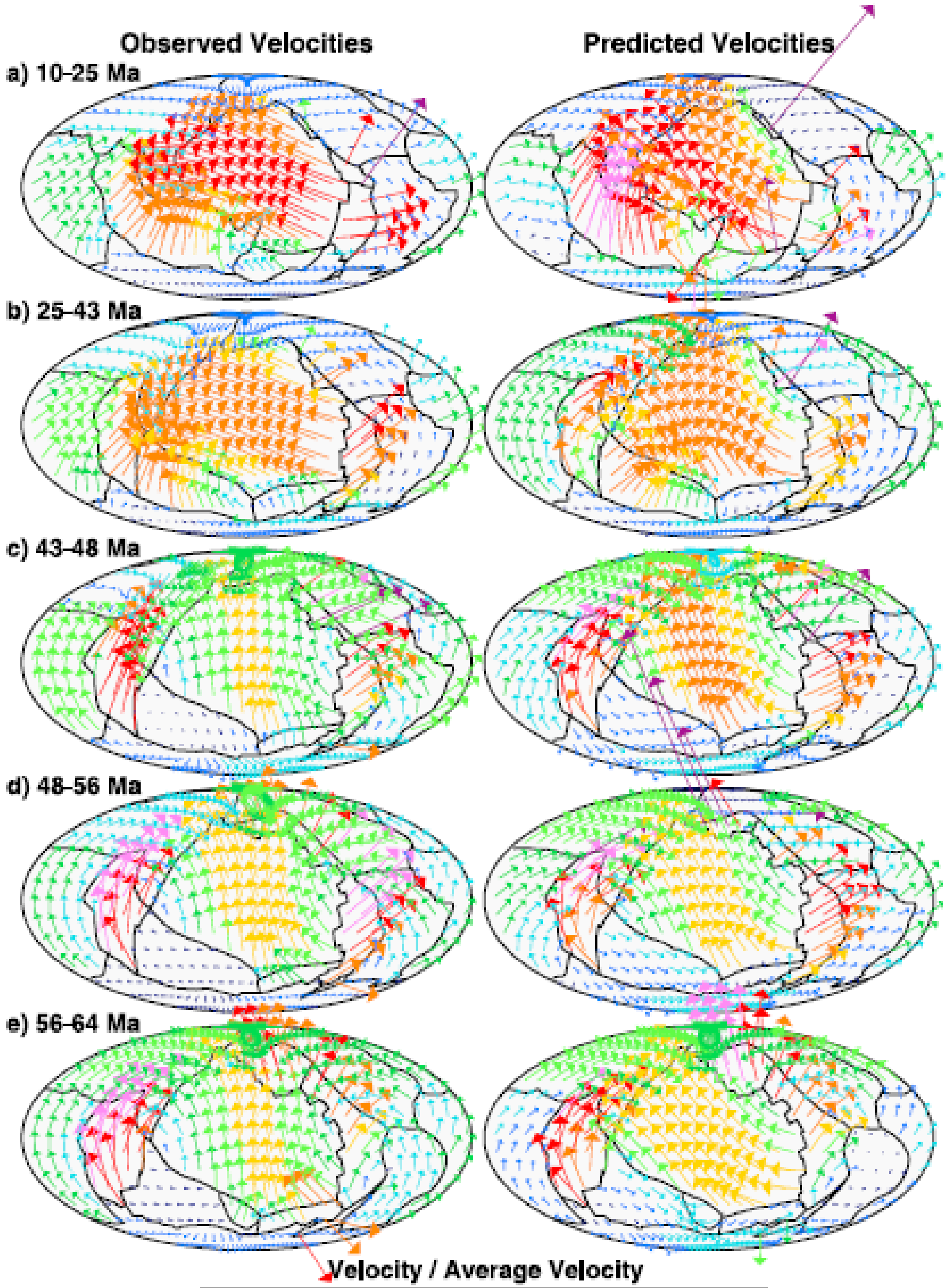

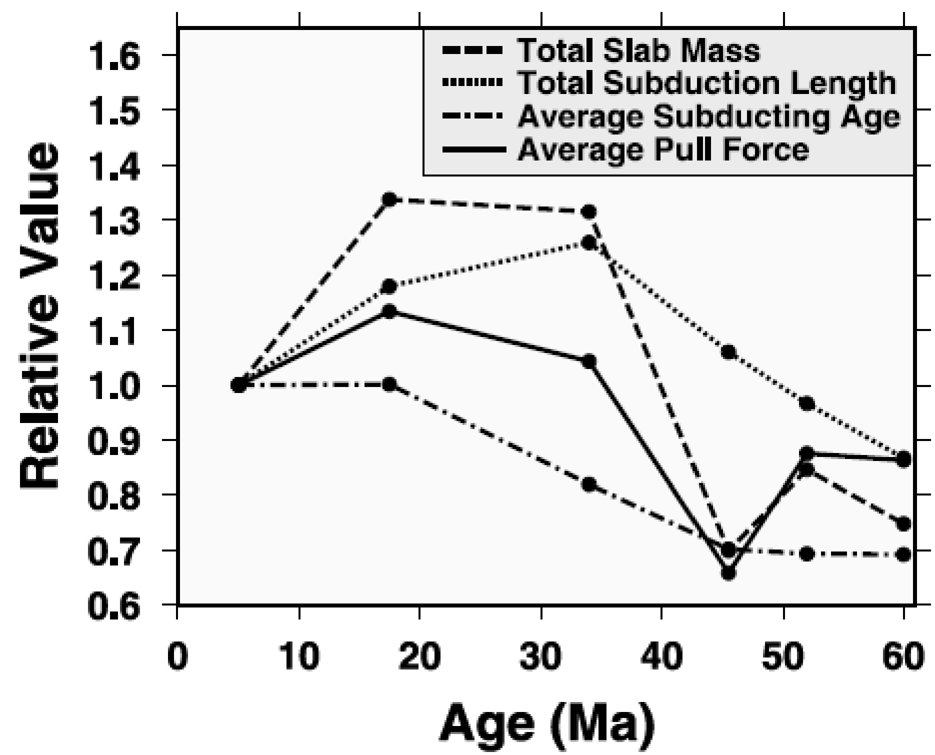

Conrad & Lithgow-Bertelloni (2004)

Global flow computations with LVVs

- Use geologic information (cratons and seafloor ages) for lithosphere
- Infer temperature anomalies from seismic tomography
- Compute 3-D, spherical mantle flow with LVVs
- Prescribe stiff cratons (cf. Conrad & Lithgow-Bertelloni, 2006)
- Solve with CitcomS (Zhong *et al.* 2000)

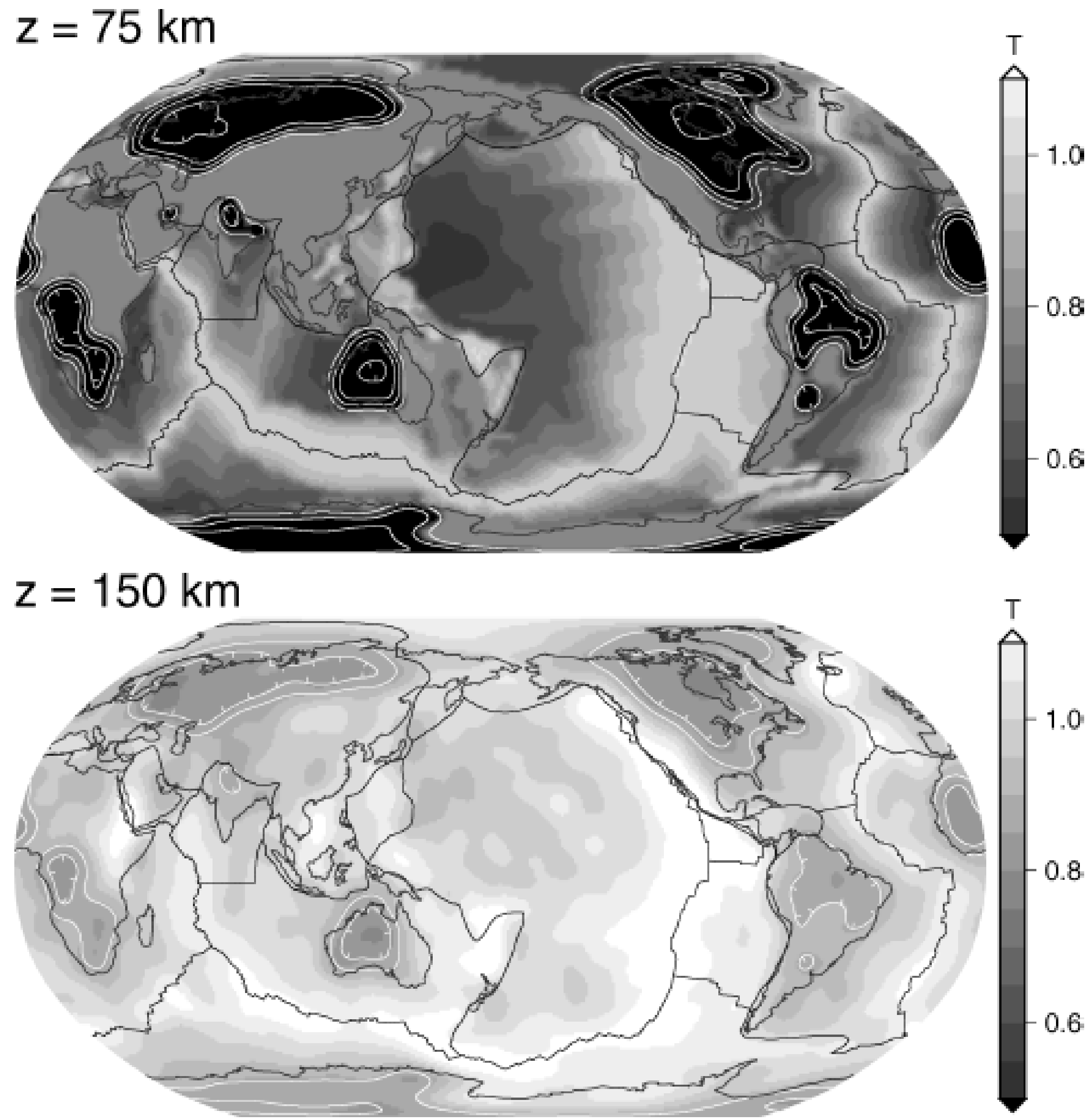

Becker (2006)

Rheology

$\dot{\eta}$: viscosity

ε: strain-rate

A) use generic temperature and/or stress dependence of viscosity on top of radial variations

B) use effective, olivine creep law with diffusion & dislocation creep

$$\dot{\varepsilon}_0 = \dot{\varepsilon}_{disl} + \dot{\varepsilon}_{diff}$$

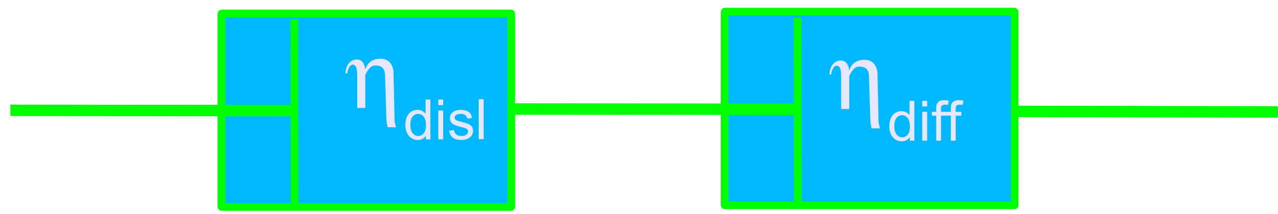

$$\eta_{\text{eff}} = \frac{\eta_{\text{disl}}\eta_{\text{diff}}}{\eta_{\text{disl}} + \eta_{\text{diff}}}$$

$$\eta = \left(\frac{d^m}{A'}\right)^{\frac{1}{n}} \dot{\varepsilon}_{II}^{\frac{1-n}{n}} \exp\left(\frac{E^* + pV^*}{nRT_r(T_c + T)}\right)$$

Global circulation models: Average mantle viscosities for dry olivine

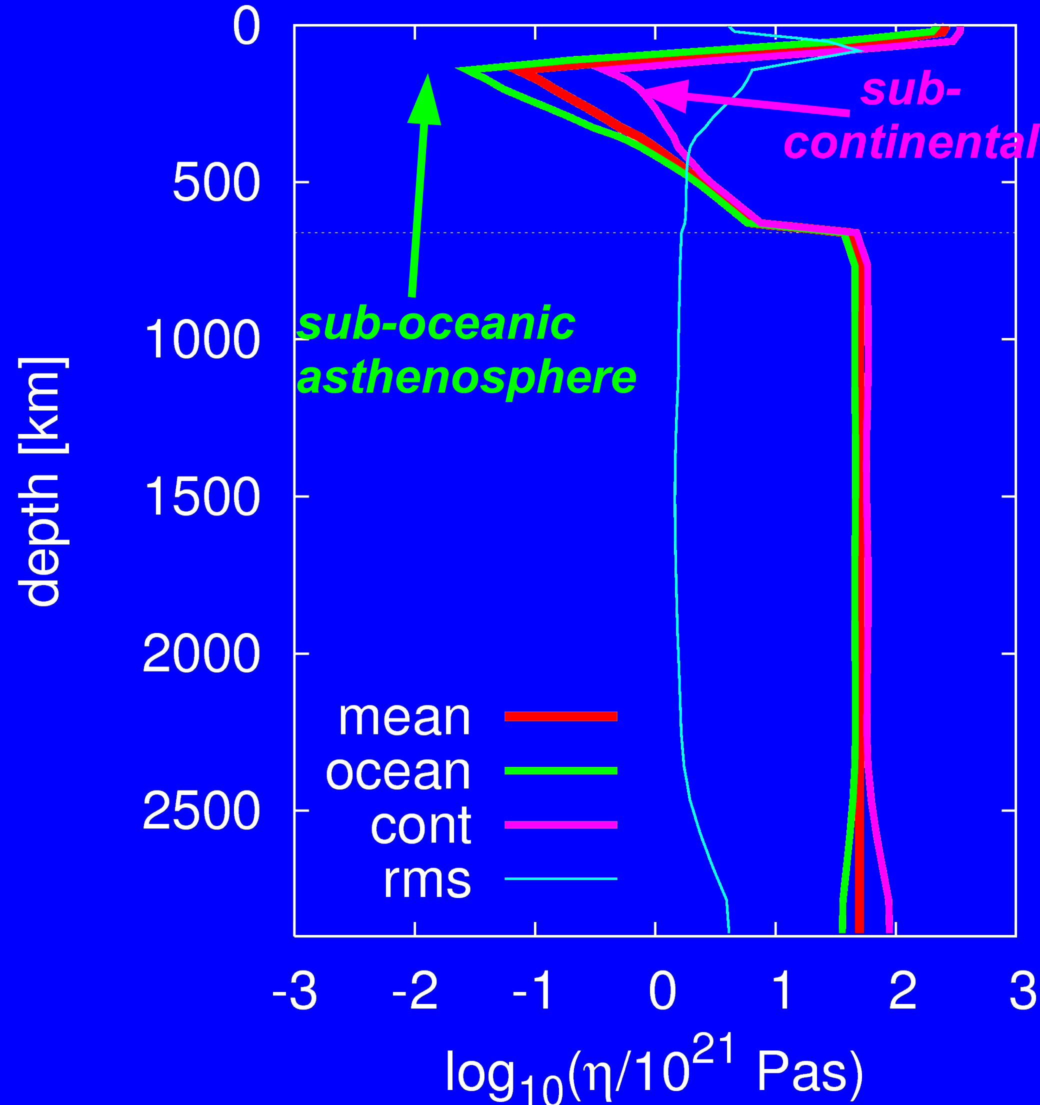

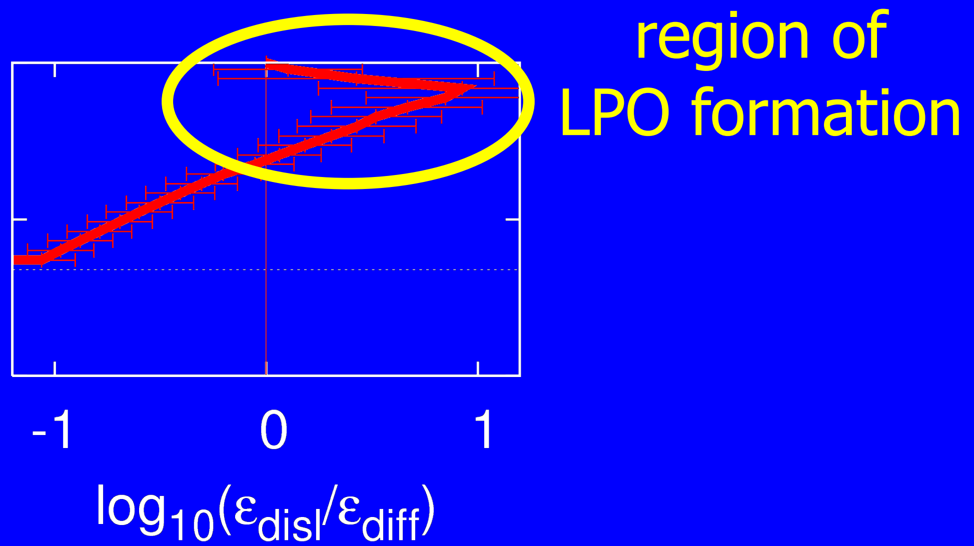

- Viscosity broadly consistent with geoid and post-glacial rebound
- Can match plate motions and other plate scores
- Depth range of dislocation creep consistent with anisotropy observations

Cadek & Fleitout (2003); McNamara et al. (2003);

Podolevsky et al. (2005); Becker (2006)

Sub-oceanic vs. continental speeds (LVV GCM @ 250 km)

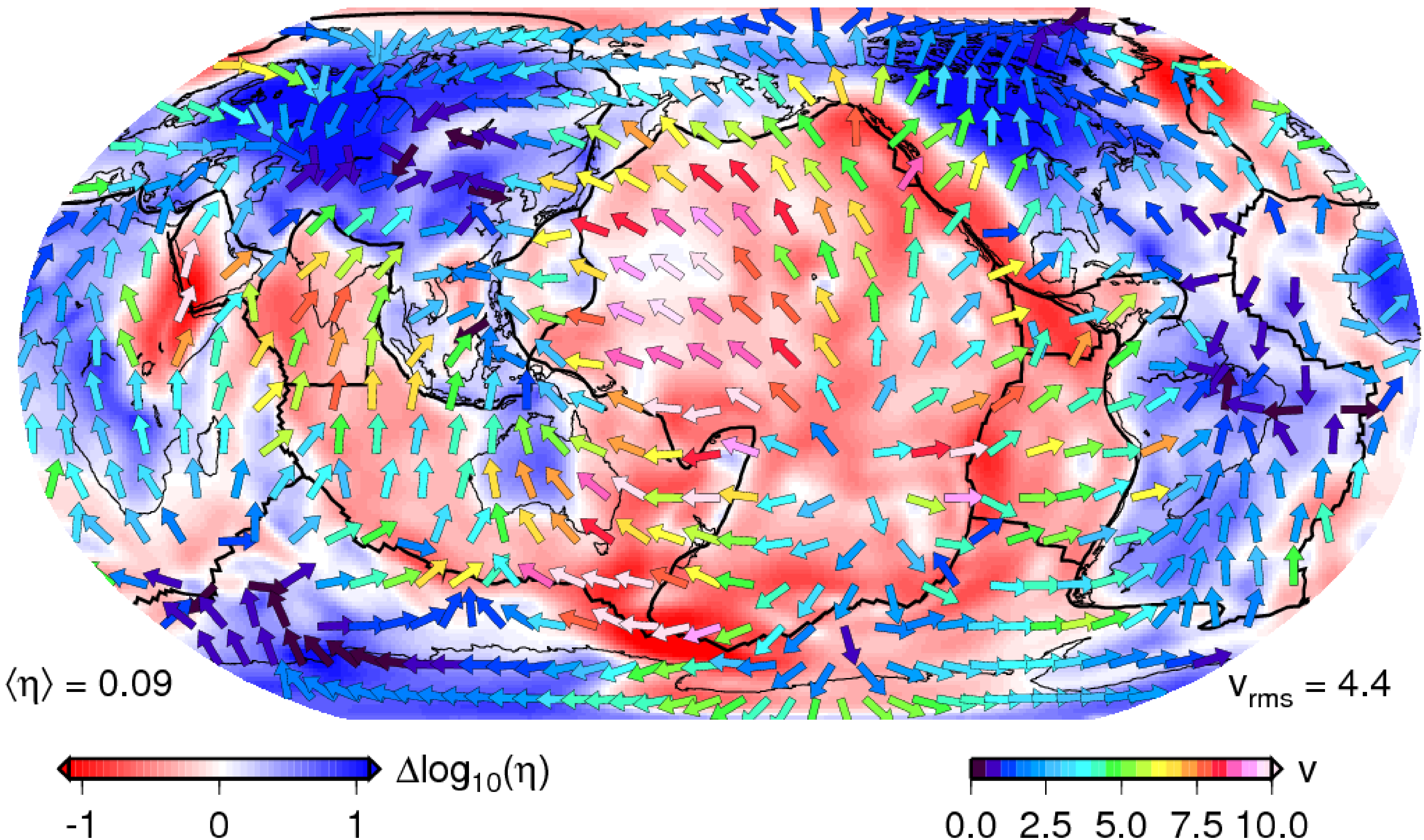

Hager & O'Connell (1981); Ricard & Vigny (1989); Zhang & Christensen (1993); Cadek & Fleitout (2003); Becker (2006)

Fit to observed net rotations

- Stiff continental keels induce net rotations of the whole lithosphere wrt. the lower mantle (cf. Ricard et al., 1991; Ribe, 1992; Zhong, 2001)
- This is seen in hotspot reference frames; poles of HS2/HS3 matched well, amplitude too low

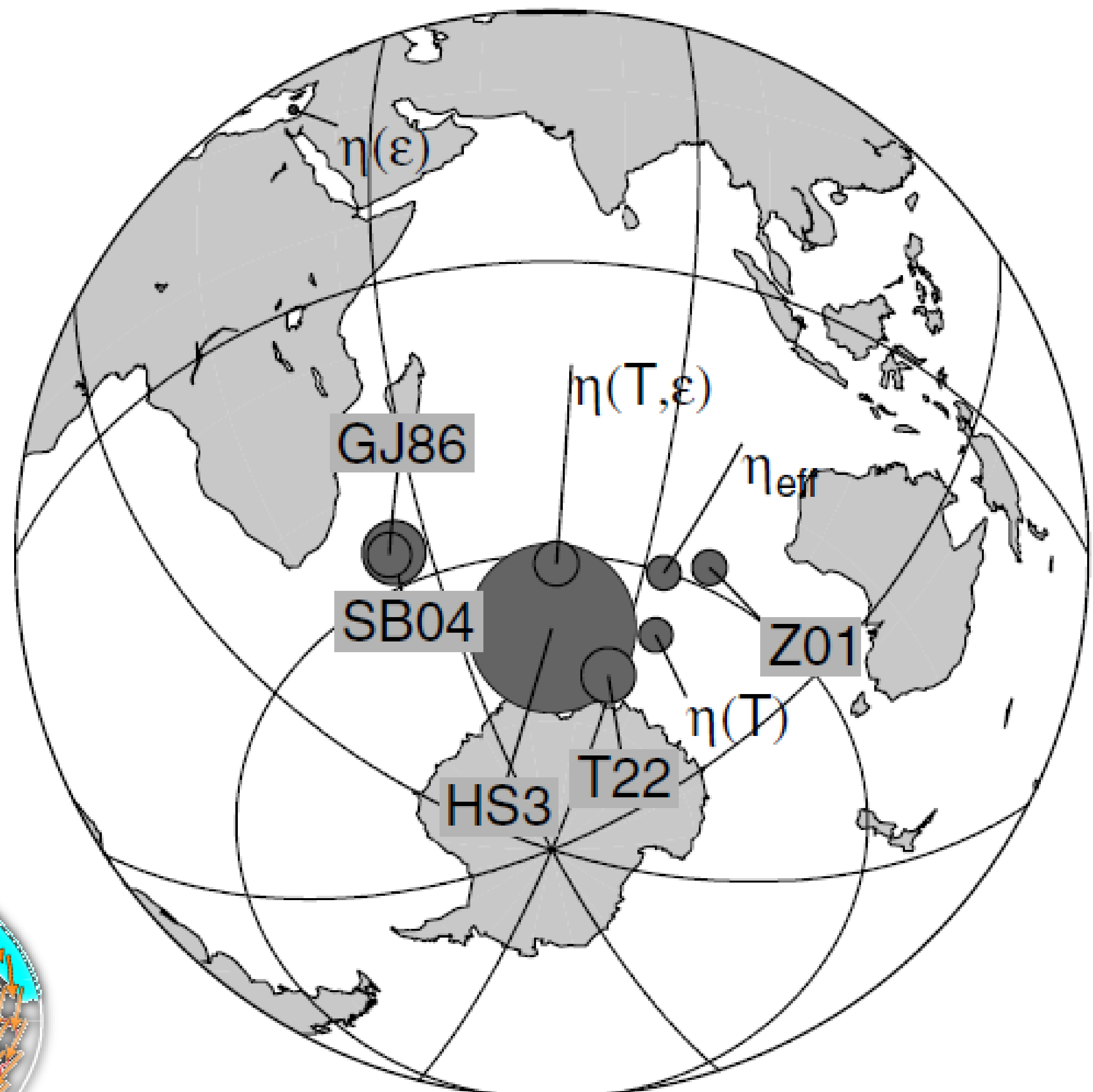

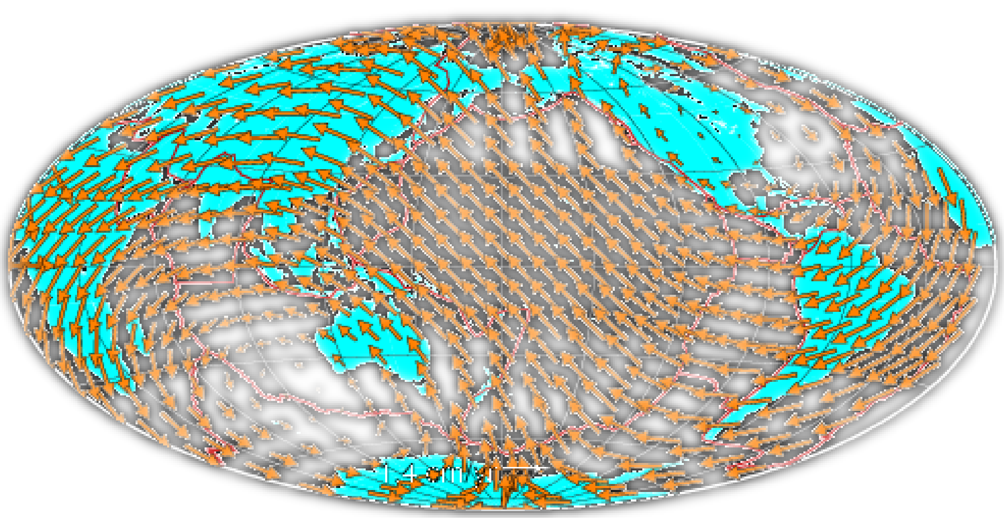

Becker (2006)

Prediction of plate scores with LVVs

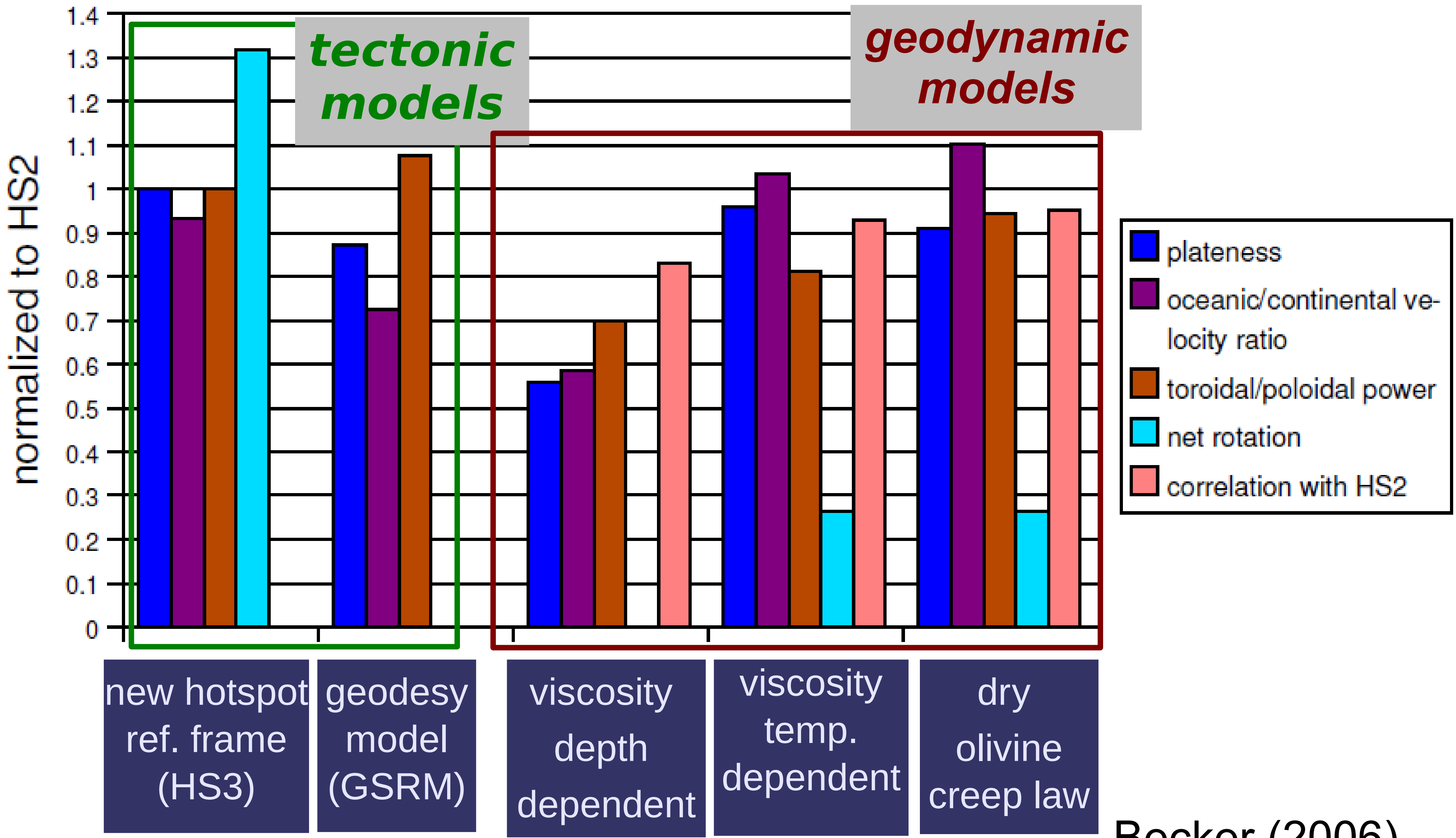

Becker (2006)

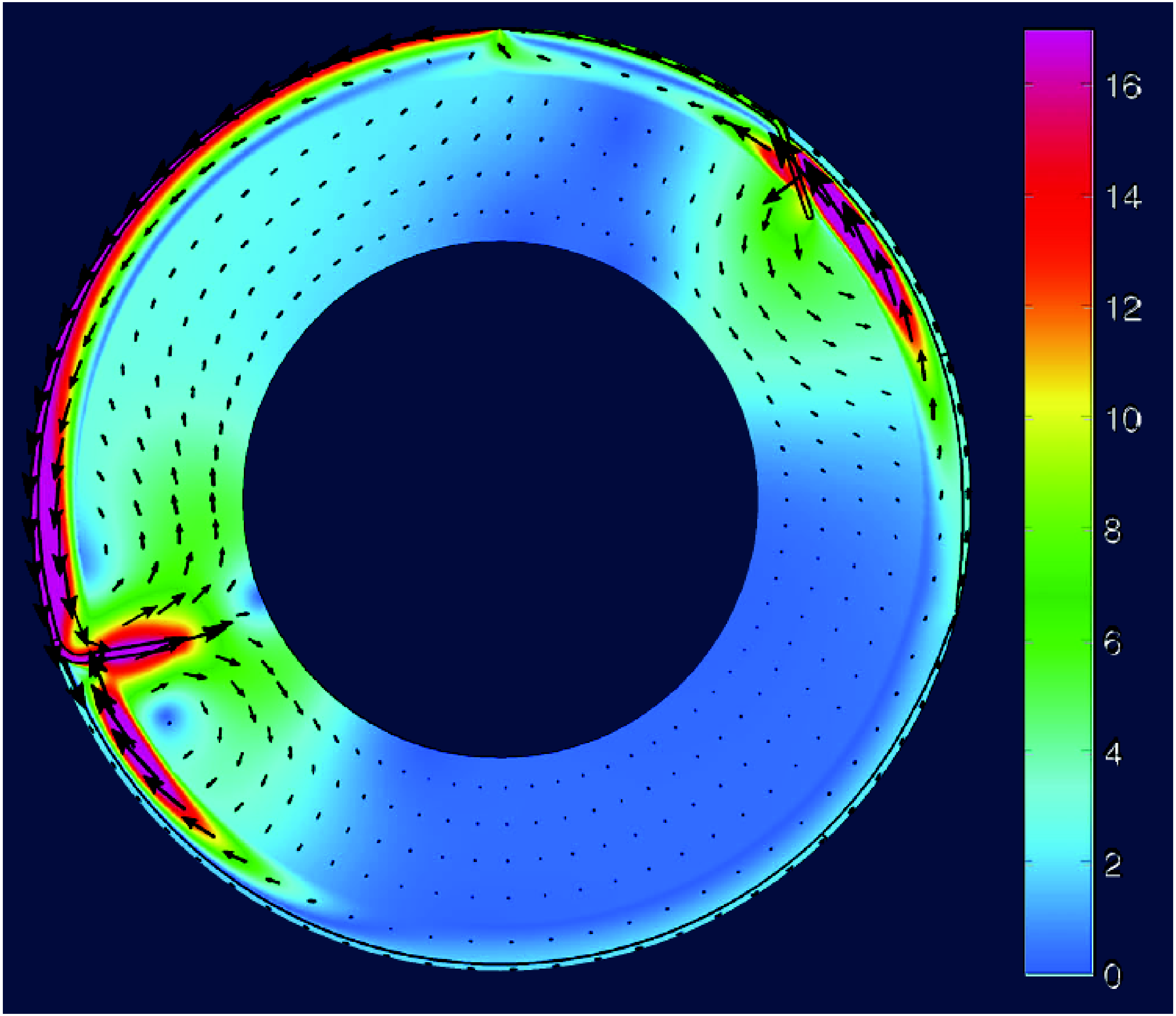

Gerault et al. (in prep)

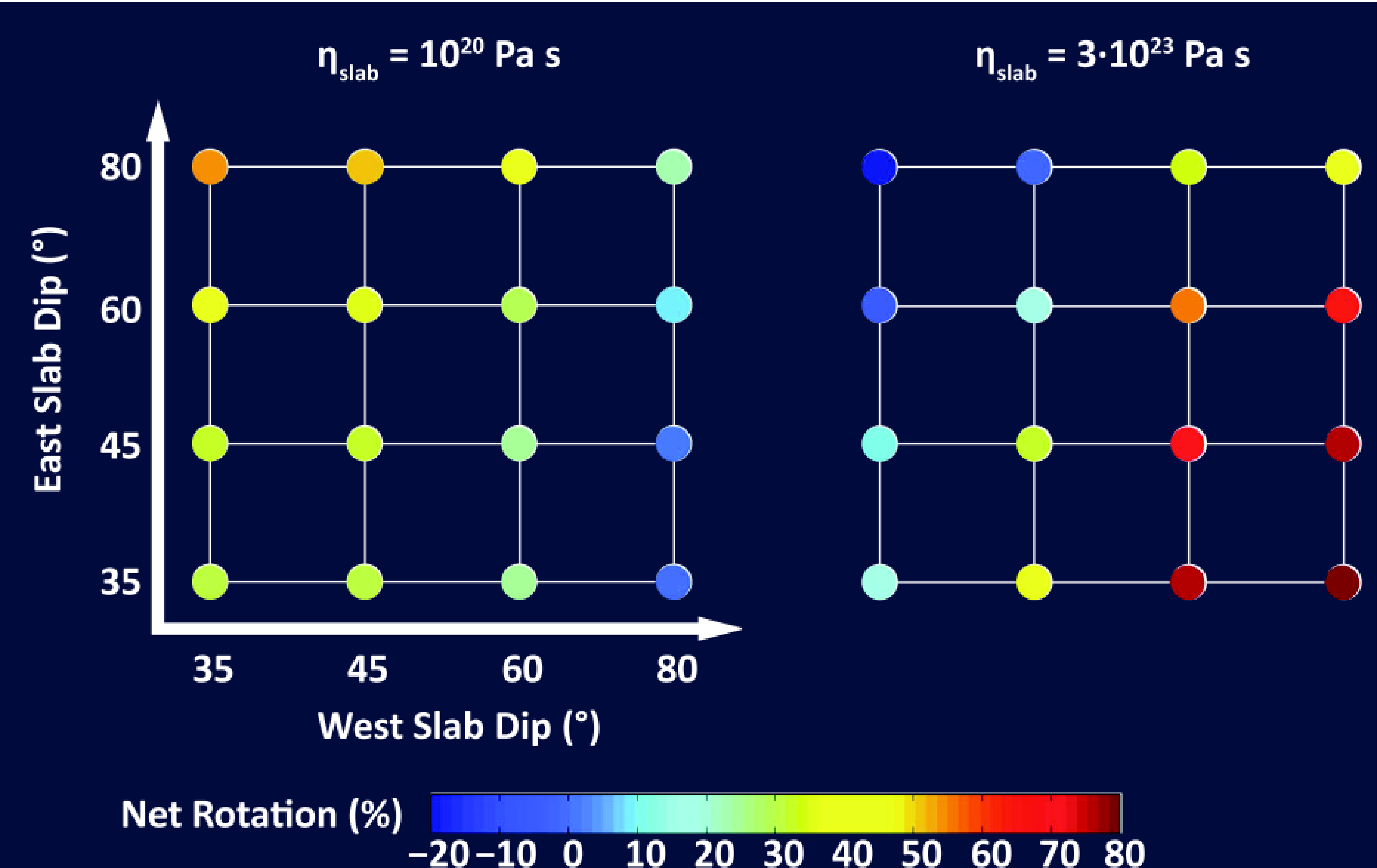

Gerault et al. (in prep)

How can we resolve the ambiguity between slab strength and lateral viscosity variations?

AMR

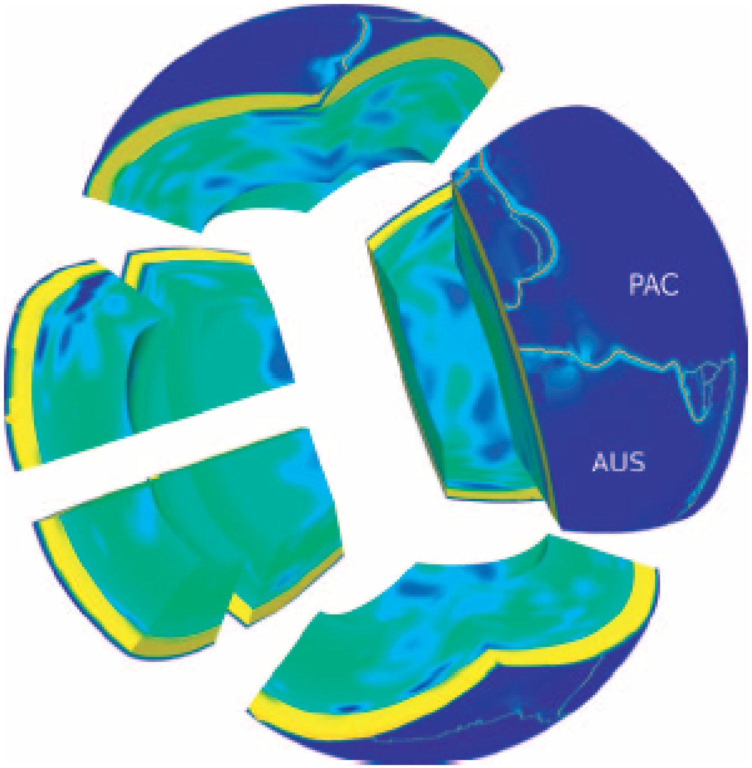

A

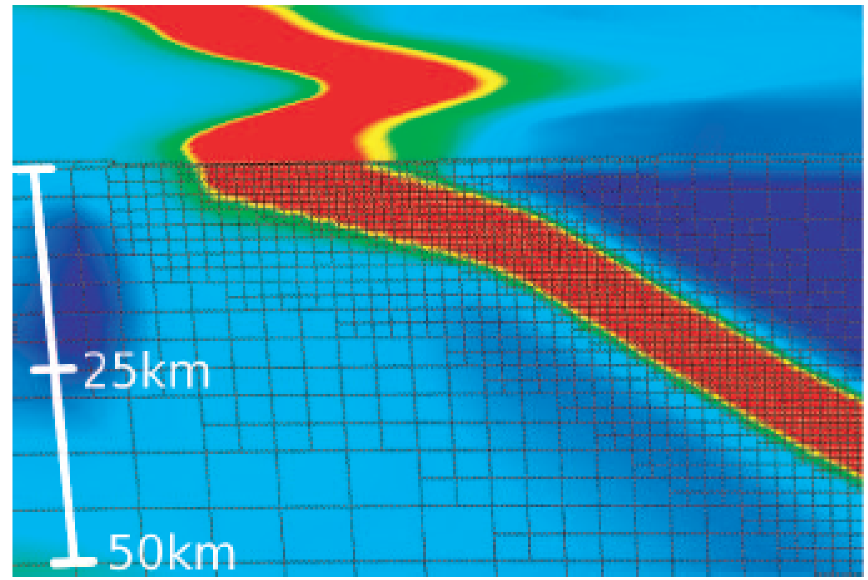

B

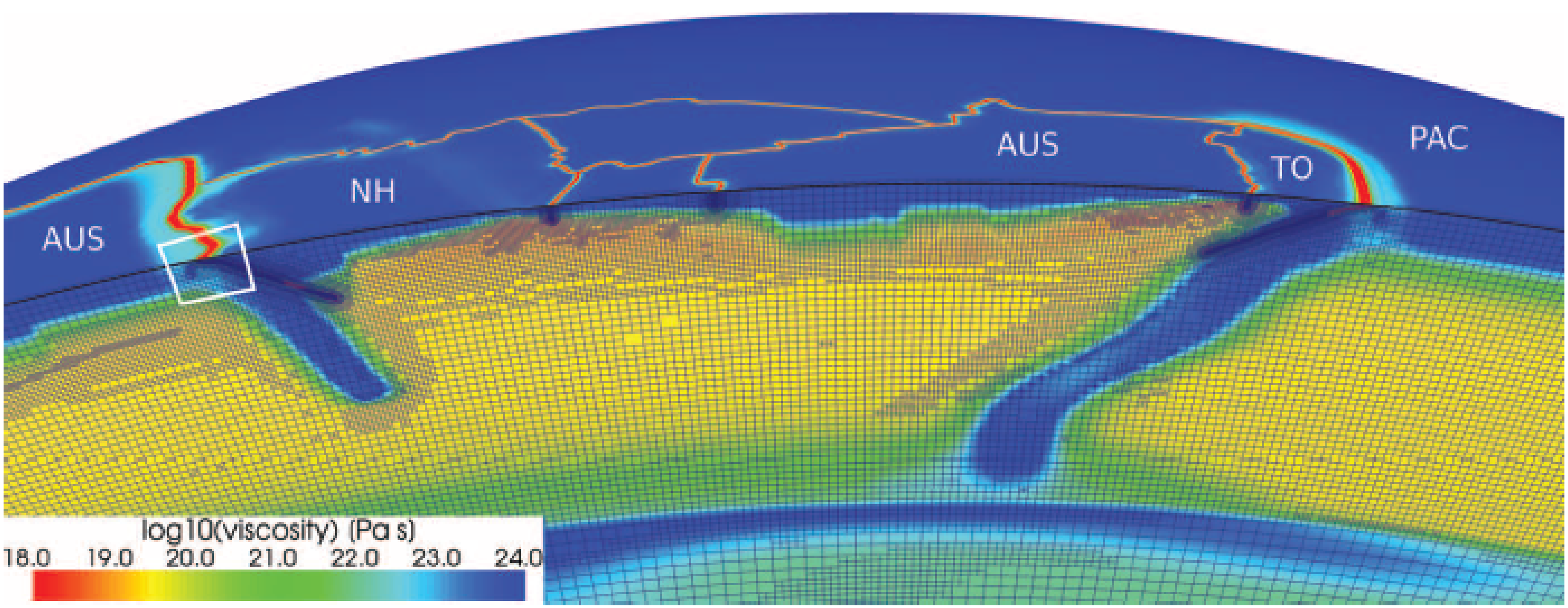

Stadler et al. (2010)

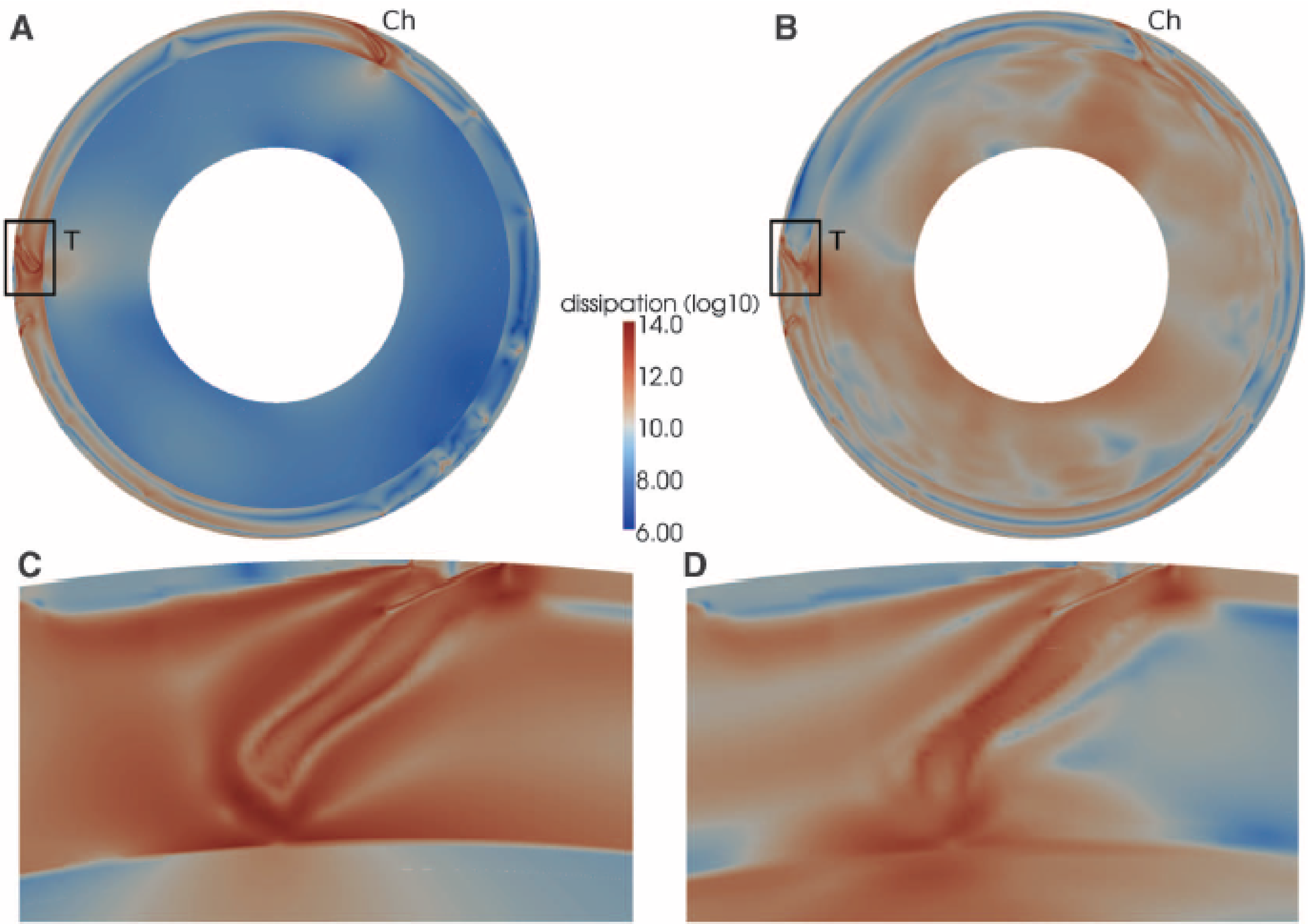

Fig. 5. Pointwise dissipation for models in cross section through small-circle at 17°S for case 6 (without lower-mantle structure) in (**A**) and through Case 8 (with lower-mantle structure) in (**B**). The Tonga area is denoted with the letter T, and the Northern Chile area with letters Ch. (**C**) Zoom-in on the Tonga area for case 6. (**D**) Same zoom-in for case 8.

Stadler et al. (2010)

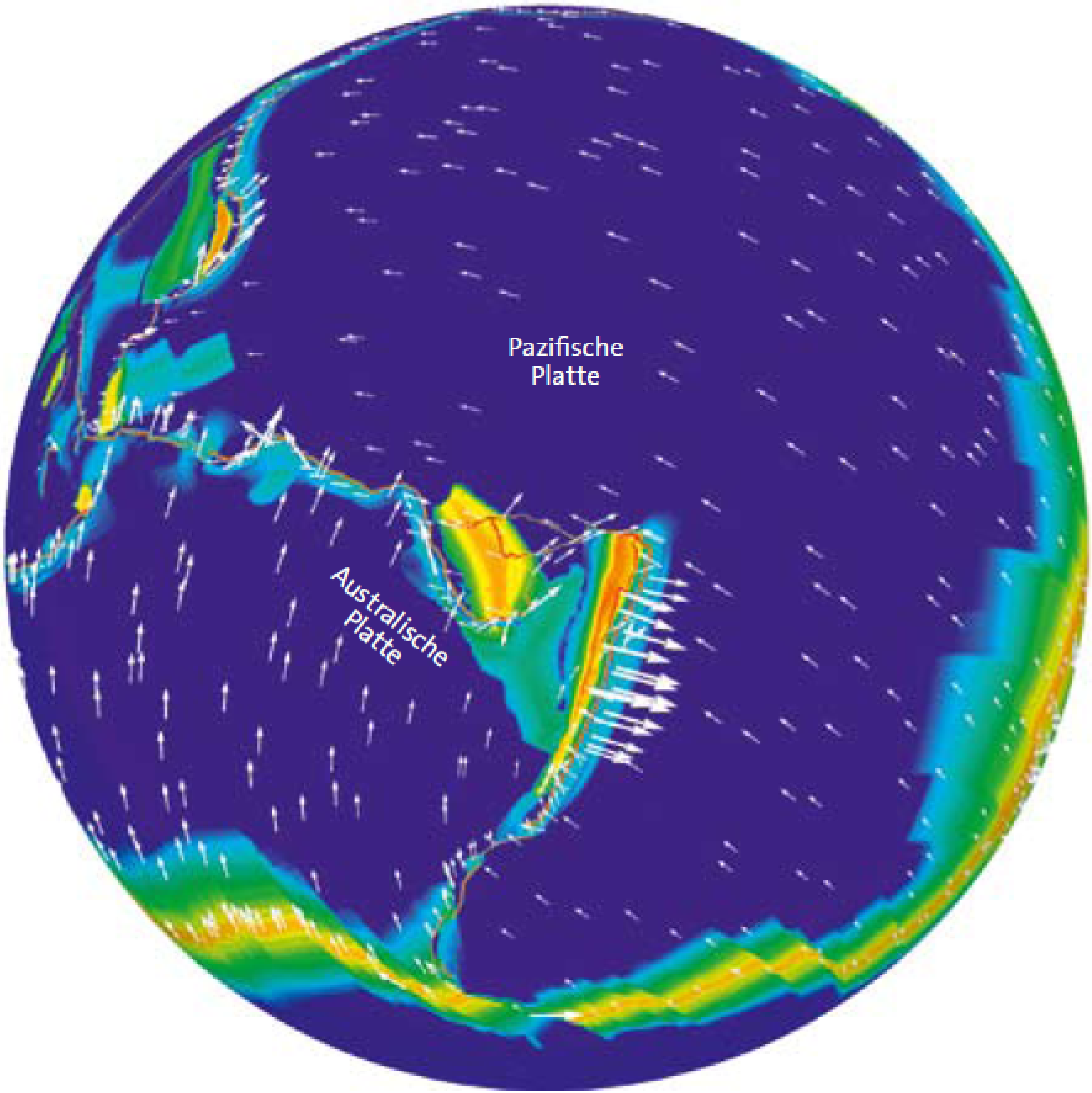

Stadler et al. (2010)

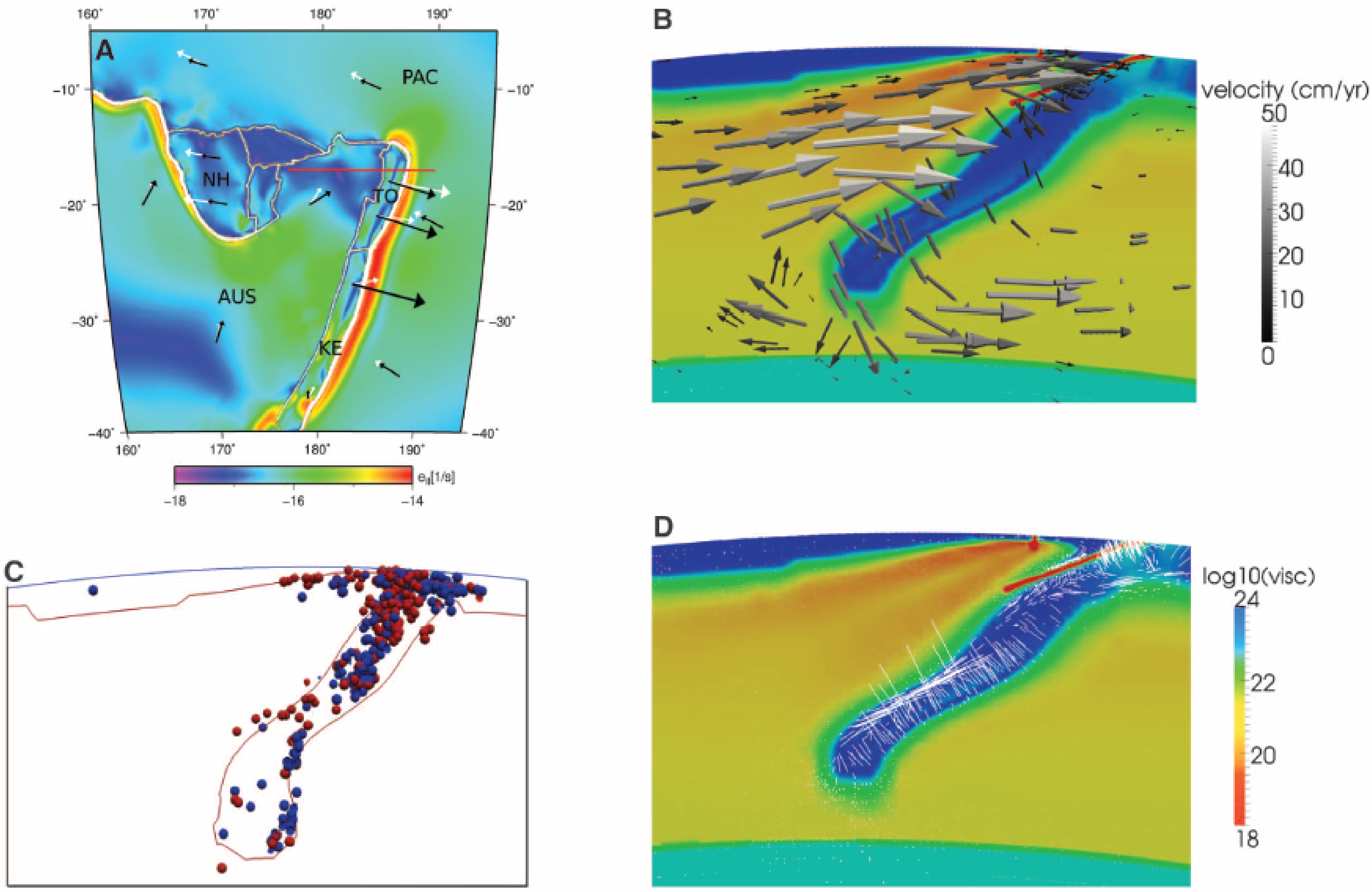

Fig. 4. (**A**) Map of surface strain rate with plate velocities for plates in a NNR frame of reference for the New Hebrides-Tonga region. Predictions are in black and white arrows from Nuvel1-NNR (*27*), with micro-plate motions from (*23*). Plates are labeled Australian, AUS; New Hebrides, NH; Tonga, TO; Kermadec, KE; and Pacific, PAC. Cross-sections in (**B**), (**C**), and (**D**) denoted by red line in (A). (B) Predicted velocity and viscosity. (C) Down-dip compression (blue) and down-dip tension (red) from CMT solutions (*22*). (D) Predicted compressional axes for case 6.

Stadler et al. (2010)

Slab seismicity

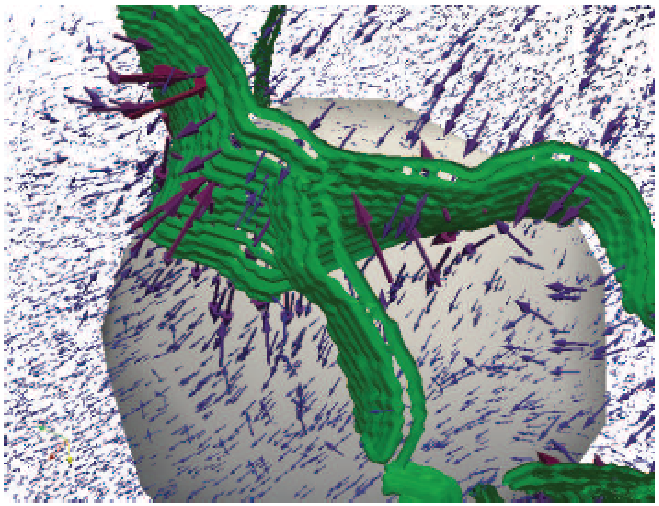

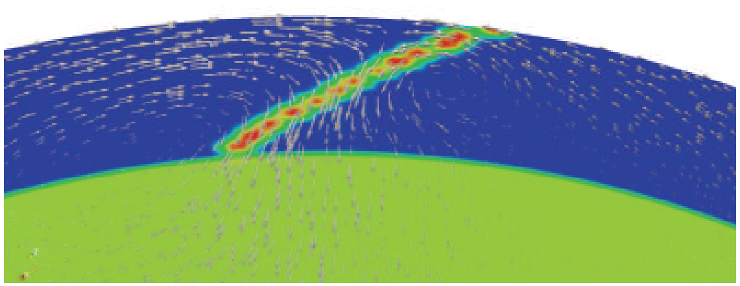

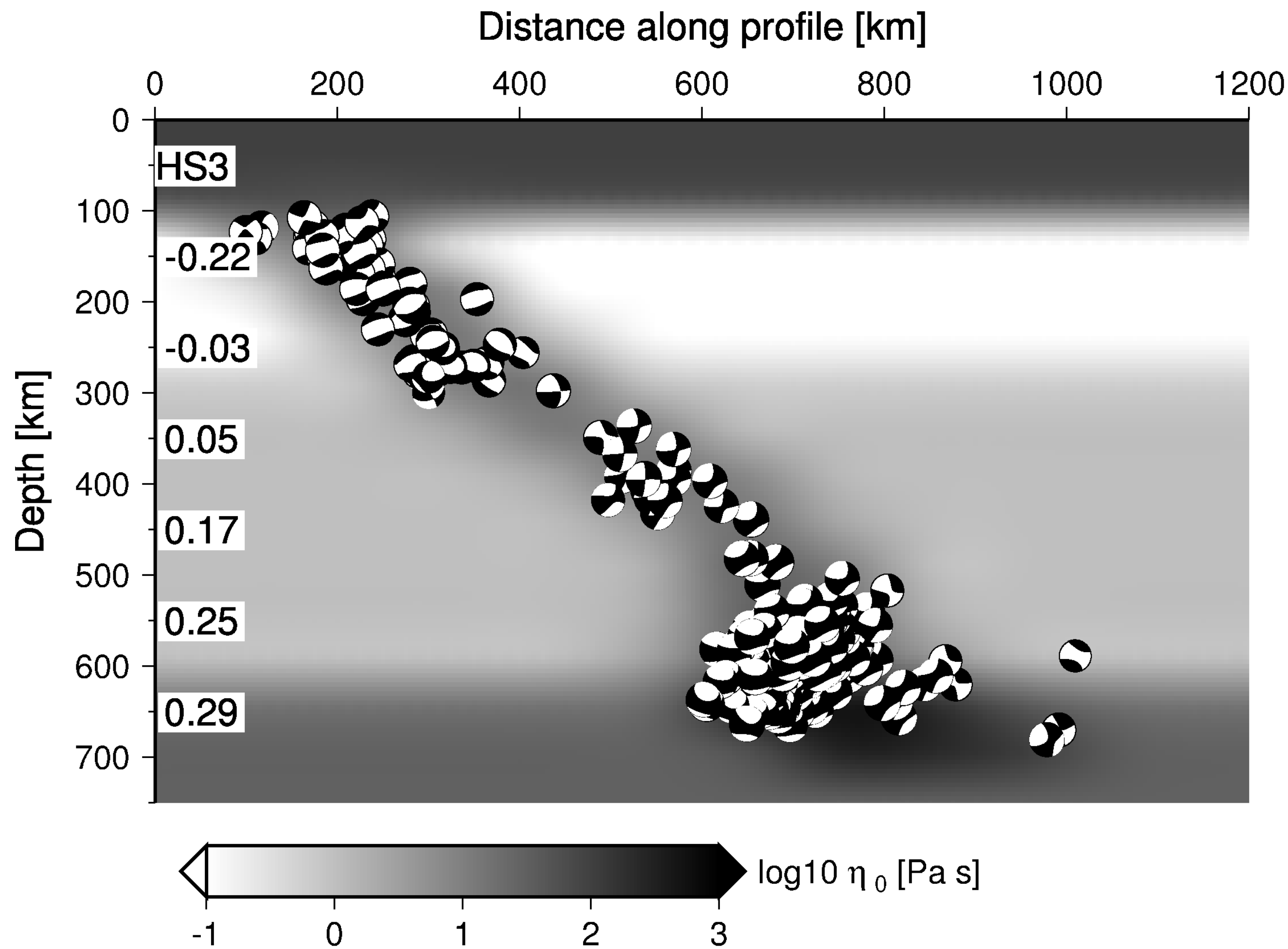

Hager & O'Connell (1979); Bevis (1988); Vassiliou & Hager (1988);
Billen and Gurnis. (2003); Bilek et al. (2005); Carminati and Petricca (2010); Alpert et al. (2010)

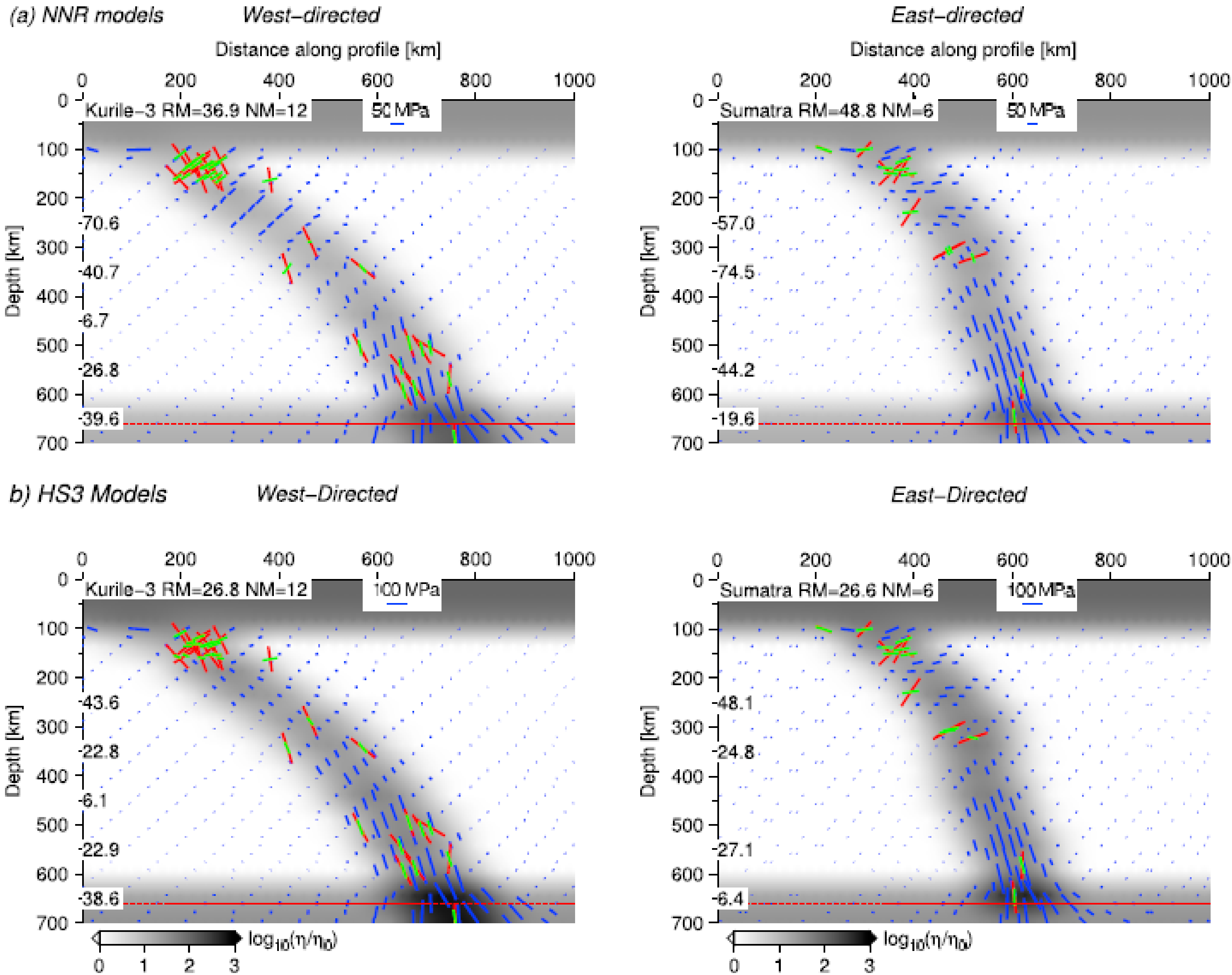

Alpert et al. (2010)

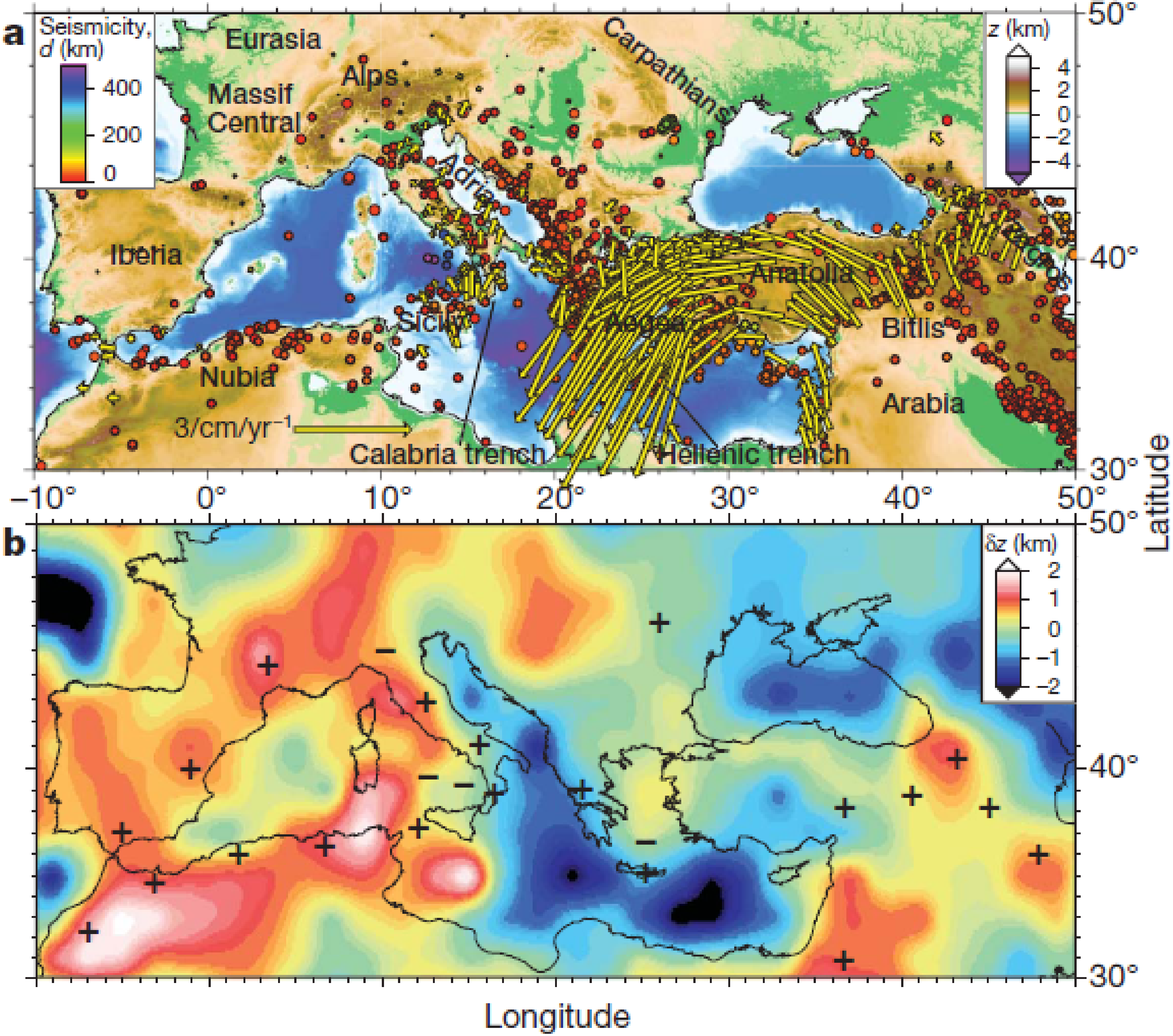

Faccenna & Becker (2010)

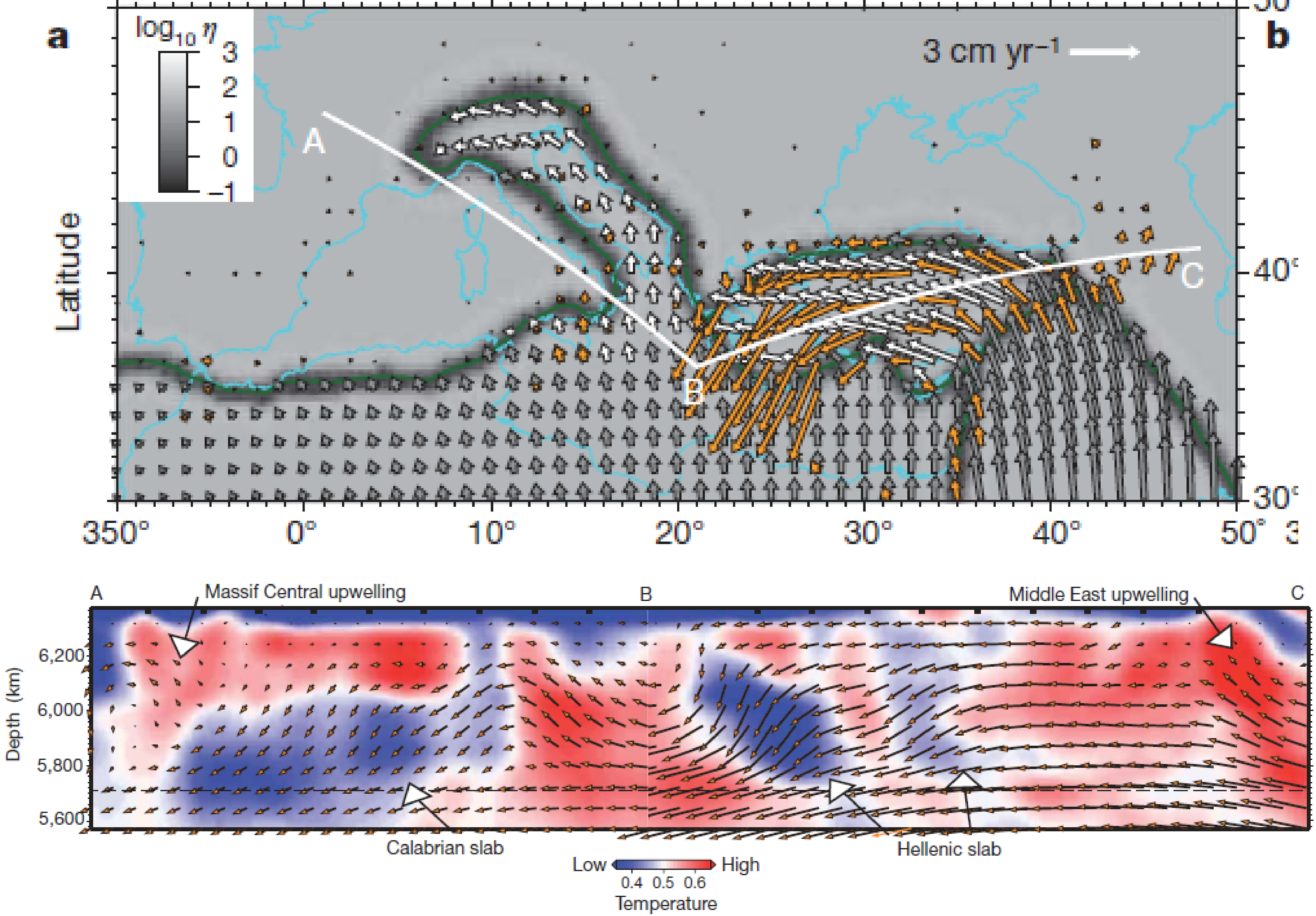

Faccenna & Becker (2010)

“observed” dynamic topography

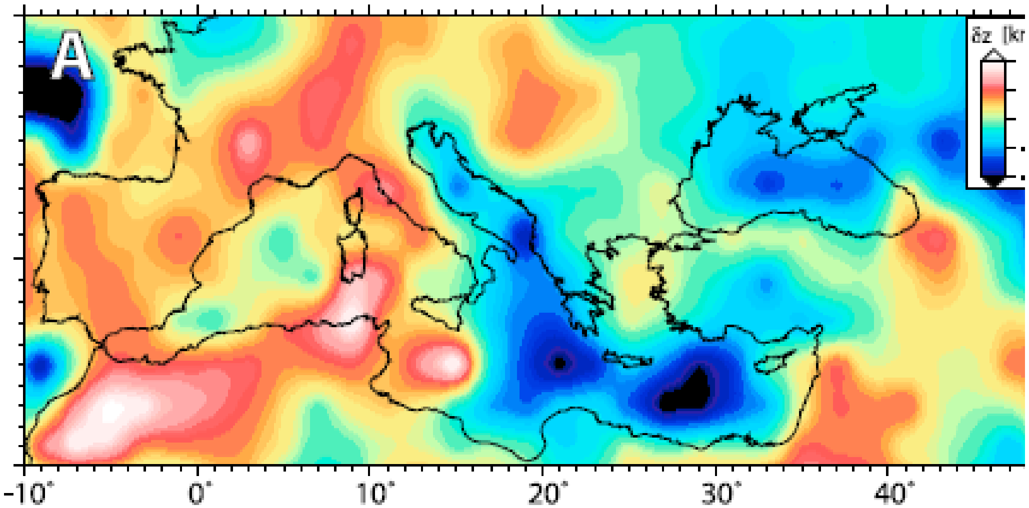

model

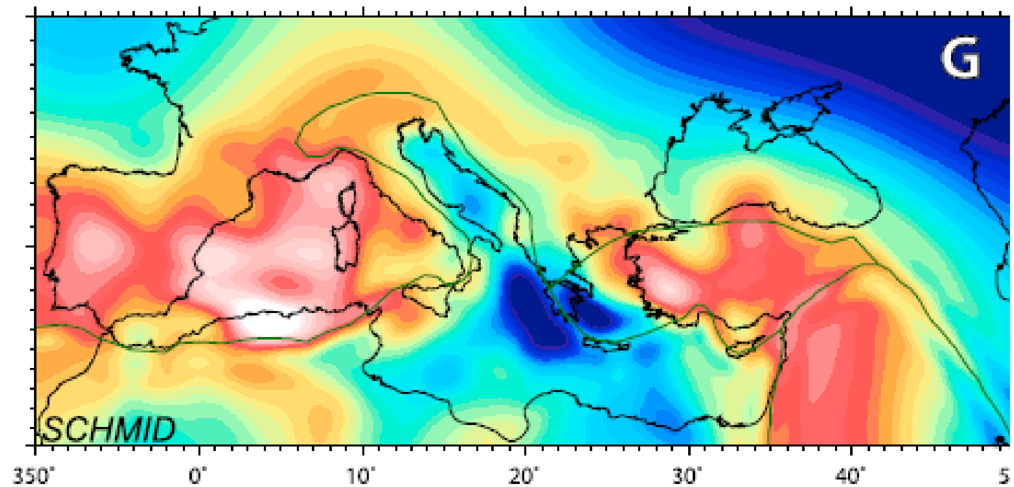

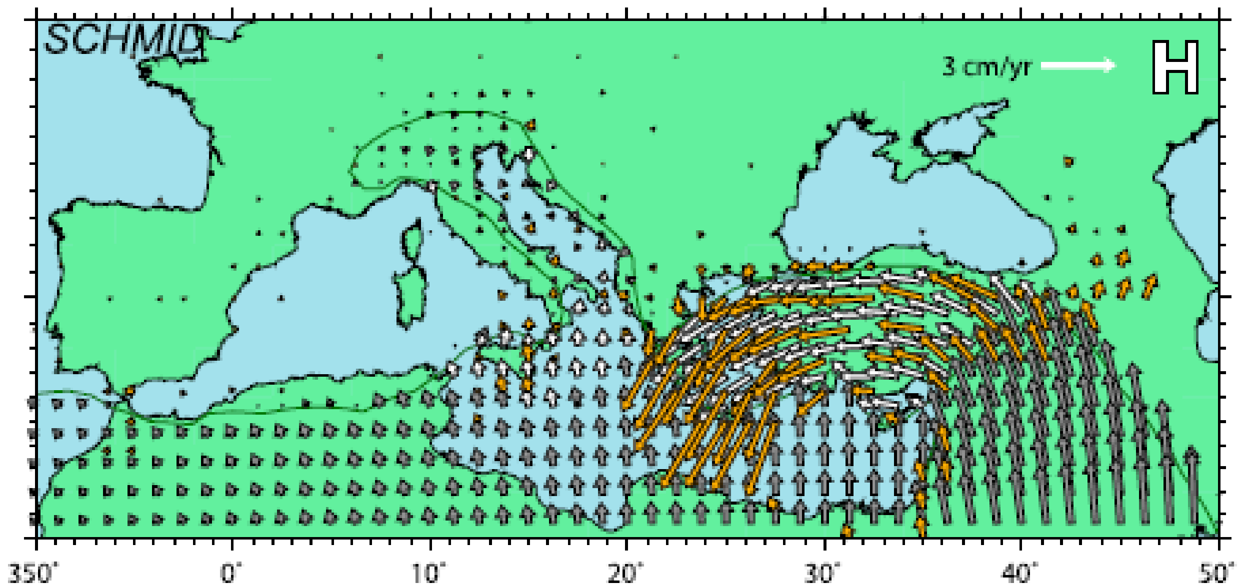

Boschi et al. (2010)

Trench dynamics

- Back-arc deformation
- Relative trench motions

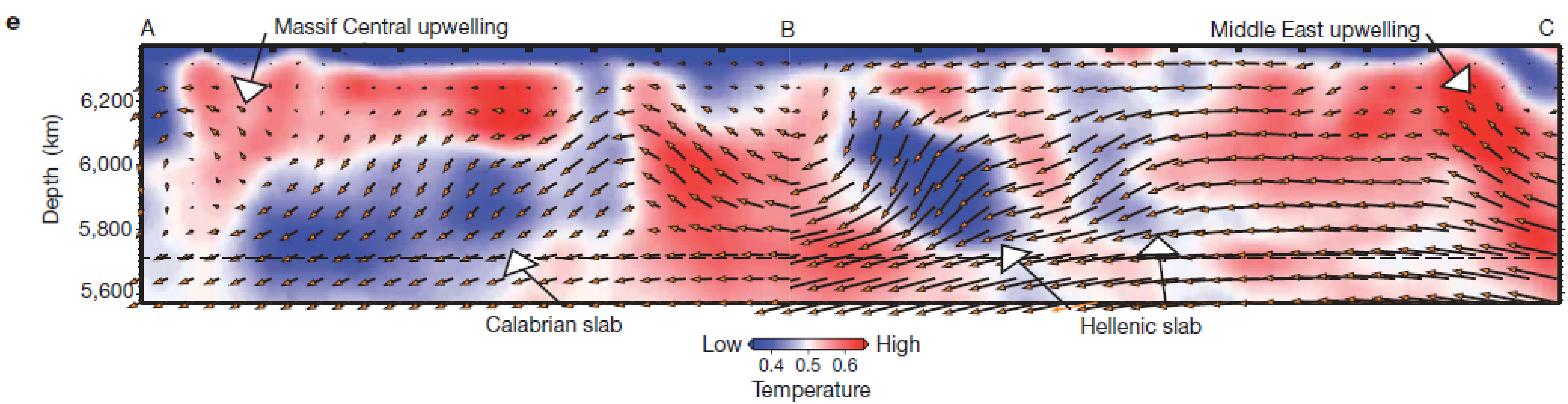

Back-arc deformation

- Distinguish between
  - absolute motion of trench and
  - back-arc deformation (shortening or extension) with respect to overriding plate

Chilean (compressional) type

Marianas (extensional) type

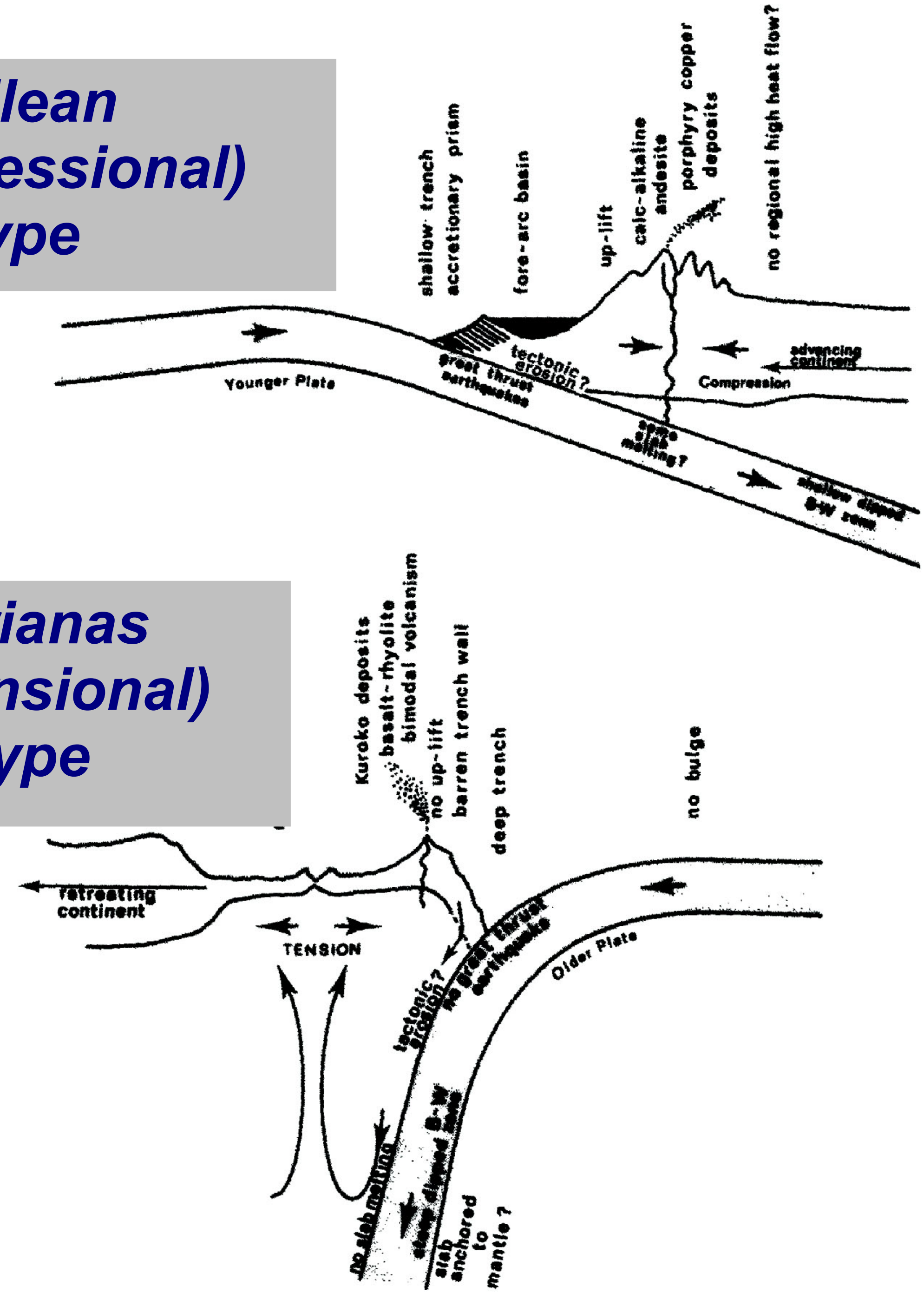

Uyeda and Kanamori (1979)

Relative trench motions

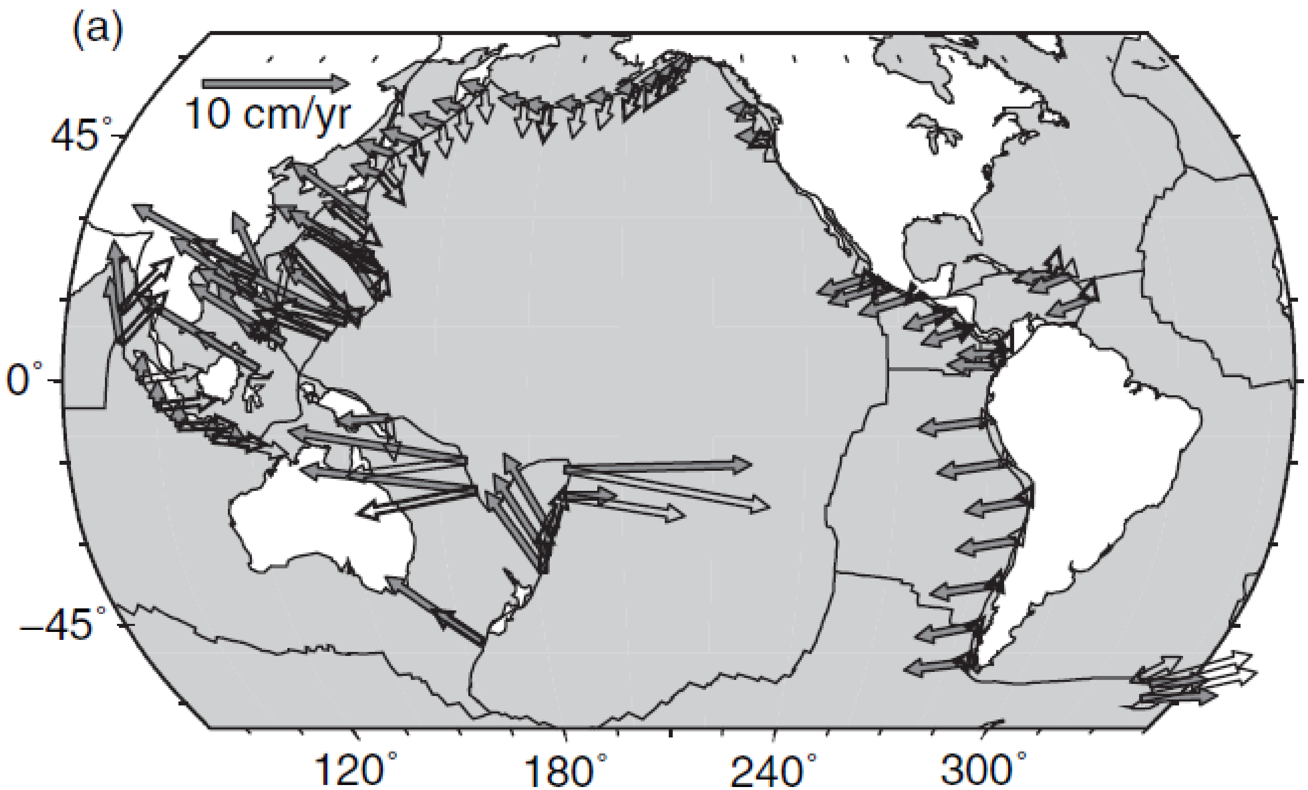

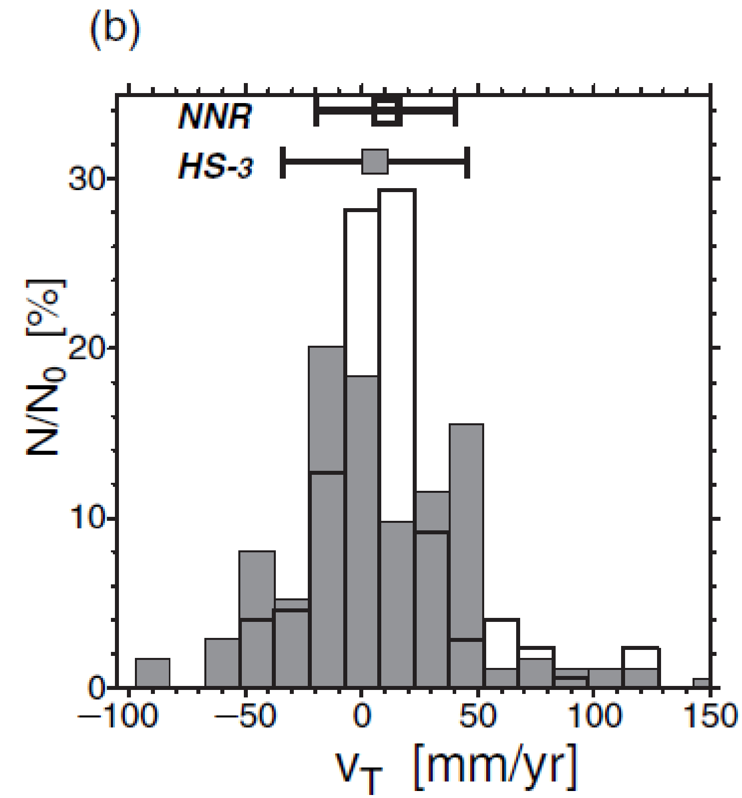

Becker & Faccenna (2009), based on Funiciello et al. (2007)

Back-arc kinematics

- Velocities:
  - Over. plate V_{OP}
  - Subduct V_S
  - Trench V_T
  - (Oc.) plate V_P
  - Back-arc V_D
- $V_s = V_P + V_{OP}$

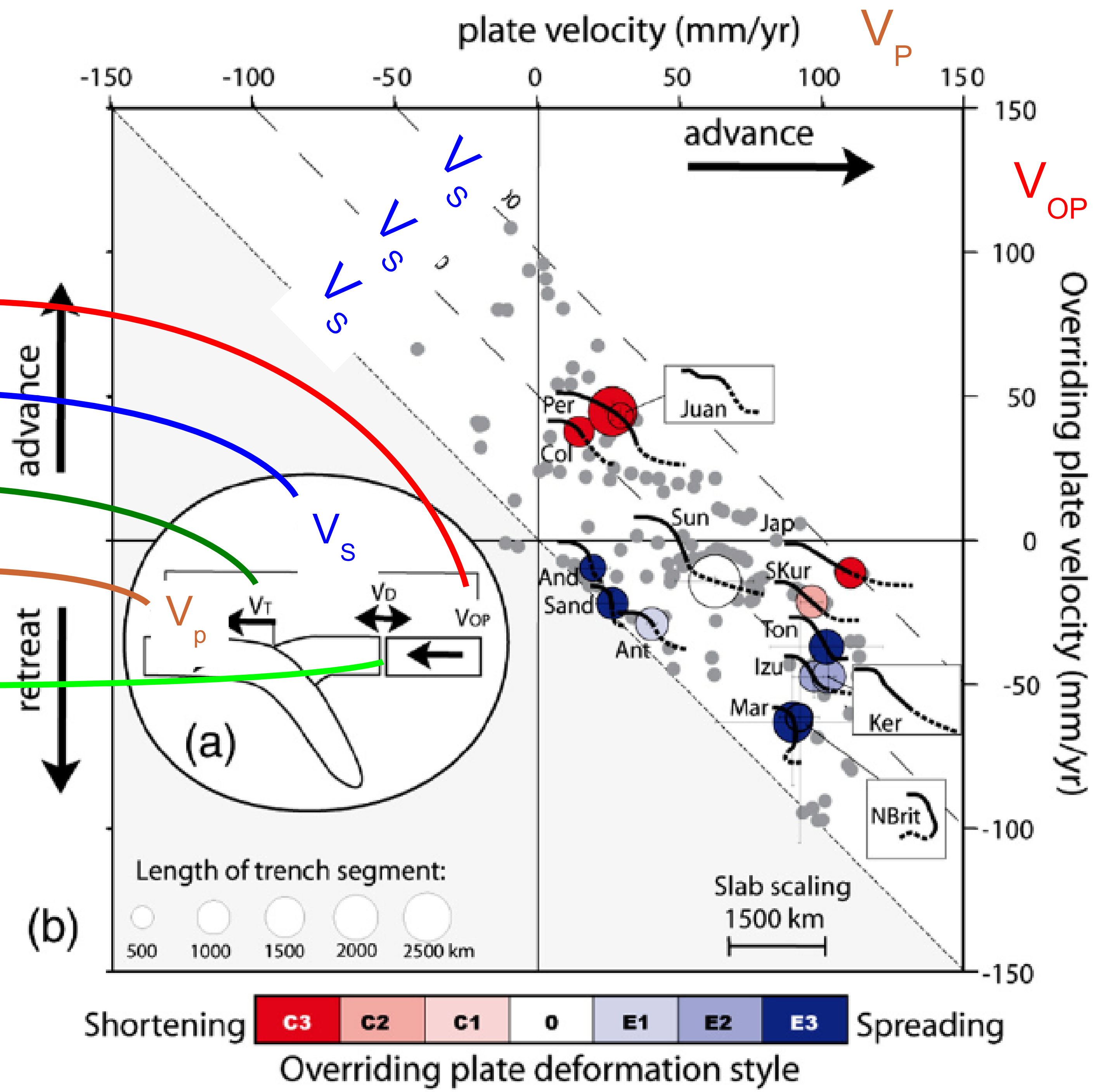

Heuret et al. (2007)

Back-arc kinematics

- Less net rotation will shift values to $v_P > 0$
- x and y axes depend on reference frame

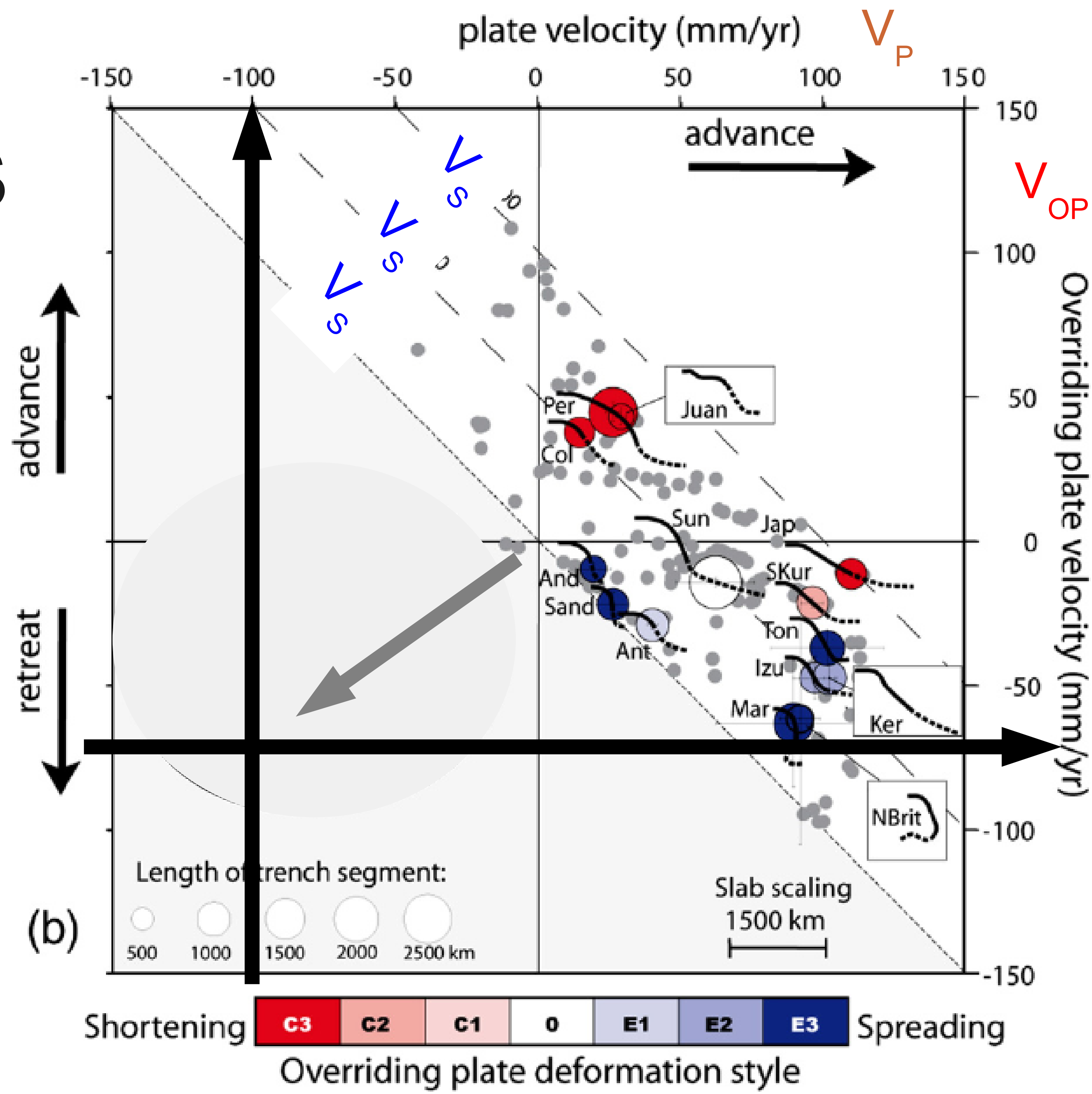

Heuret et al. (2007)

Back-arc kinematics

- V_S is roughly constant, ~ independent of reference
- If V_S > 5, back-arc shortening
- If V_S < 5, back-arc extension
- Slab anchoring effect

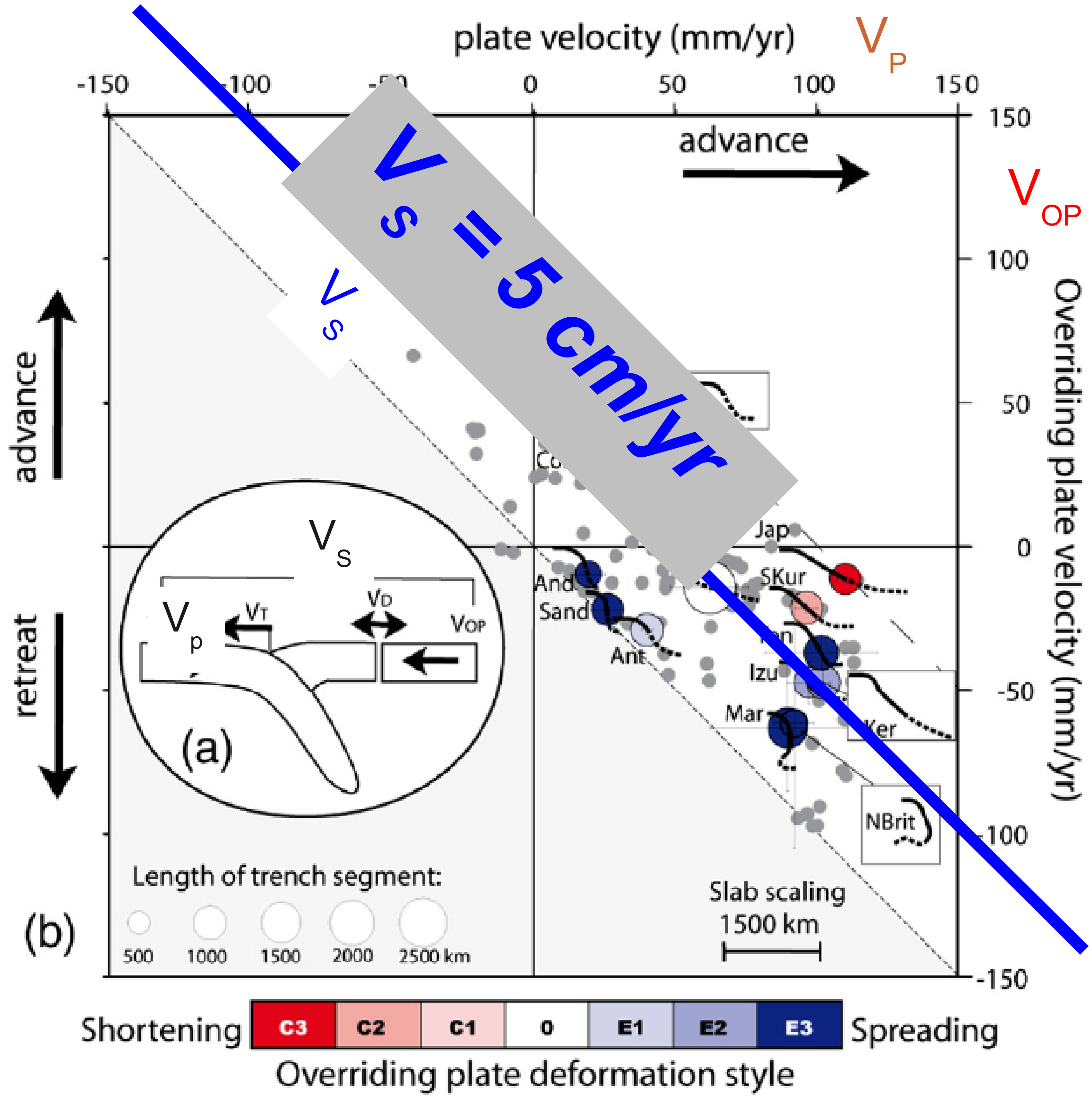

Heuret et al. (2007)

Back-arc dynamics

- Similar behavior found in lab for stiff slab experiments
- Compressional and extensional response of back-arc determined by V_S compared to subduction (modified Stokes) velocity V'

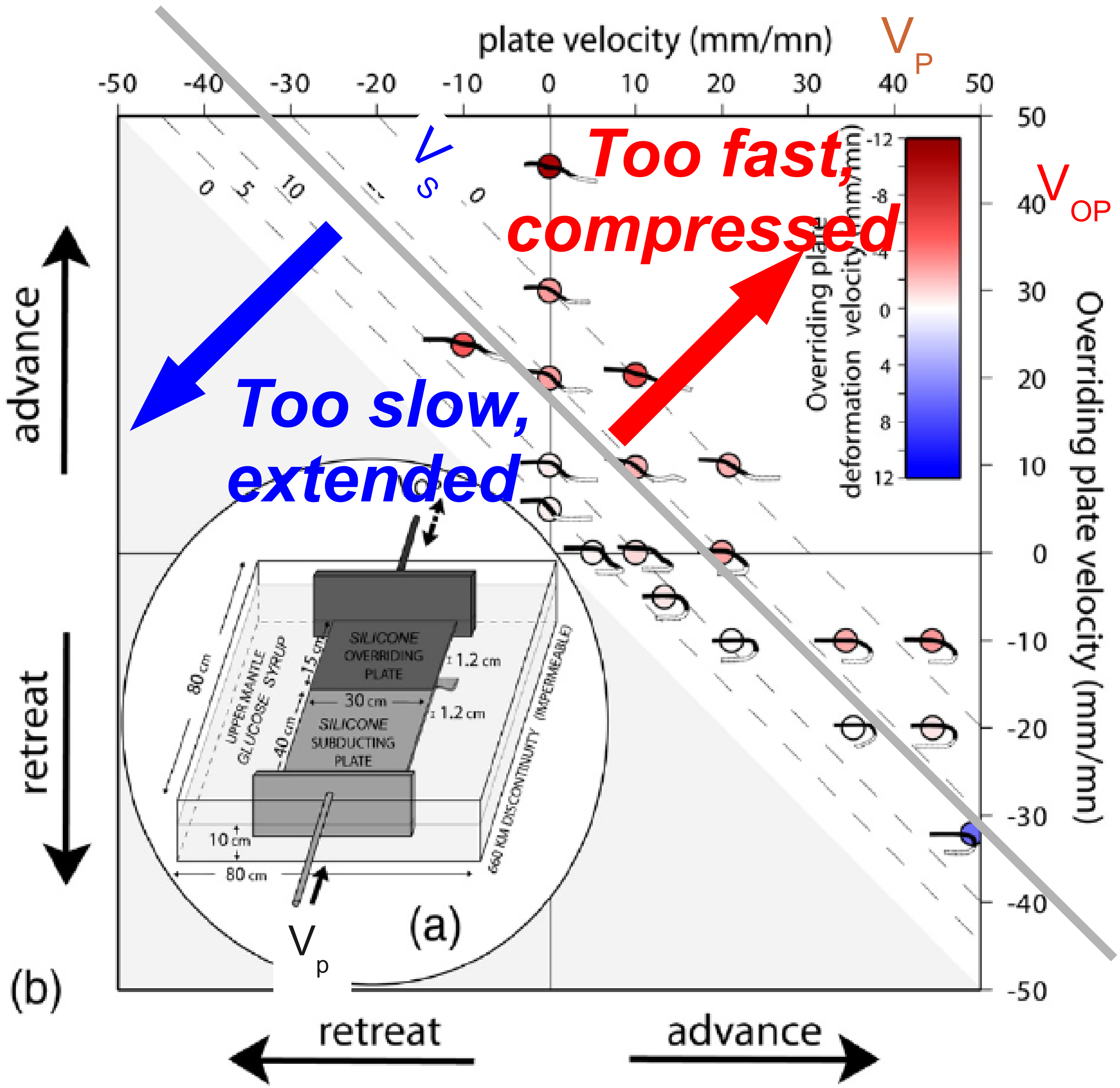

Heuret et al. (2007)

What controls trench motions?

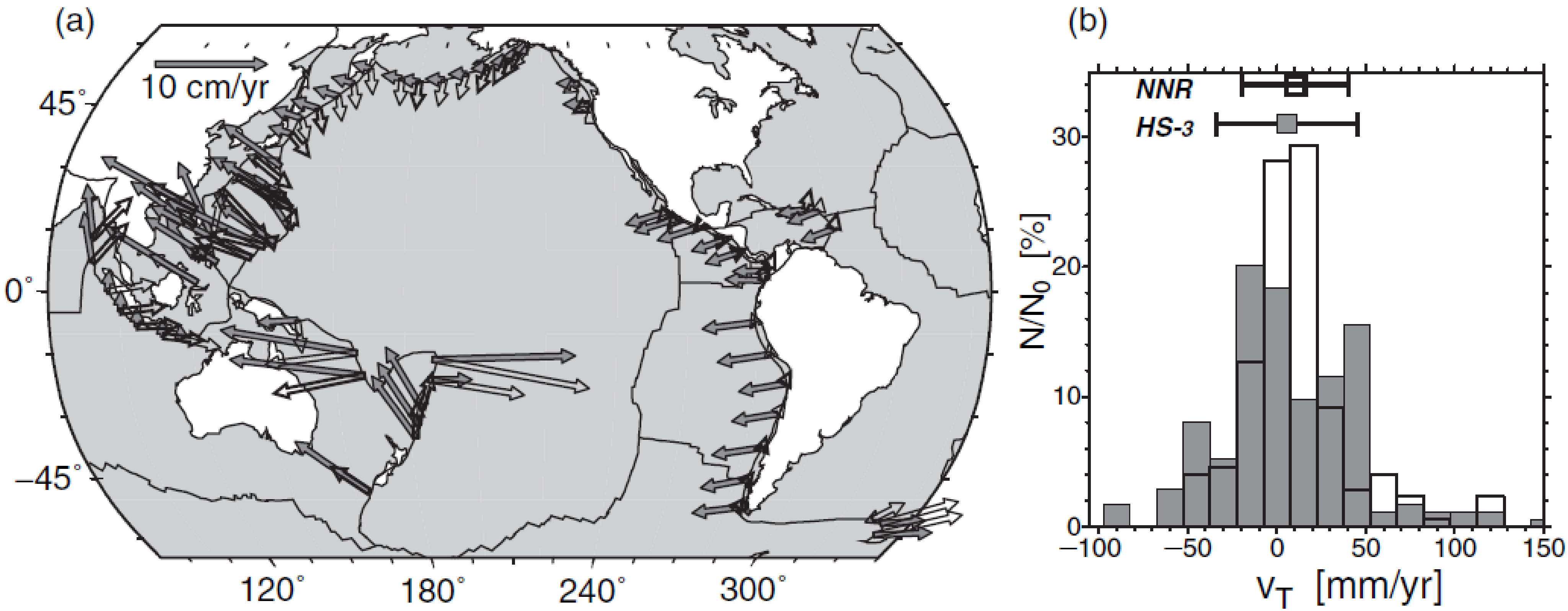

Becker & Faccenna (2009), based on Funiciello et al. (2007)

Instantaneous slab flow field

- Toroidal flow increases with slab width and peaks at moderate viscosity contrasts

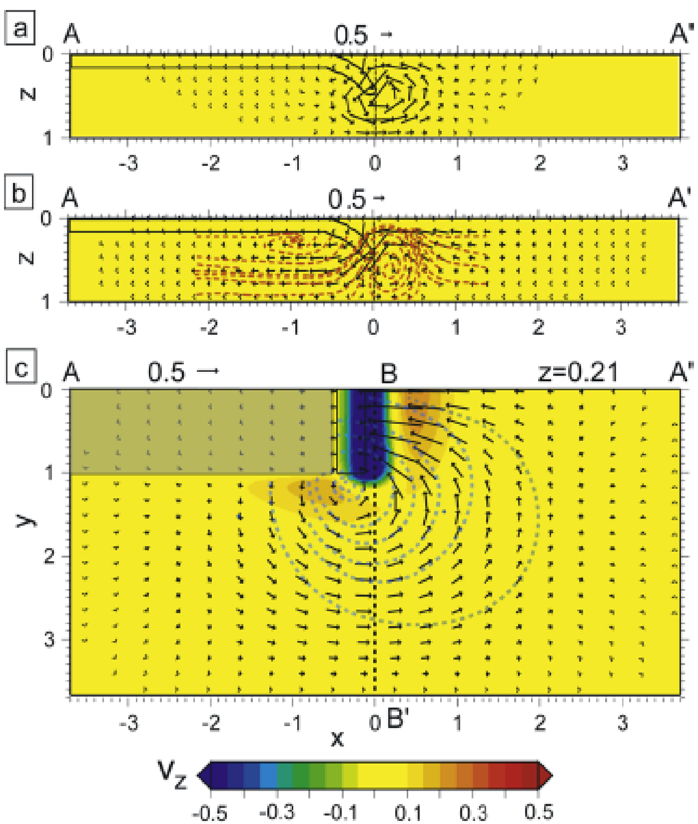

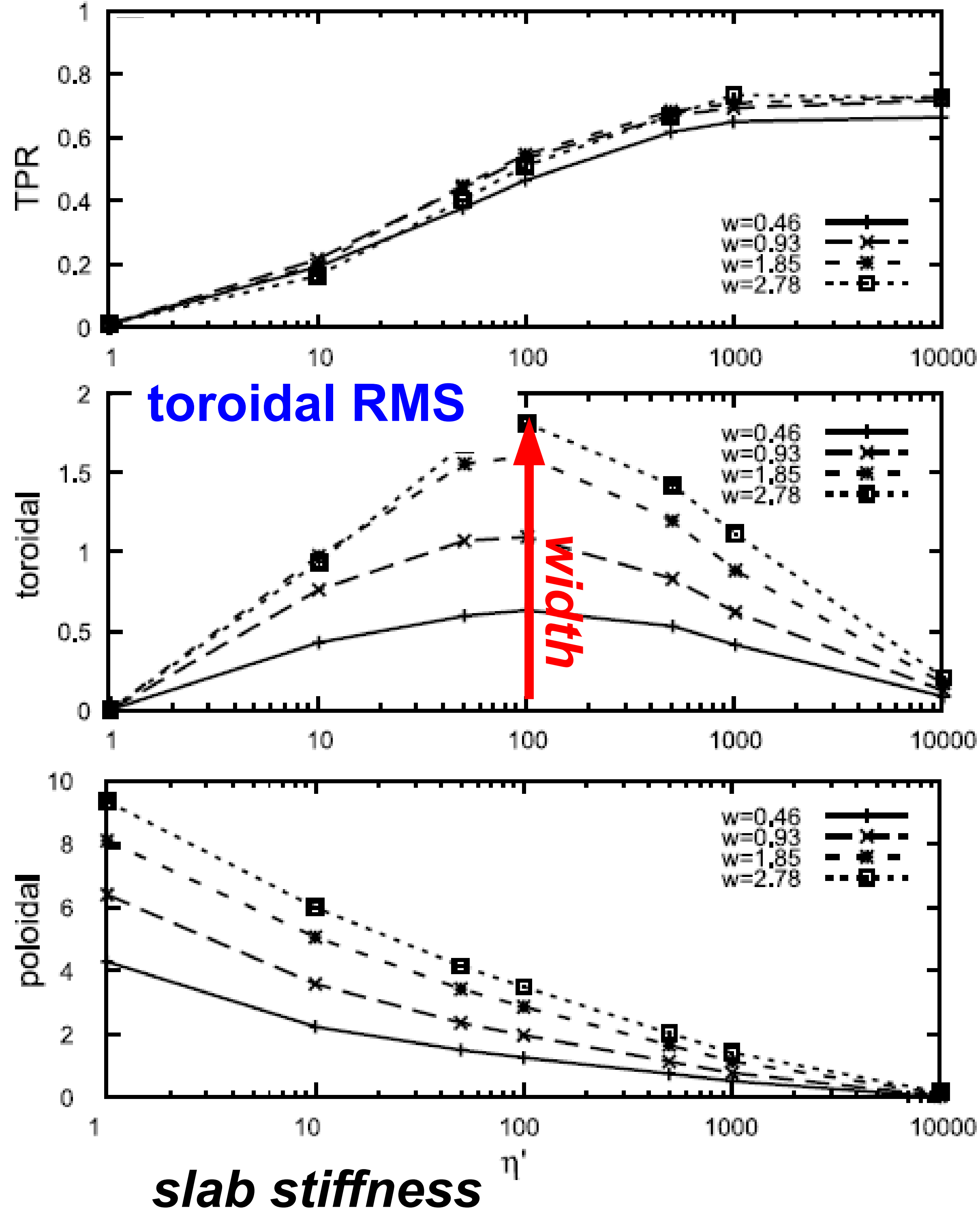

Piromallo et al. (2006)

The role of slab width for toroidal flow

- Inverse relationship between slab with and retreat rate Dvorkin et al. (1993) and Bellahsen et al. (2005)
- Royden & Husson (2006) provide analytical approximation for effect of slab width on the pressure due to toroidal flow

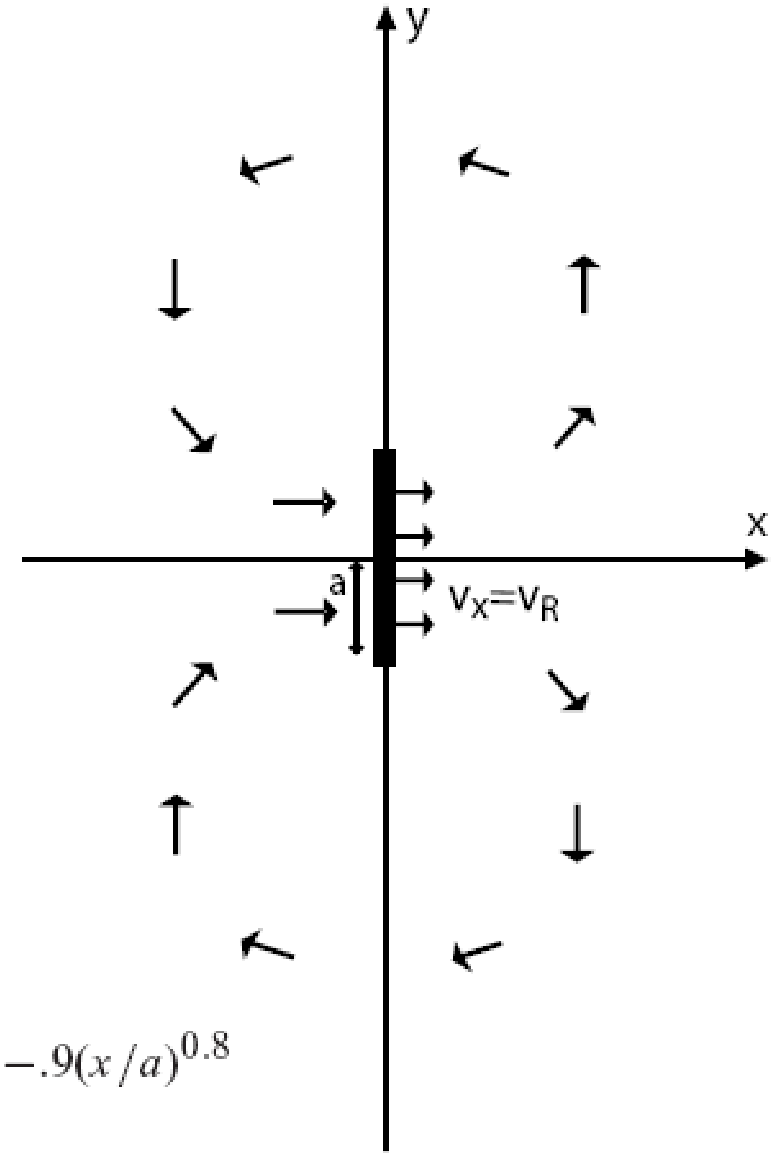

$$P_{\mathrm{visc}}(x,0) = \frac{12\mu a}{\lambda^2}\left[v_R - \left(\frac{v_t + v_m}{2}\right)\right] e^{-.9(x/a)^{0.8}}$$

Royden & Husson (2006)

$V_T = f(W)$ applied to nature

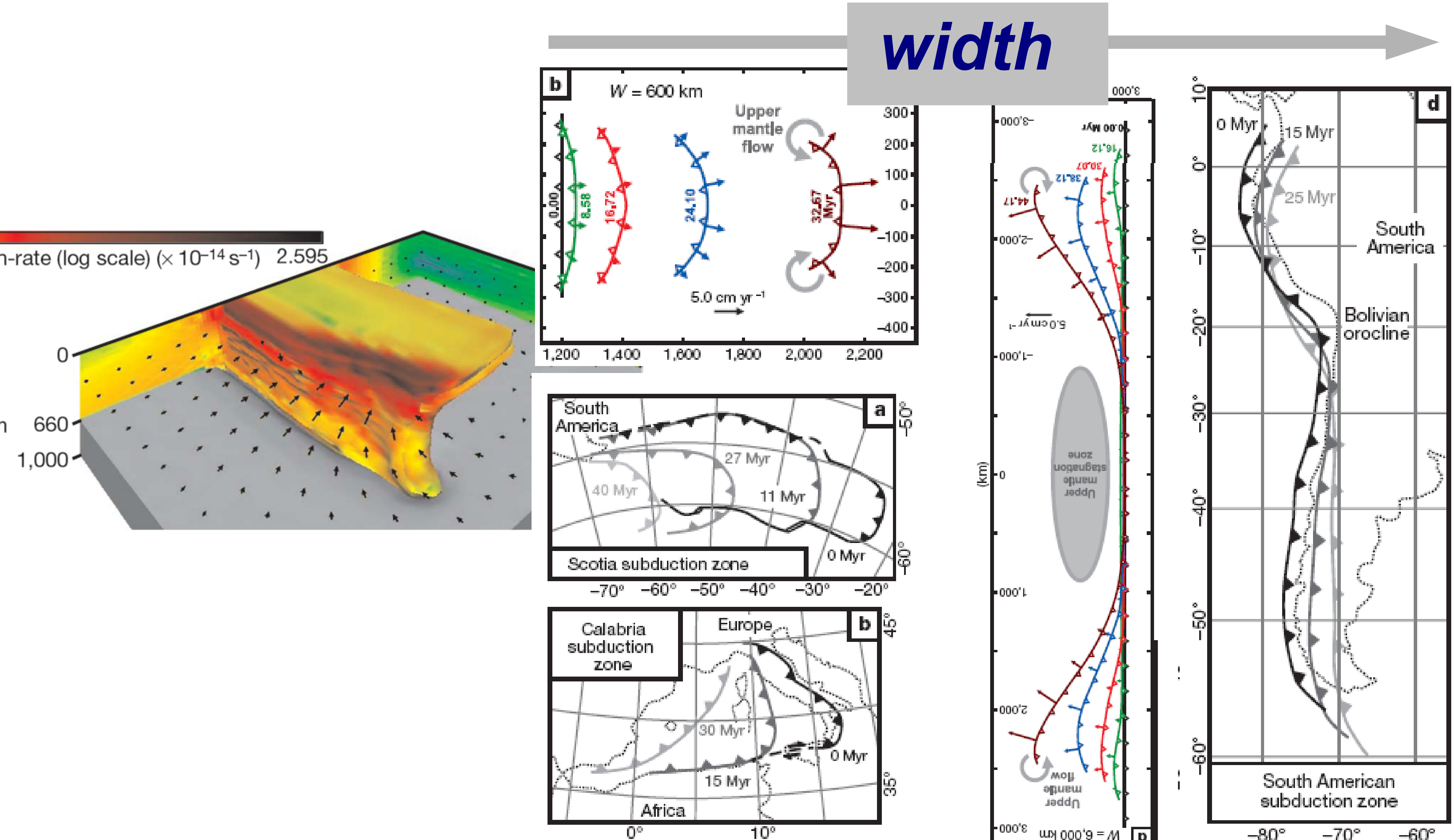

Schellart et al. (2007)

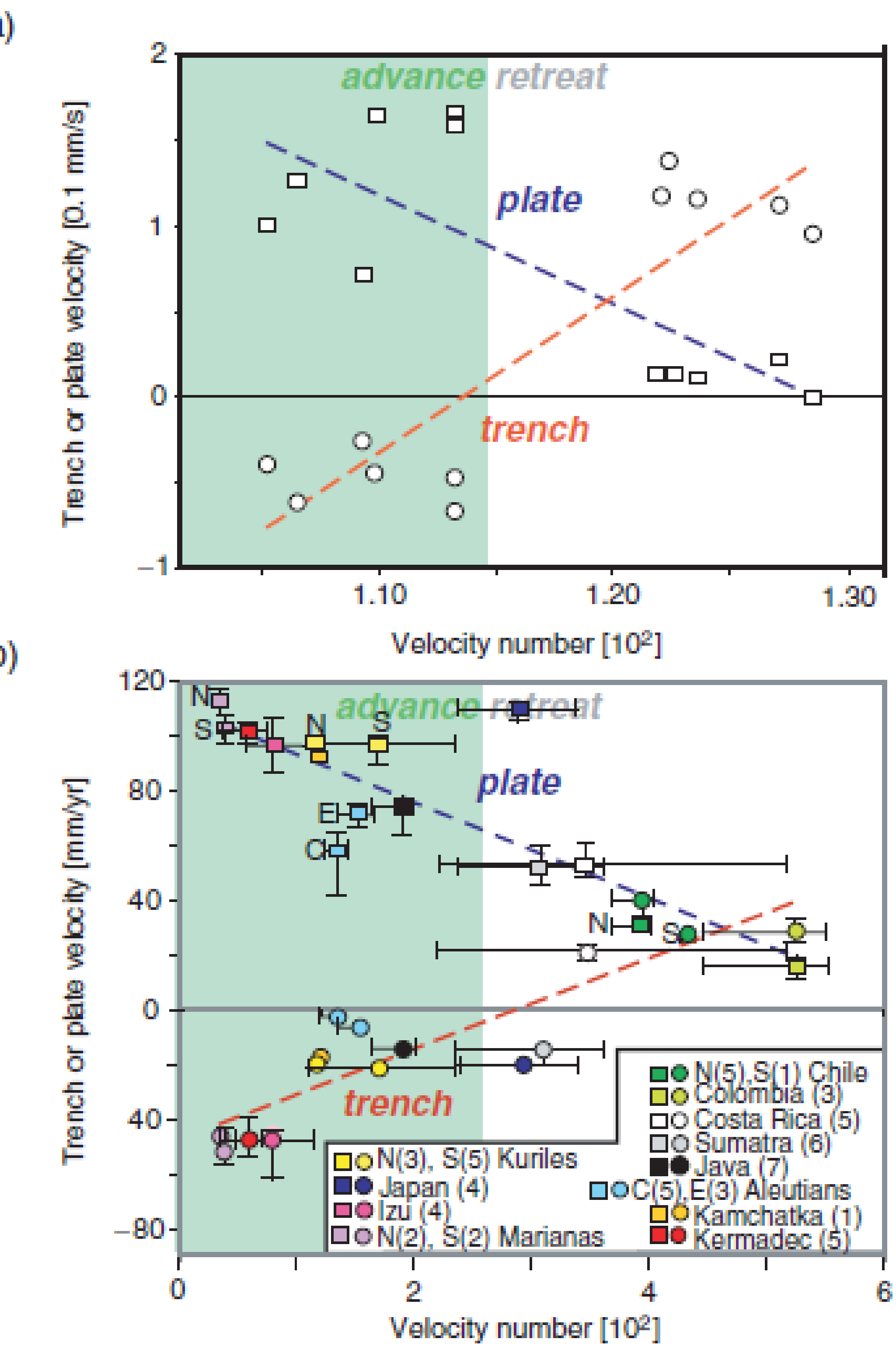

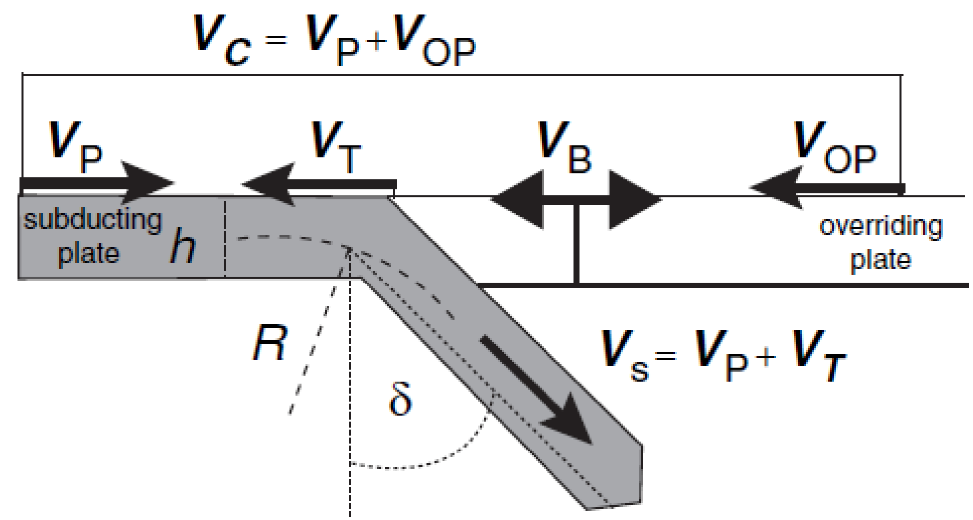

Fig. 3 Regional subduction zone kinematics and slab geometry parameters. We assume that all intra-plate deformation is localized in the back-arc deformation rate, V_B (positive for extension), and all velocities are trench-normal components. Plate (V_P), trench (V_T, positive for rollback) and overriding plate (V_{OP}, positive toward the trench) velocities are all computed in an absolute reference frame. The convergence rate at the trench, V_C, is given by $V_P + V_{OP}$ with this sign convention, and the sinking velocity of the slab, V_S, is partitioned between V_P and V_T. (We assume $V_T = V_{OP} + V_B$, so $V_S = V_P + V_{OP} + V_B$).We also indicate the width of the slab and plate, h, and the approximate bending radius at the trench, R, as well as the slab dip angle, δ. For more elaborate dip angle descriptions, see Jarrard (1986) and Lallemand et al. (2005)

Faccenna et al. (2007)

Trench rollback as f(ref frame)

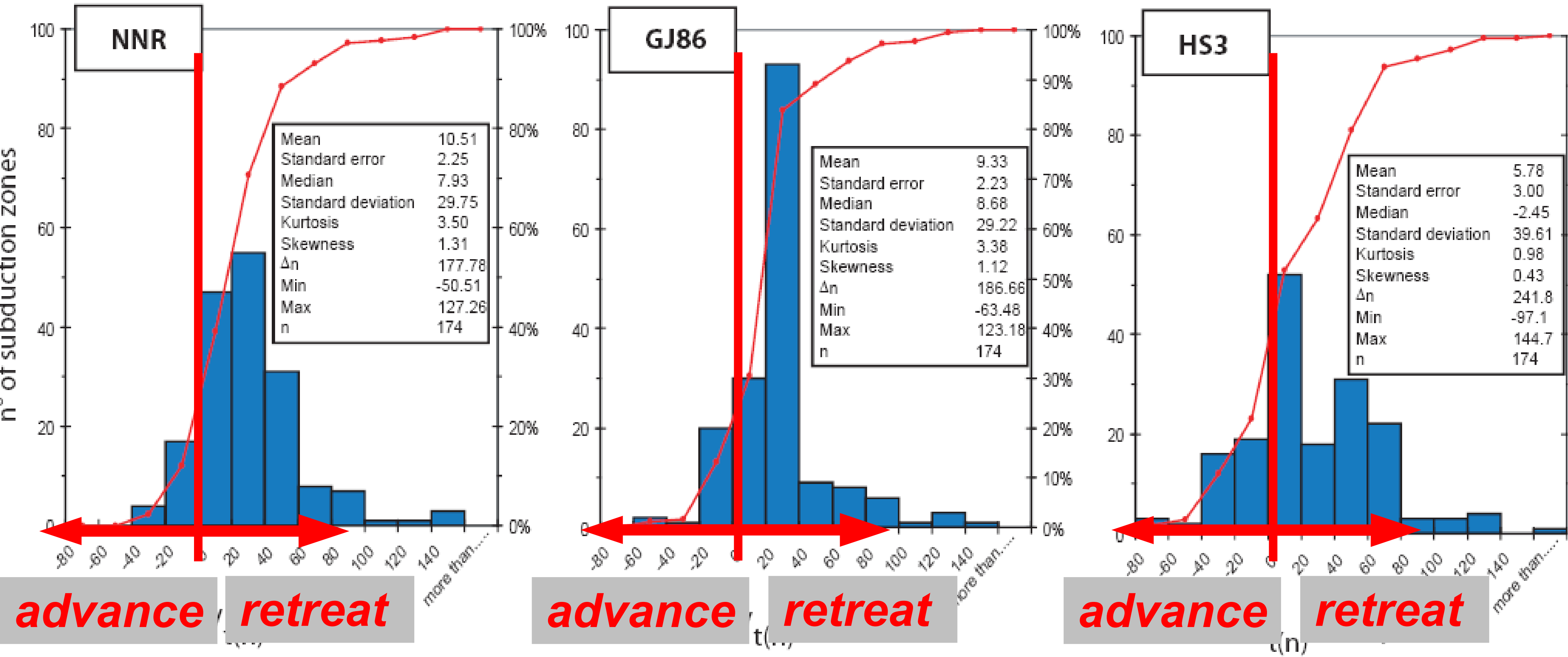

- Most (but probably not all) trenches retreat away from the overriding plate

Funiciello et al. (2008)

V_p – V_t scaling in nature as f(ref. frame)

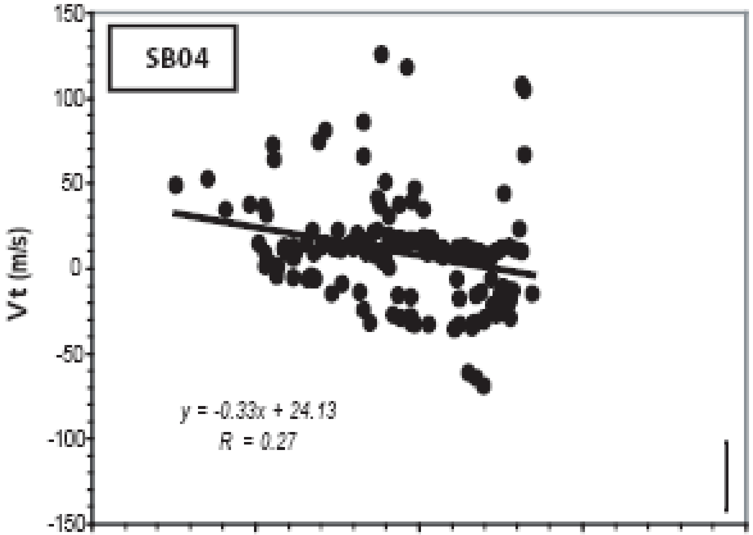

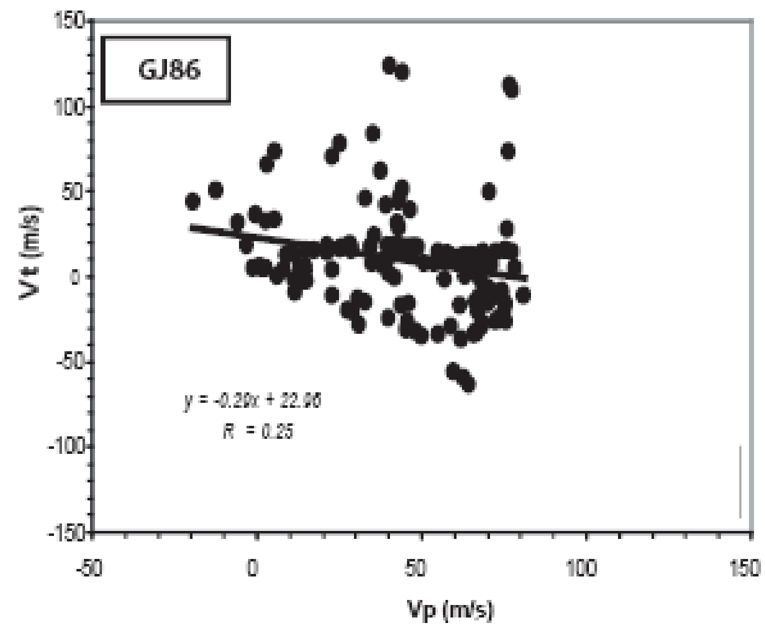

Funiciello et al. (2008)

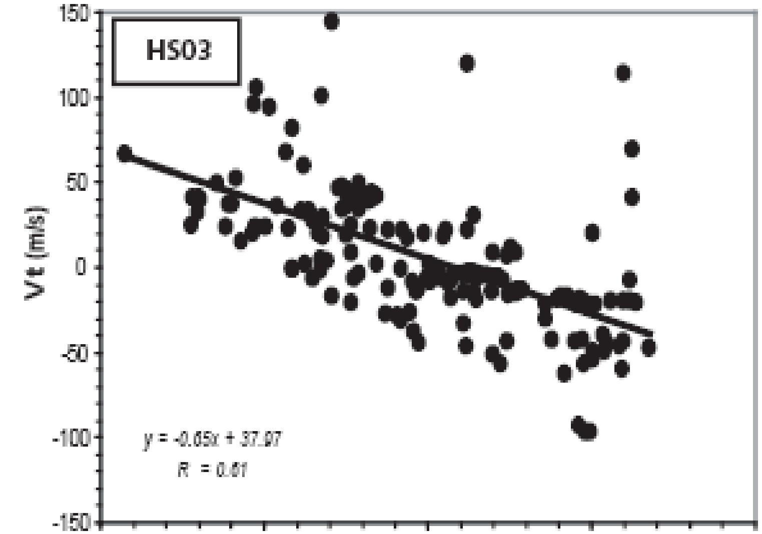

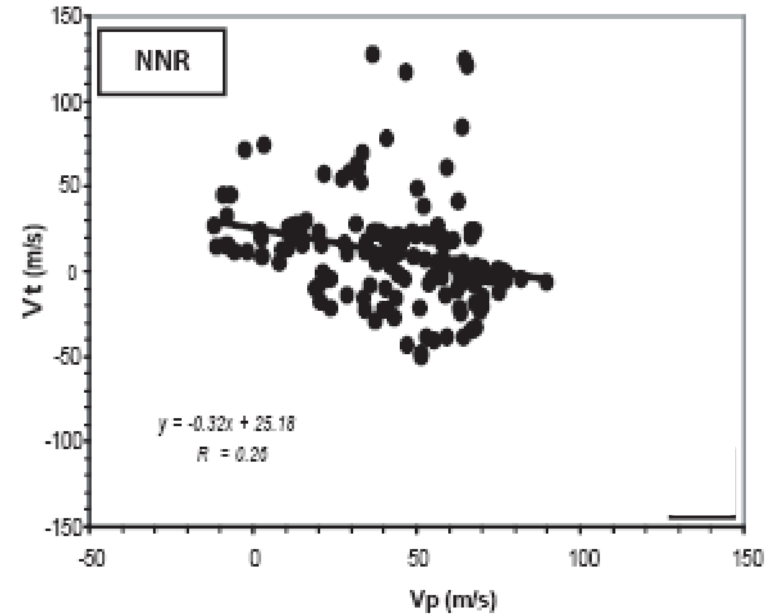

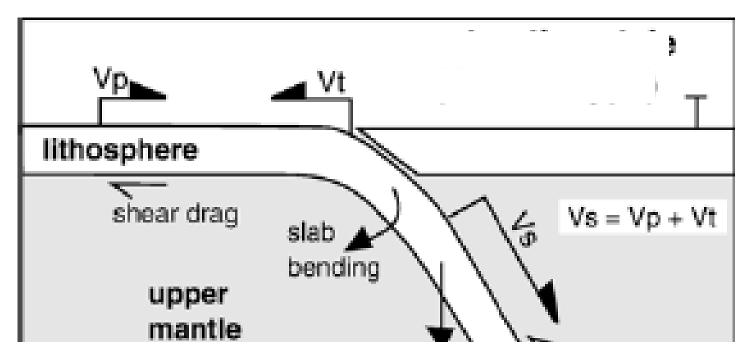

Fig.12 Laboratory model behavior for free ridge models with different slab/mantle ratios η′ and normalized subduction velocities (V' of eq. 7, divided by a normalized Stokes velocity to remove the effect of buoyancy changes at constant mantle viscosity). Models are from Bellahsen et al. (2005), Funiciello et al. (2008) (diamonds), and Schellart (2004b) (circles). Dashed lines are approximate divisions of model behavior; figure is modified from Funiciello et al. (2008)

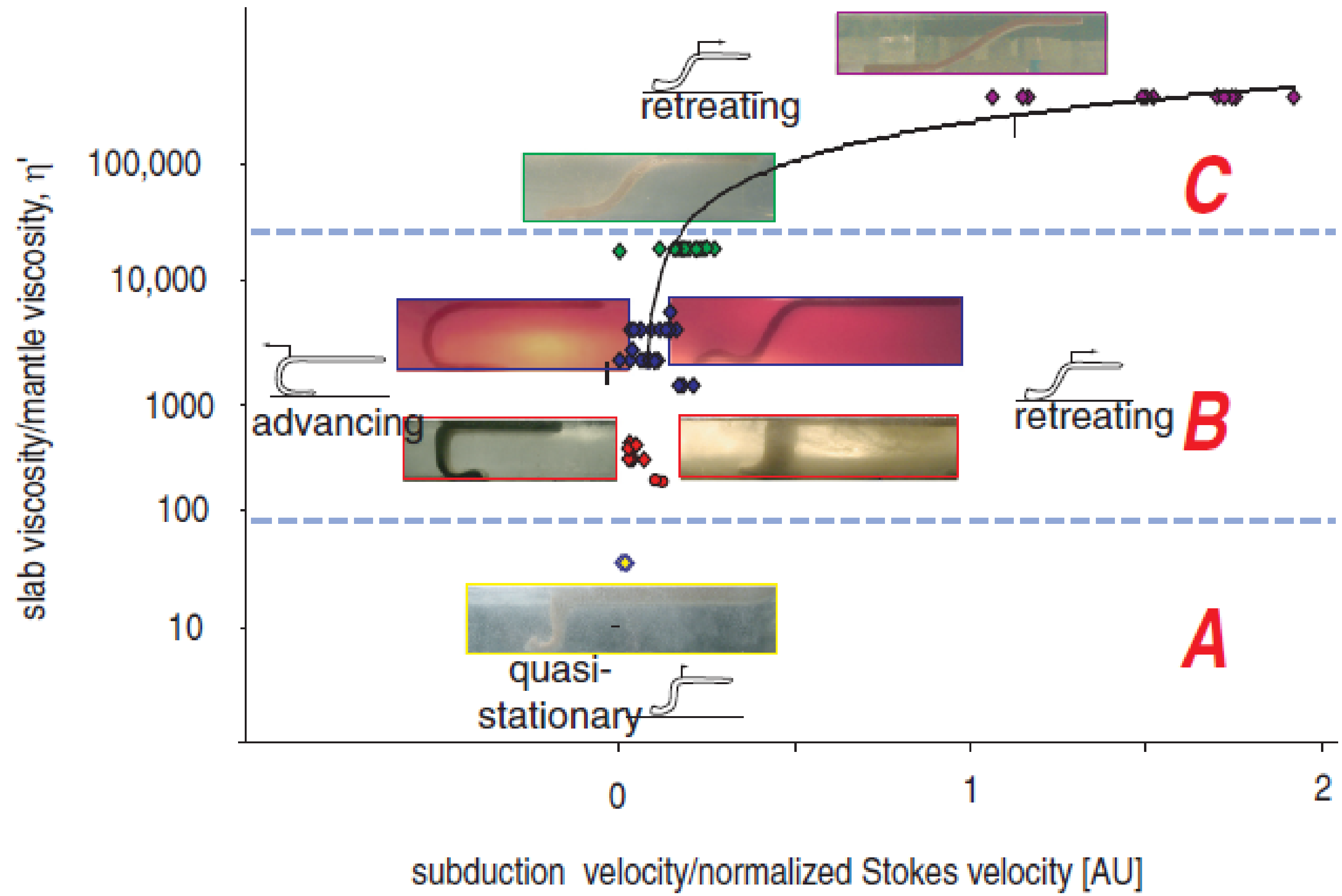

Funiciello et al. (2008)

$V_p - V_t$ scaling in the lab as f(slab viscosity)

Funiciello et al. (2008)

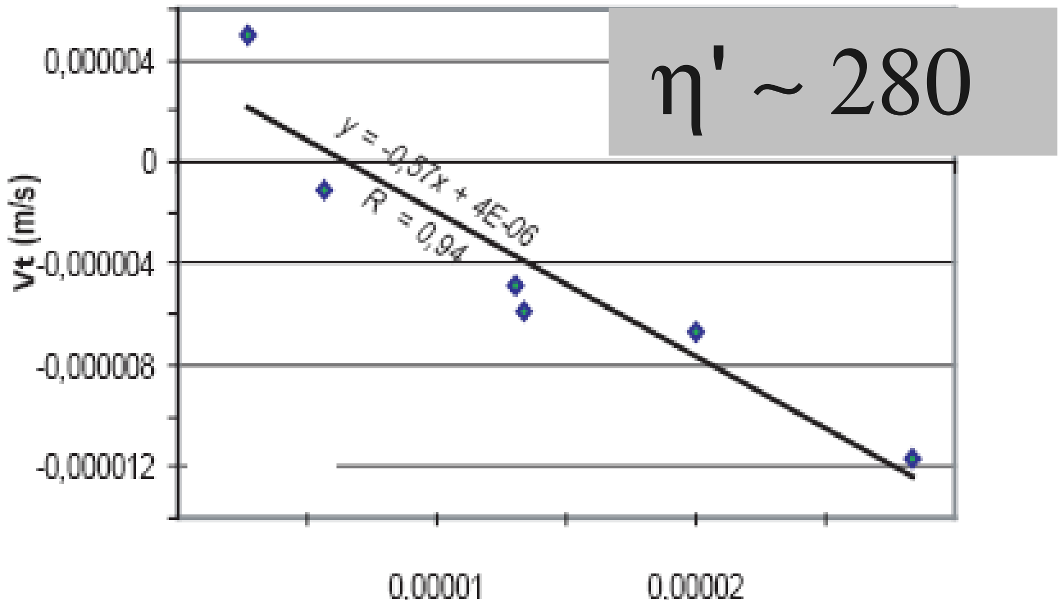

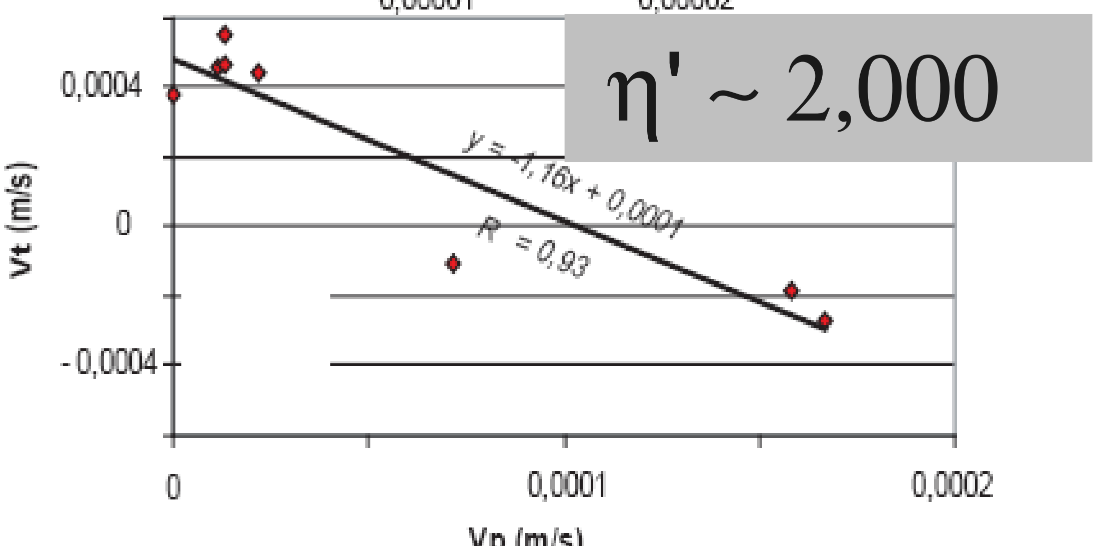

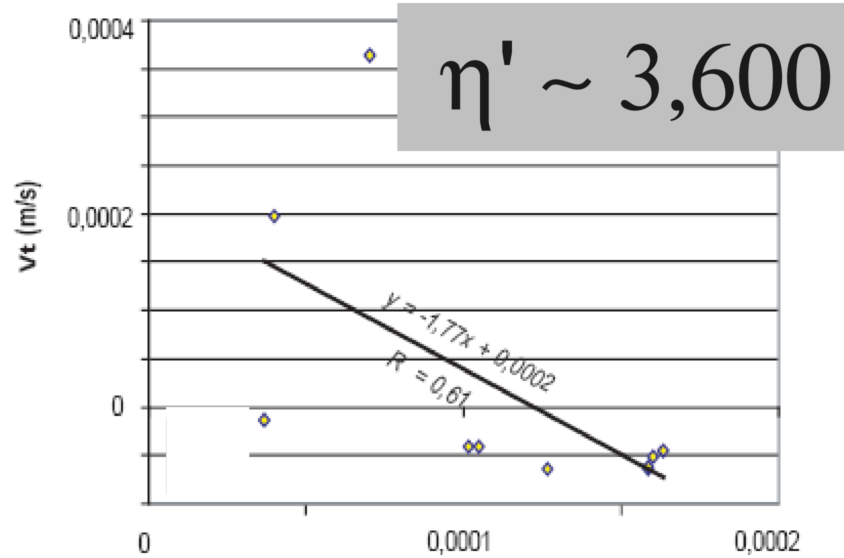

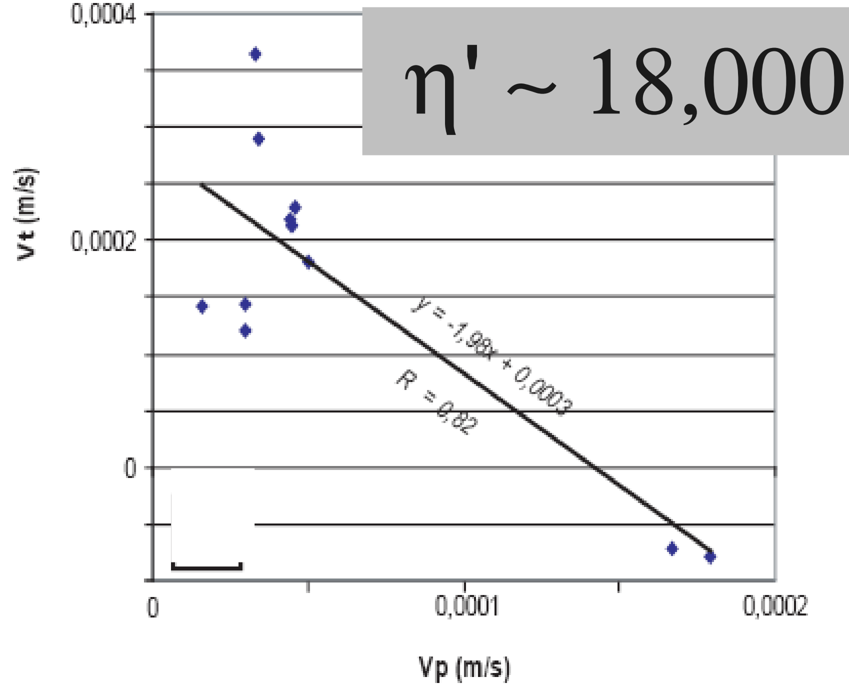

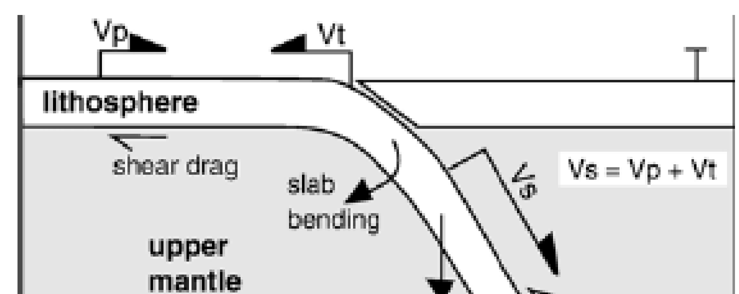

Let's turn it around

- Assume free slab, fluid experiments are meaningful models for the Earth
- Assume that subduction velocity (balance of slab pull, bending and viscous drag) is useful
- Assume $V_p \sim 1/V_T$ relationship holds as $f(\eta')$
- Assume that net rotation of the lithosphere is at least partially related to regional slab dynamics

Let's turn it around

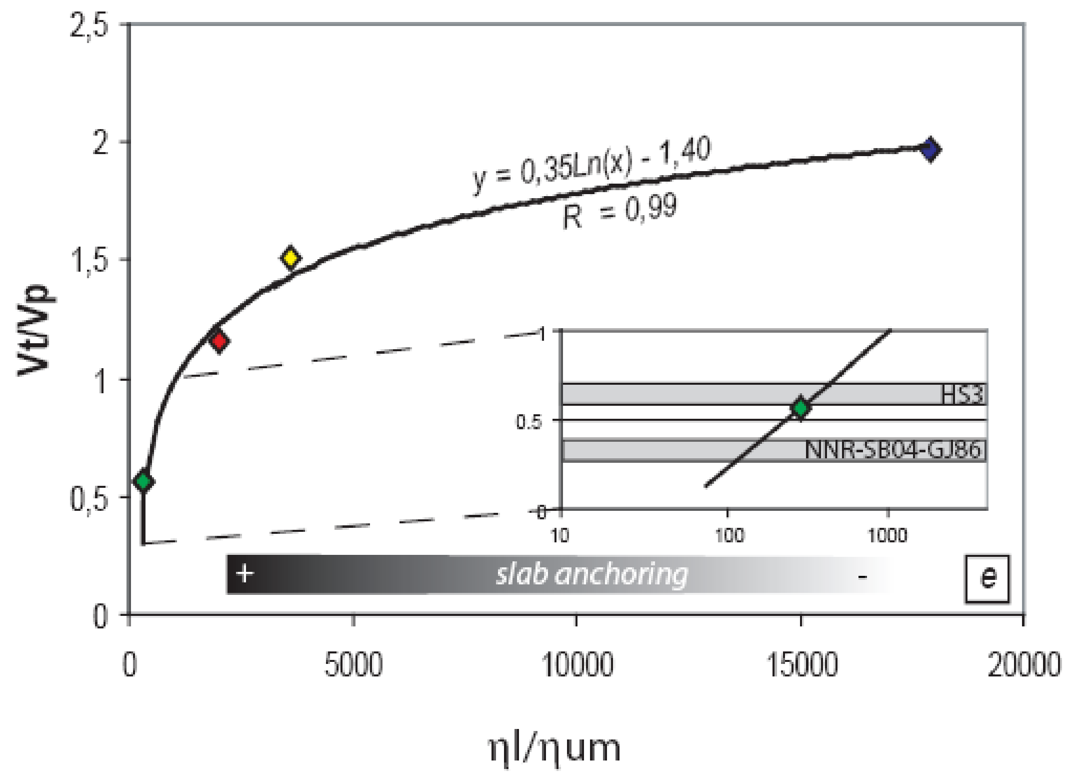

Funiciello et al. (2008)

- Range of best-fit scaling for $V_T \sim 1/V_P$ corresponds to viscosity ratios η' of ~ 150 ... 350
- This is borderline in the advancing/retreating regime (or maybe not, according to Ribe, 2010)

Seismic anisotropy

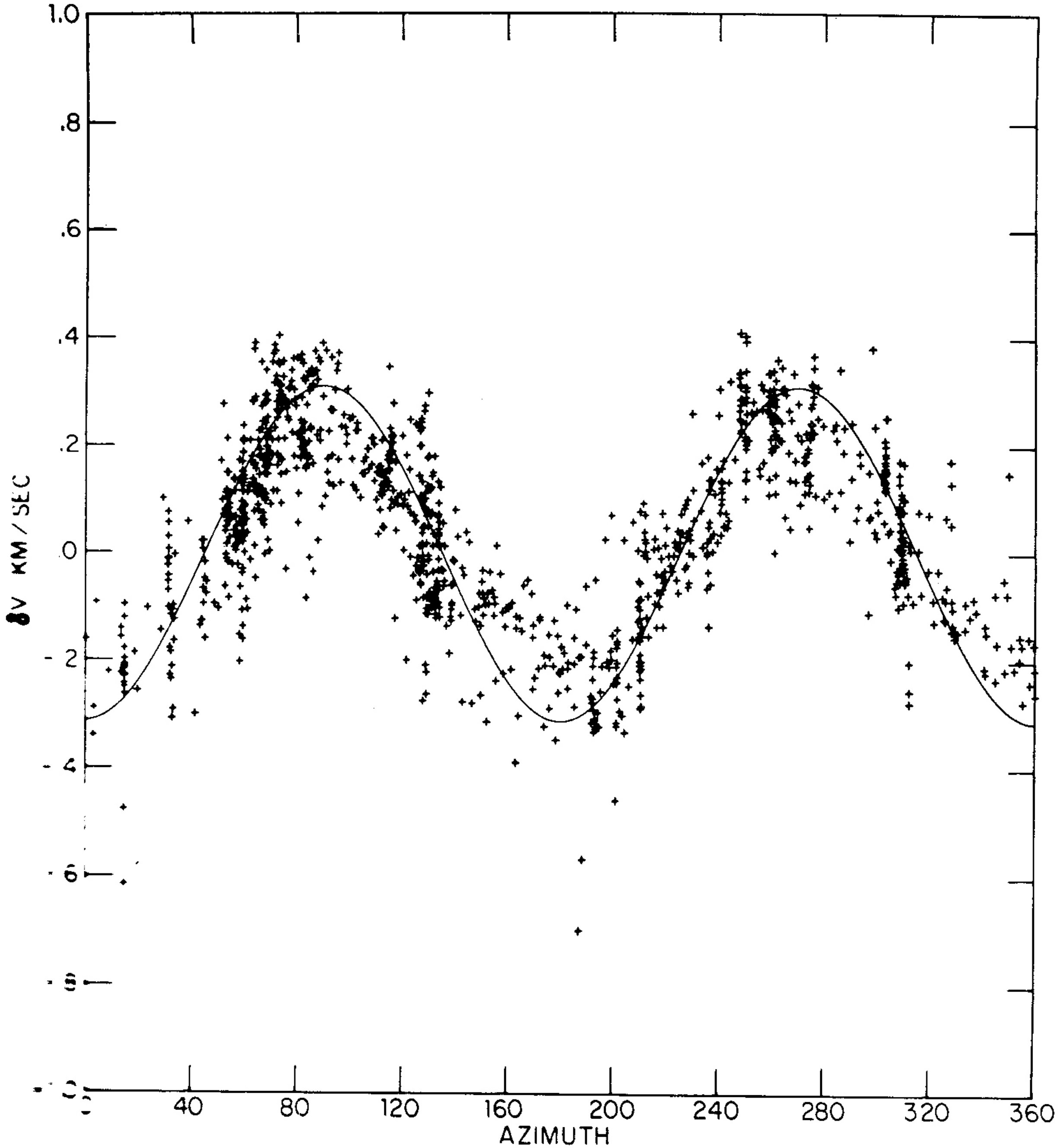

FIGURE 3-1
Combined data from Hawaii region showing velocity anisotropy given as deviations from the mean velocity of 8.159 km/sec plotted as a function of azimuth. (*From Morris, Raitt, and Shor*, 1969, *with permission. Copyright American Geophysical Union.*)

Shear wave splitting

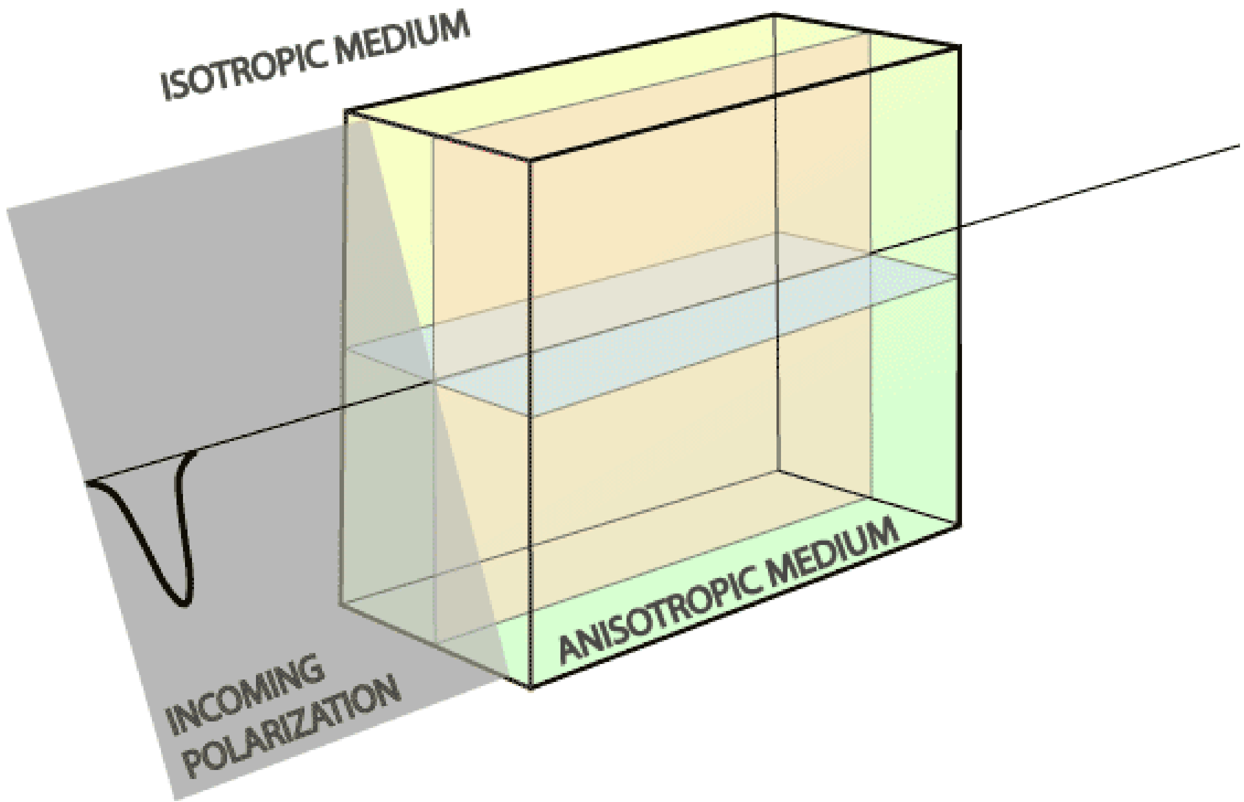

garnero.asu.edu

Shear wave splitting in anisotropic media

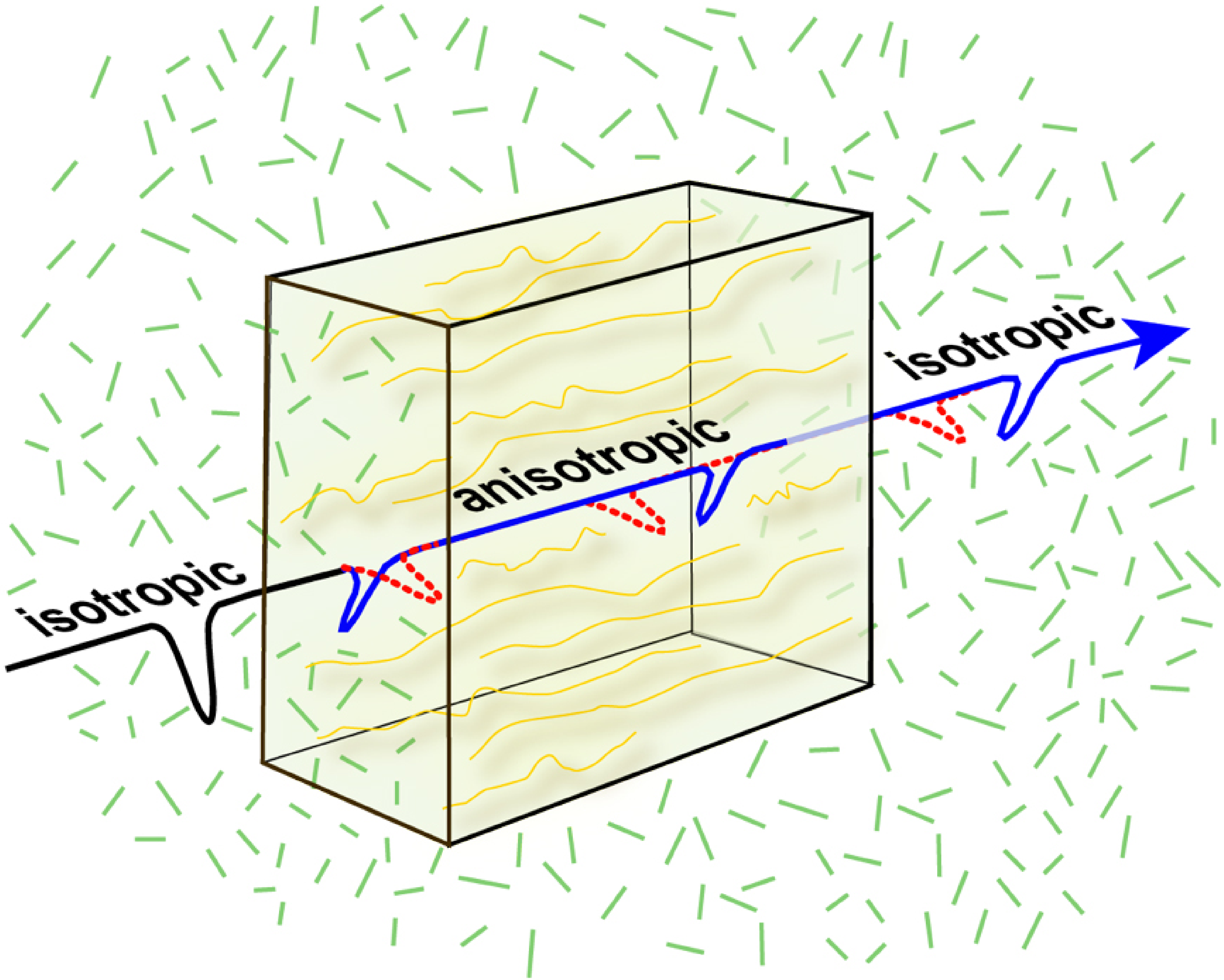

garnero.asu.edu

(After Crampin, 1981)

Causes of seismic anisotropy

Predicted elastic anisotropy

- individual minerals
- aggregates: lattice preferred orientation (LPO)
  - build up by dislocation creep
    - lines up with flow (most of the time)

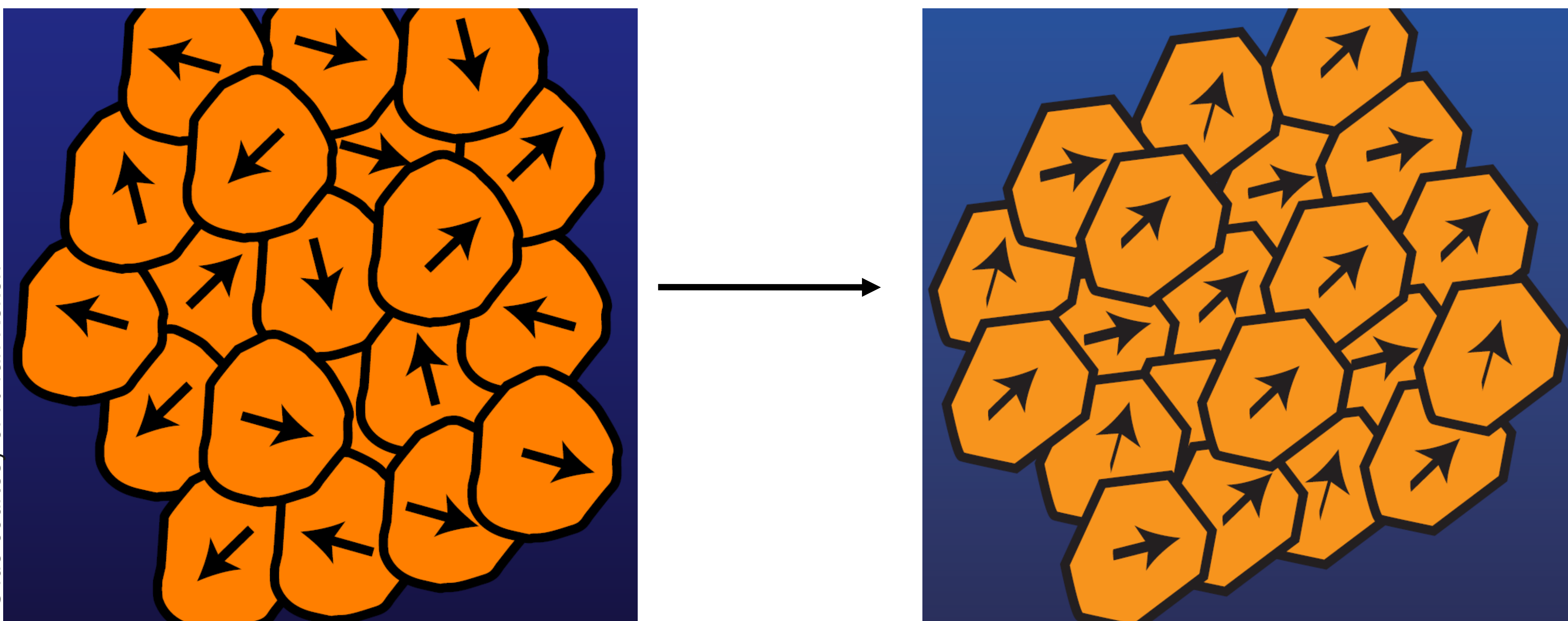

Slide courtesy of P. van Keken

Effect of water/stress

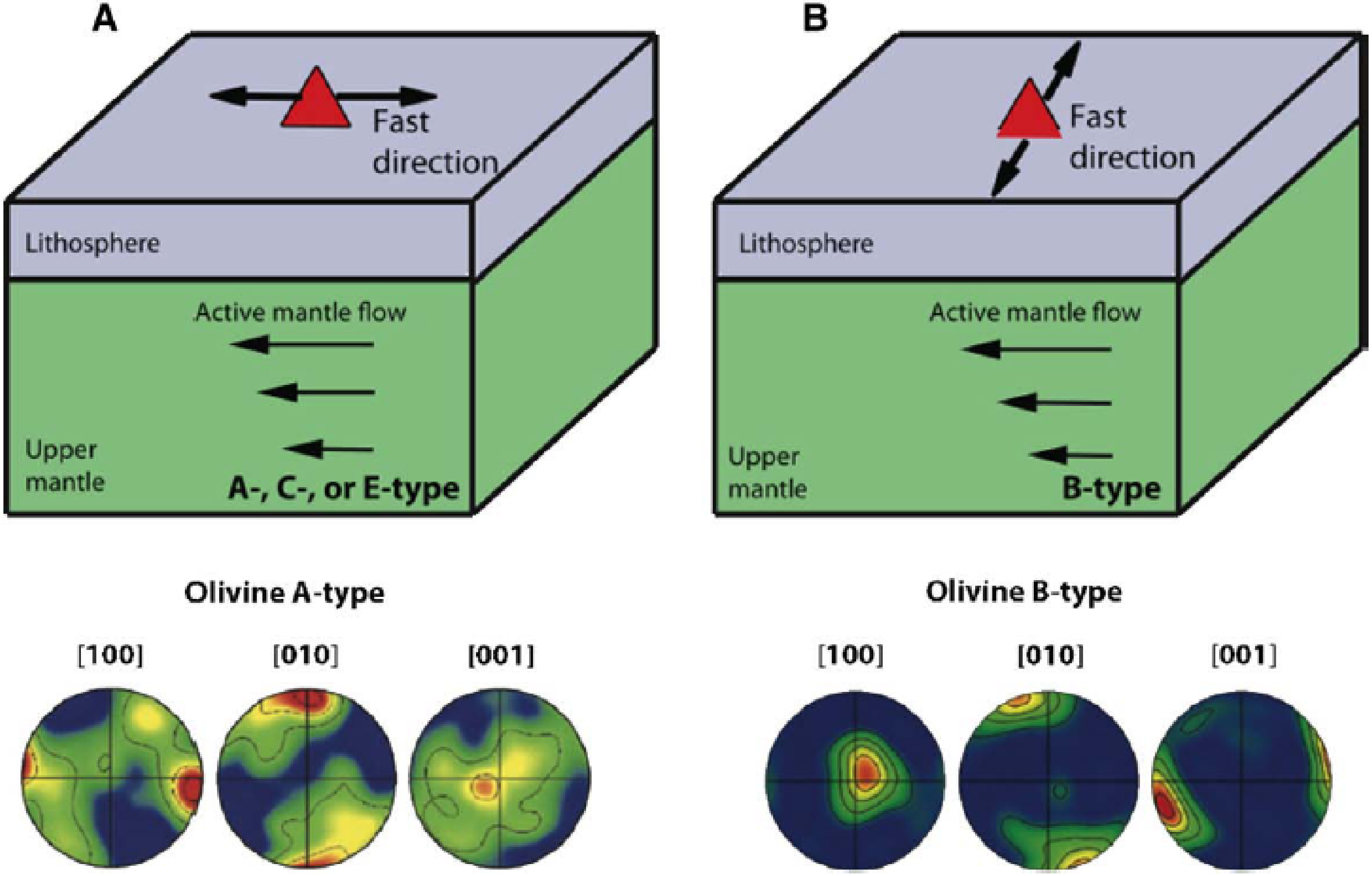

Long and Becker (2010)

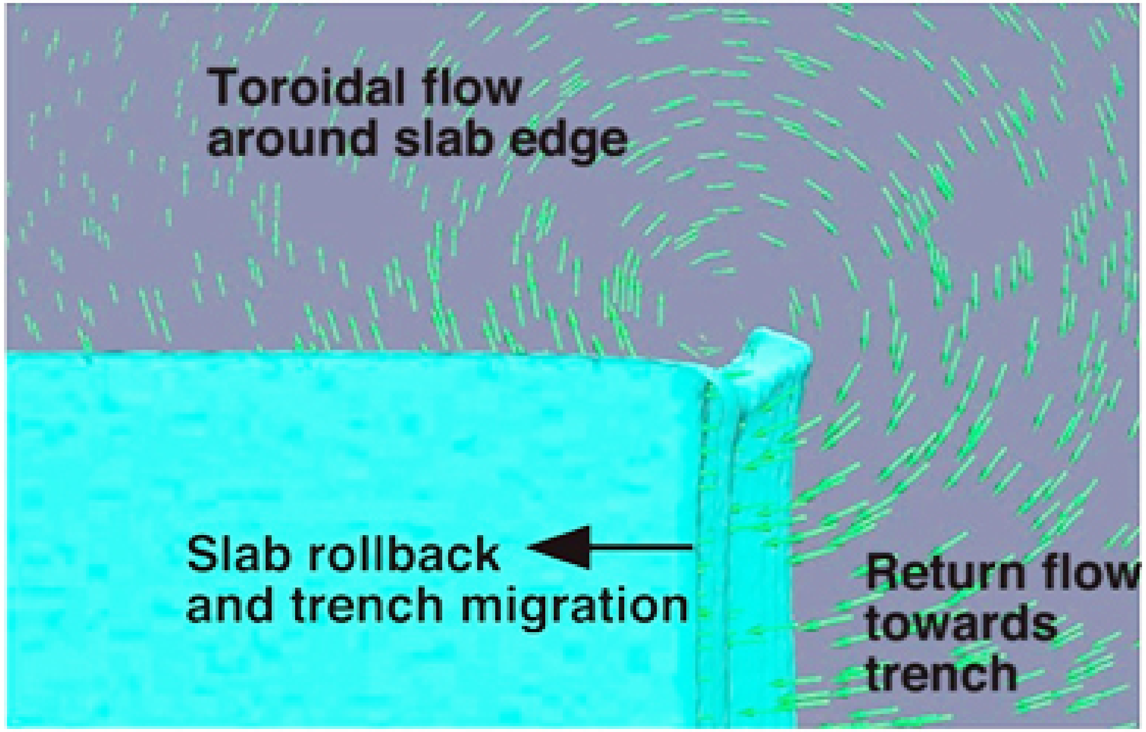

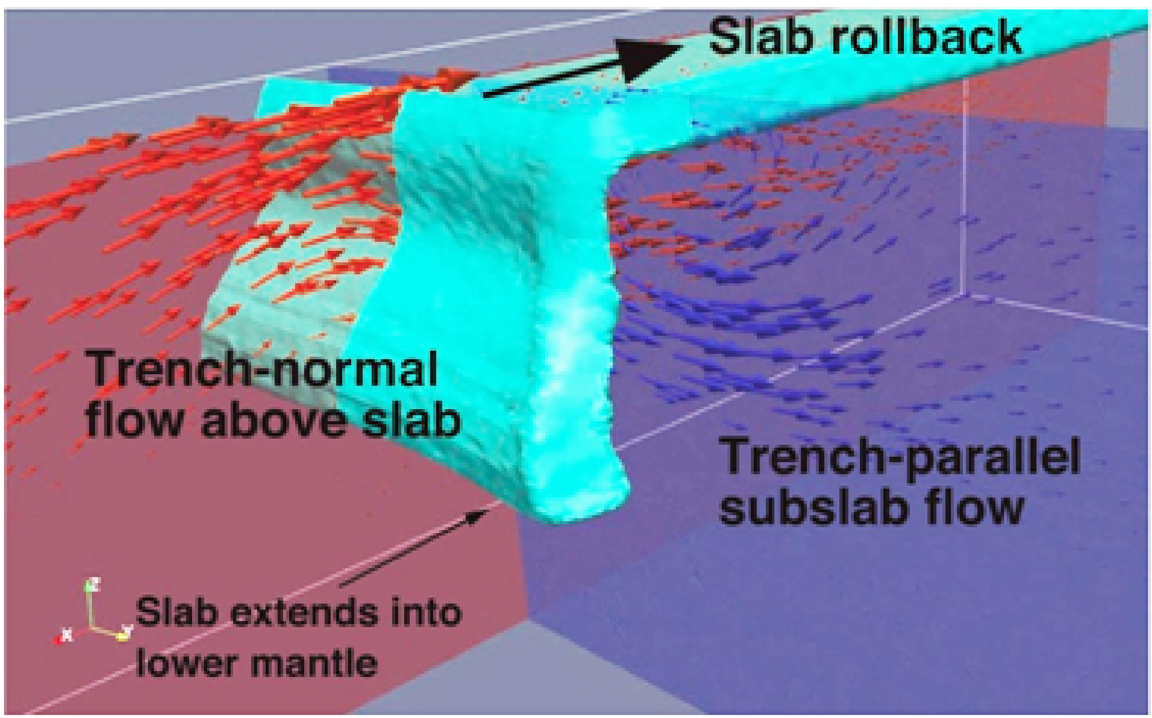

Long and Becker (2010)
See also Buttles and Olson,
EPSL, 1998

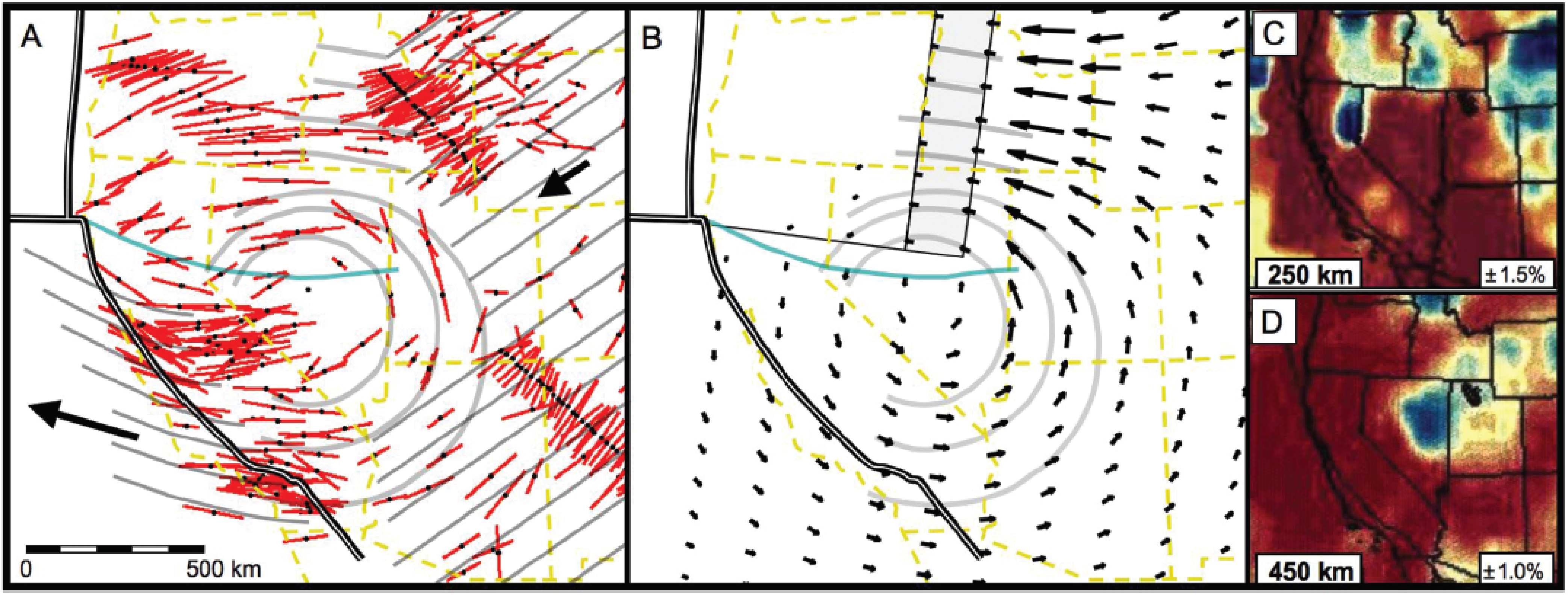

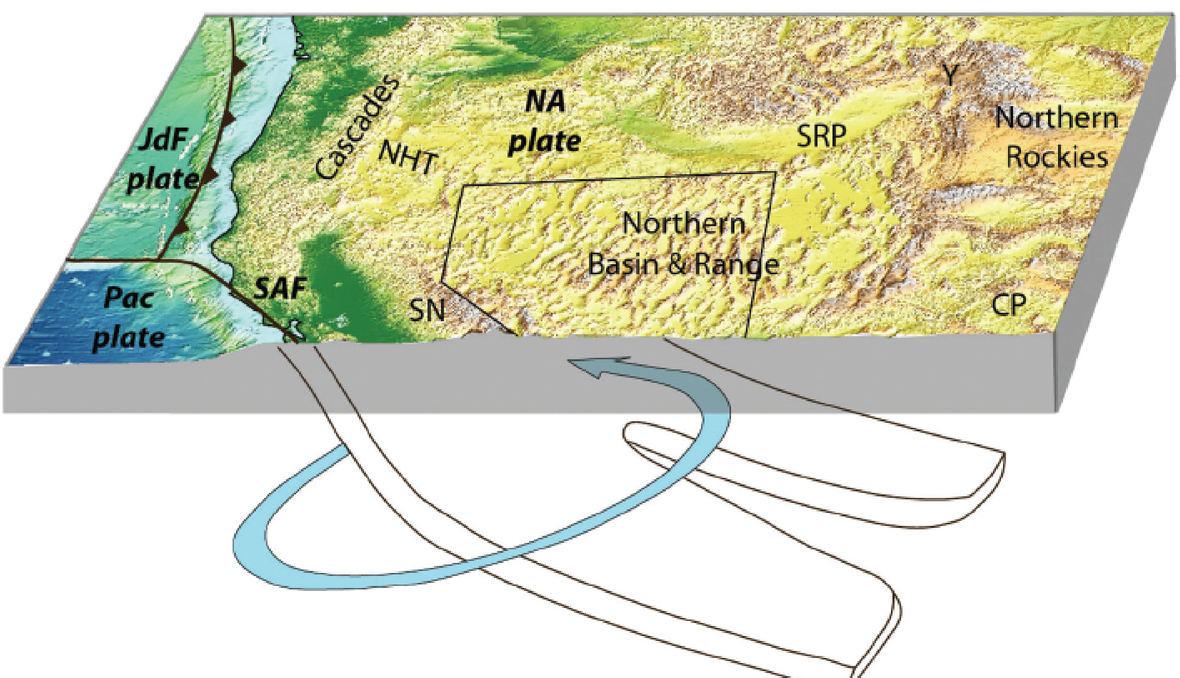

Zandt & Humphreys (2008)

SZ Anisotropy

Spreading Center Anisotropy

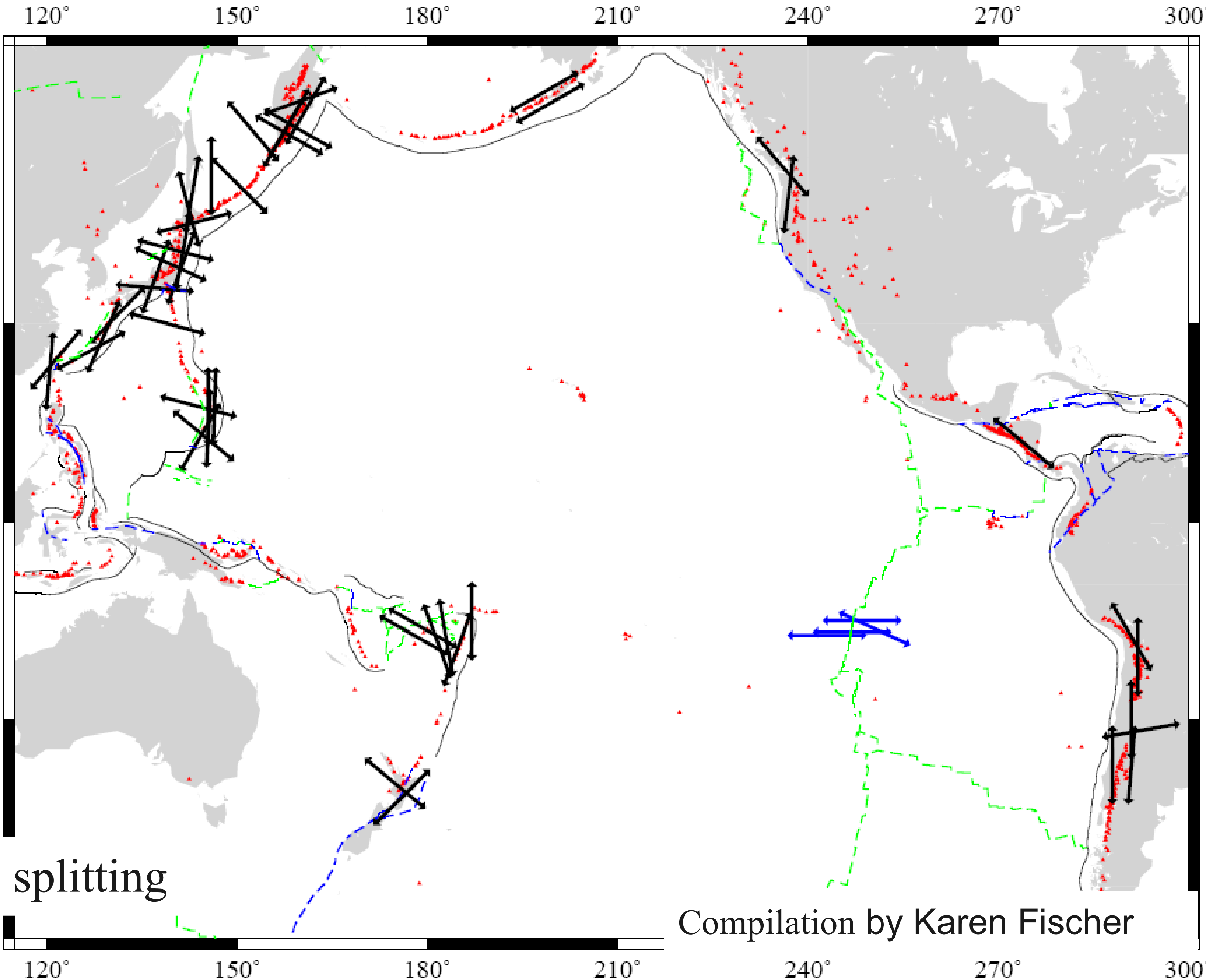

S wave splitting

Compilation by Karen Fischer

Slide courtesy of P. van Keken

teleseismic

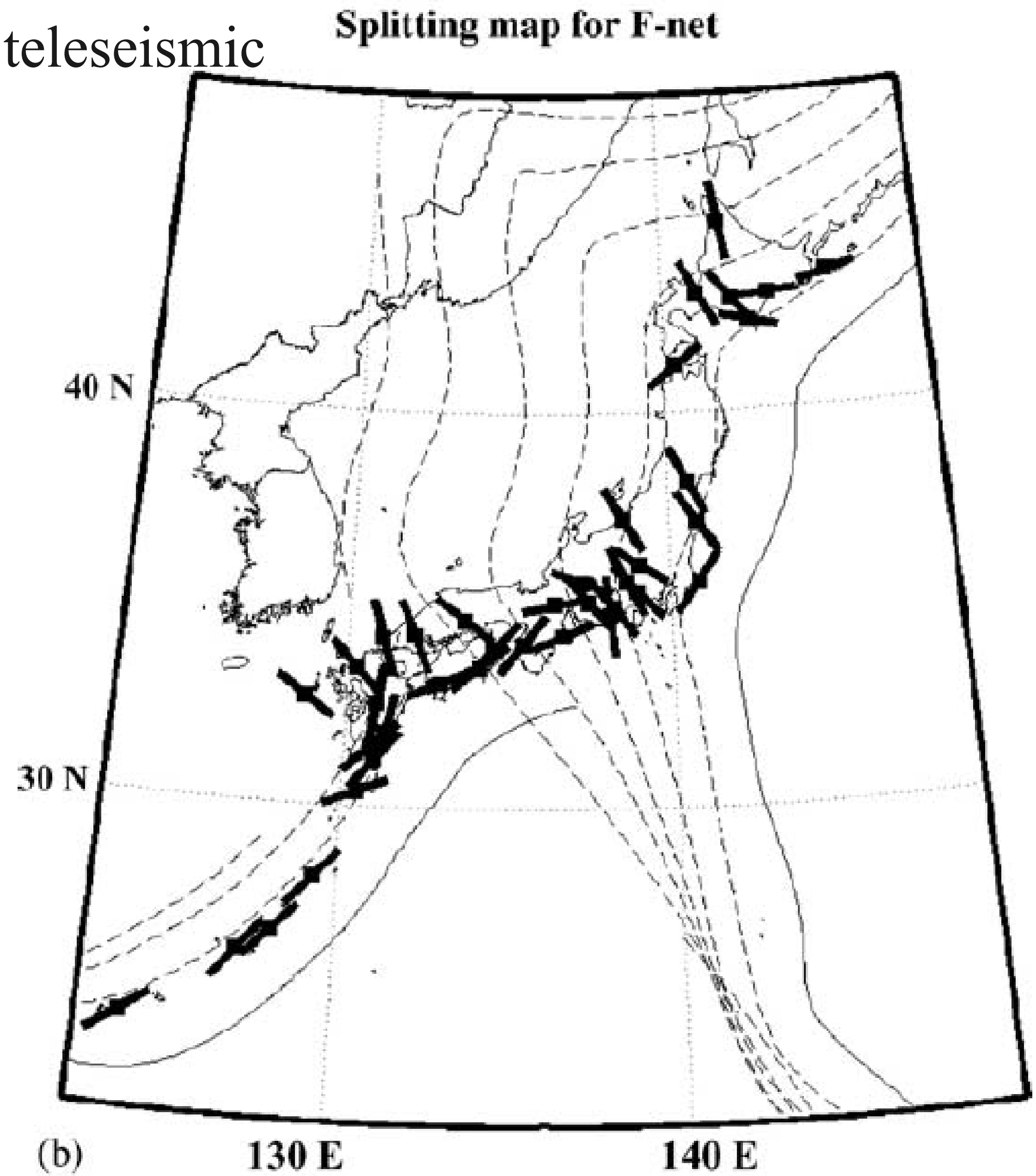

Long and van der Hilst, PEPI, 2005

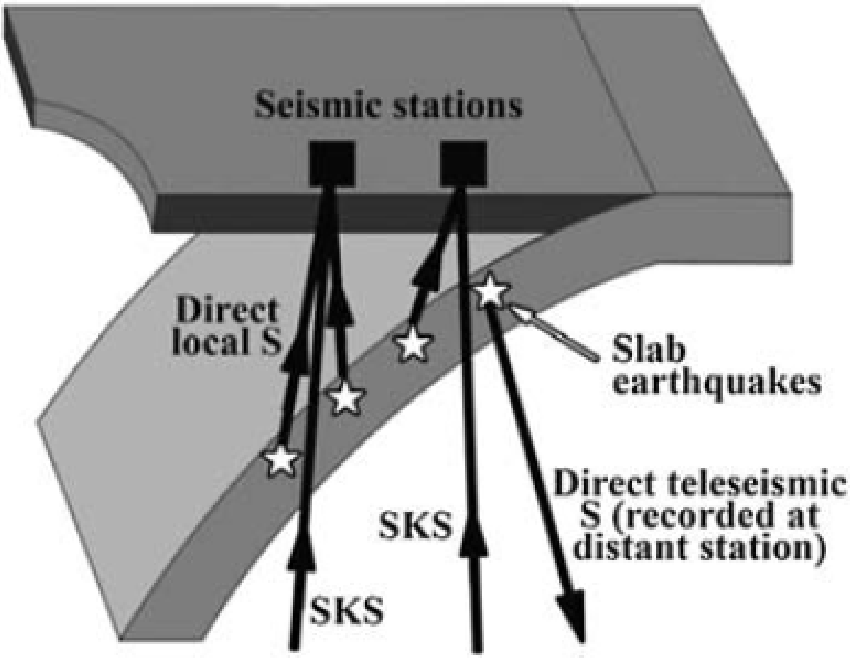

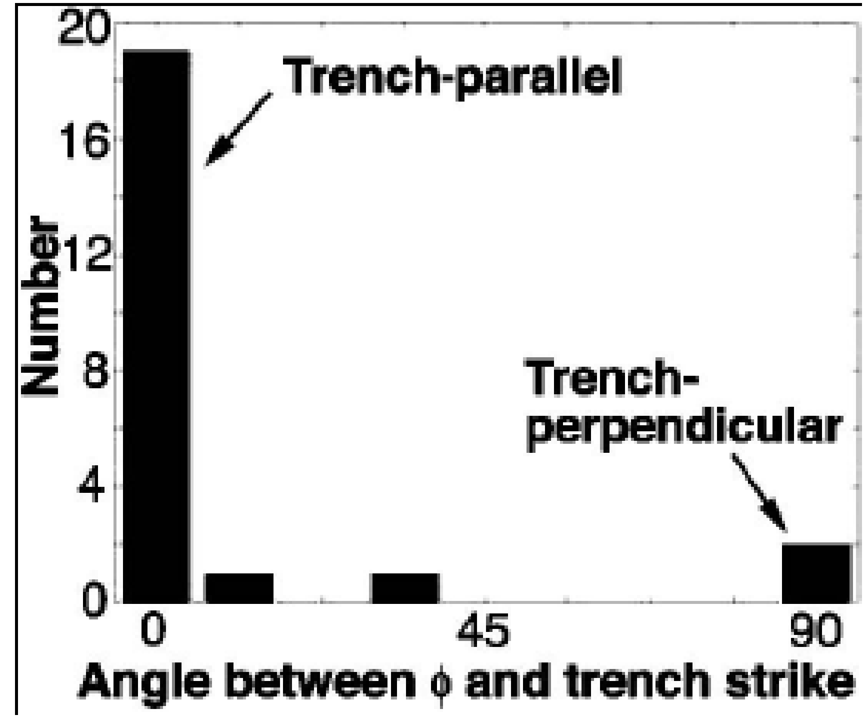

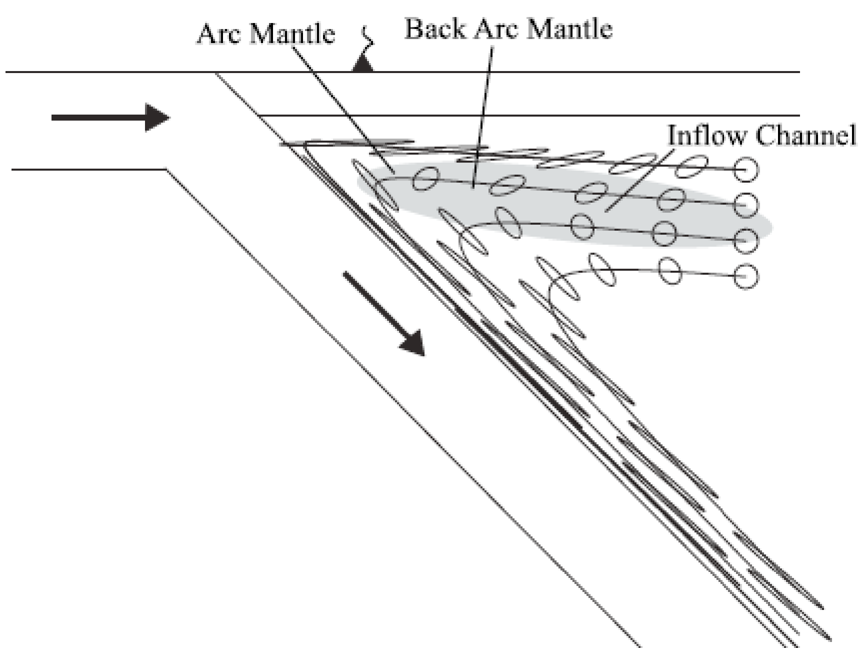

Long and Silver, JGR, 2009

Along-arc flow

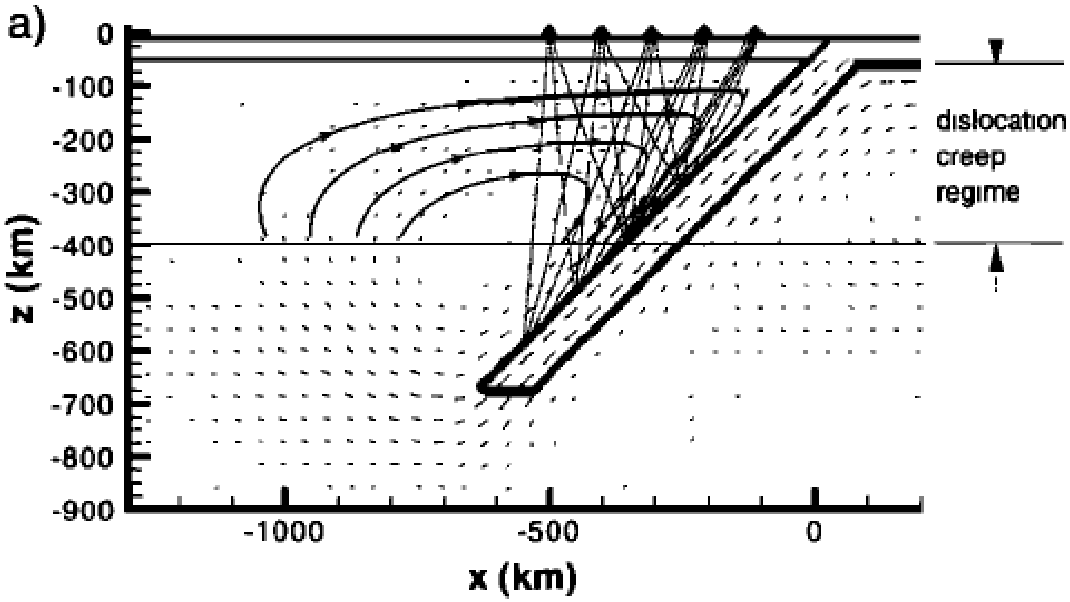

- Flow -> FSE -> LPO
- LPO -> 3D C_{ij}
- C_{ij} -> waveforms
- Waveforms -> split

0 cm/yr

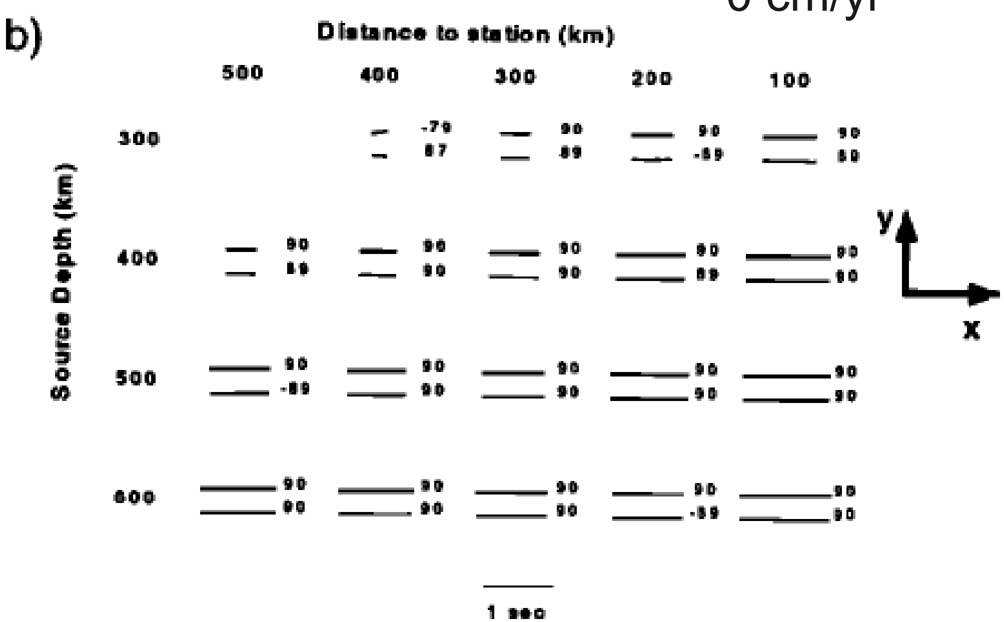

3 cm/yr

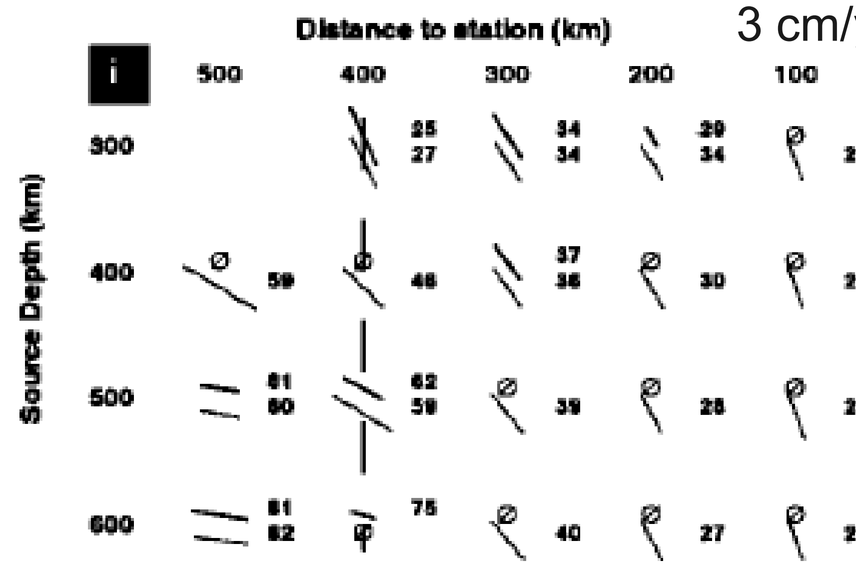

Hall et al. (2000)

Kneller and van Keken, Gcubed, 2007

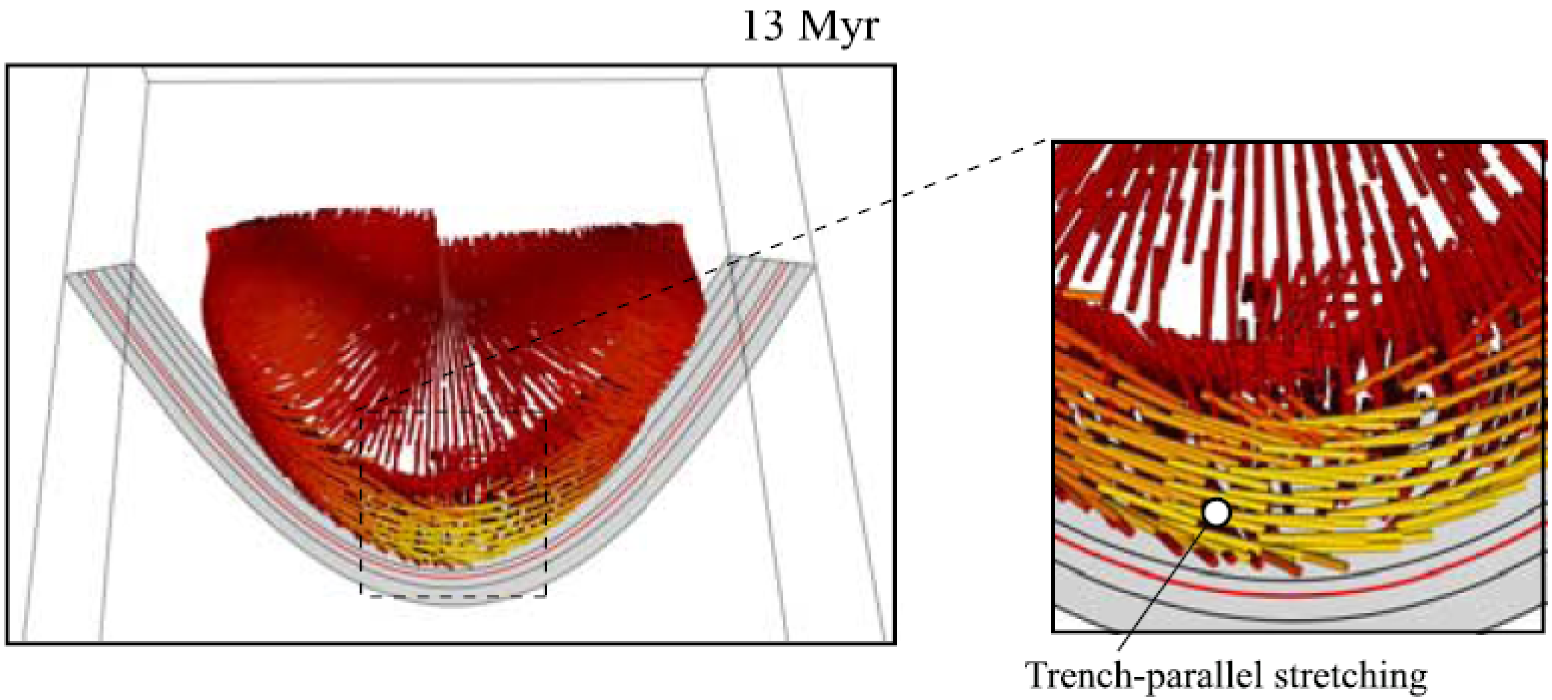

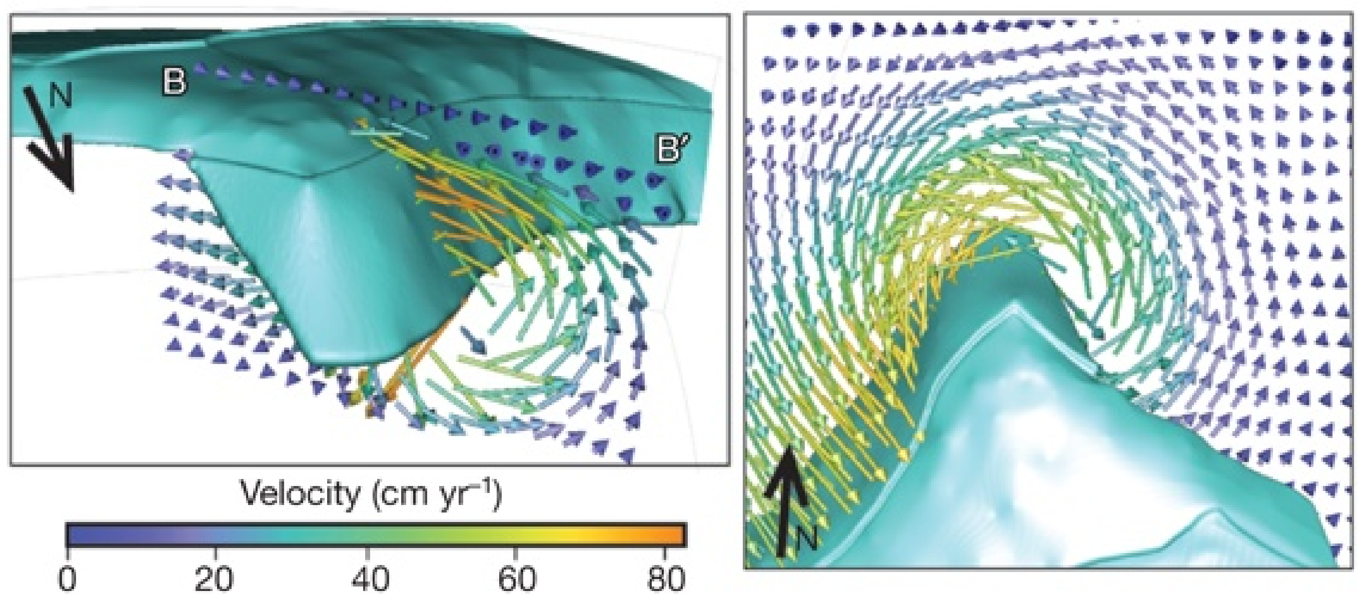

Jadamec and Billen, Nature, 2010

3D flow due to trench geometry (curvature, slab dip changes)

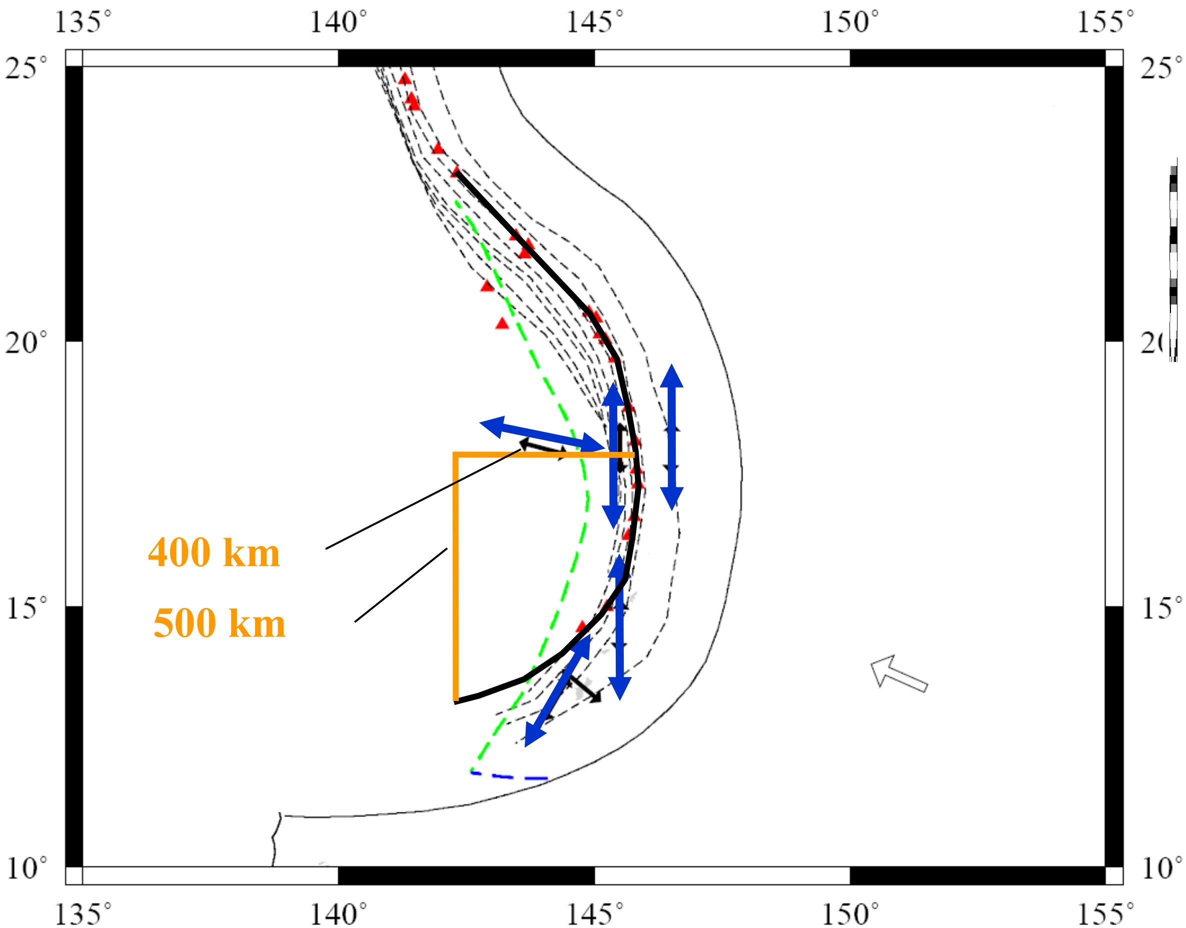

Splitting: Pozgay et al., GJI, 2007

Contours: Syracuse and Abers, G-cubed, 2006

Maximum stretch directions

400 km

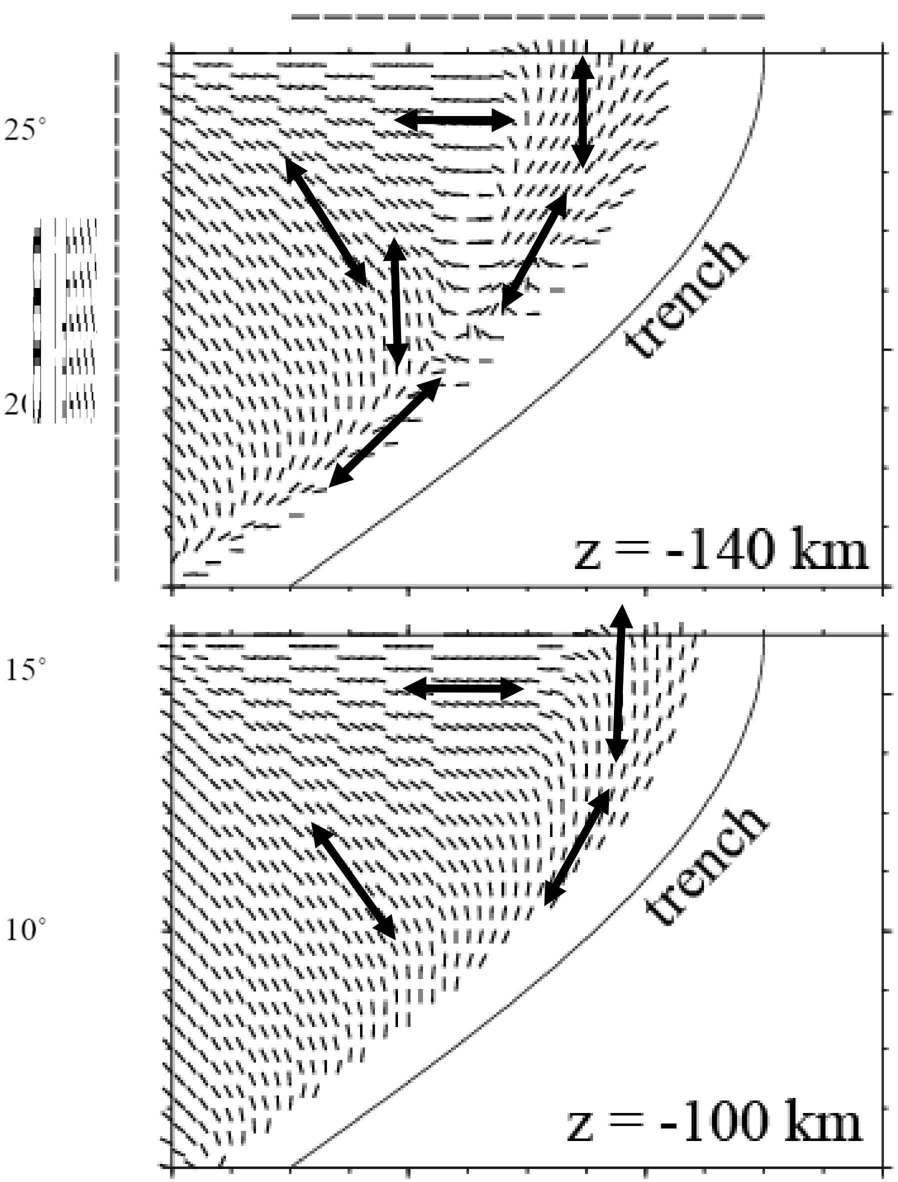

Kneller and van Keken, Nature, 2007

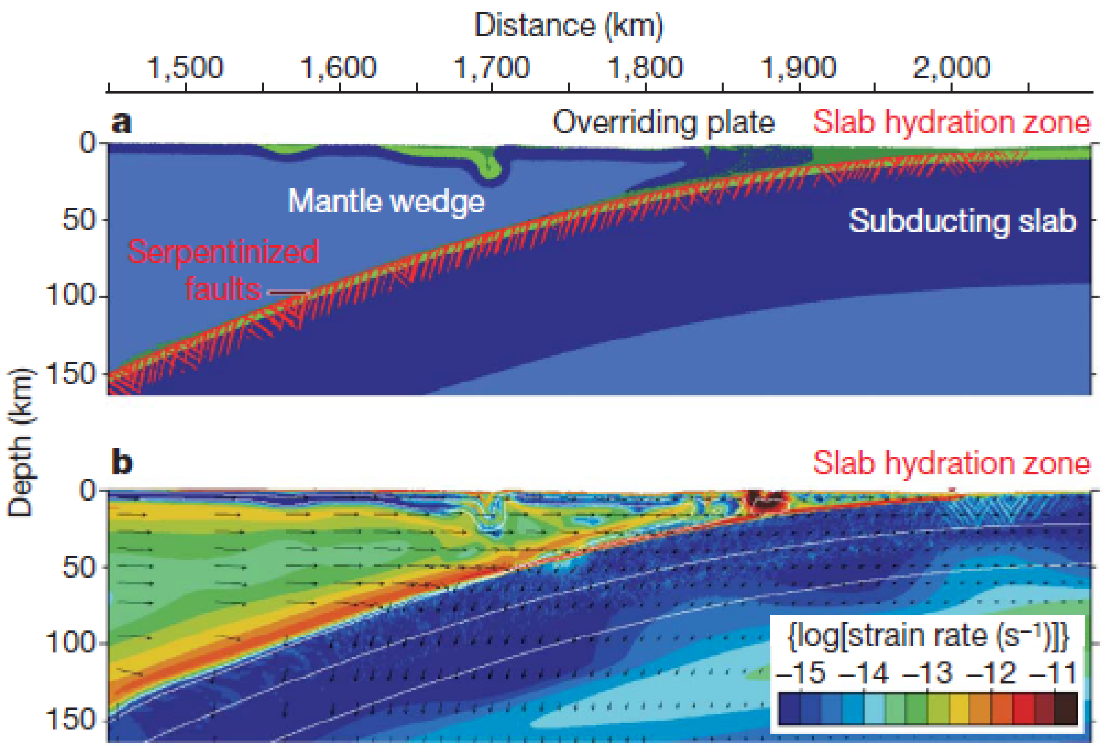

Figure 1 | Thermo-mechanical two-dimensional model of a spontaneously bending oceanic plate. a, Compositional map. Serpentinized faults are trenchward dipping but sets of antithetic and seaward-dipping faults are occasionally visible. Light green is gabbroic oceanic crust; basalt and sediments are shown in dark green. **b,** Strain rate map. Fault activation due to the bending of the plate occurs mainly at the trench in the upper layer of the slab. Arrows indicate the direction of material displacement. White lines are isotherms in °C (see Methods for details of the numerical model).

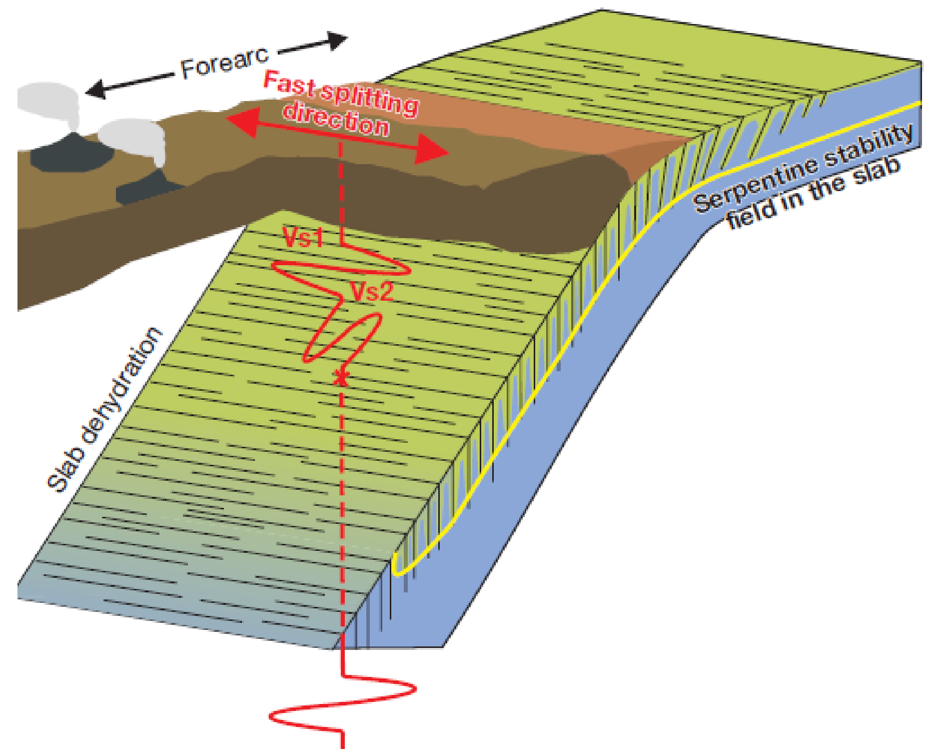

Faccenda et al. (2008)

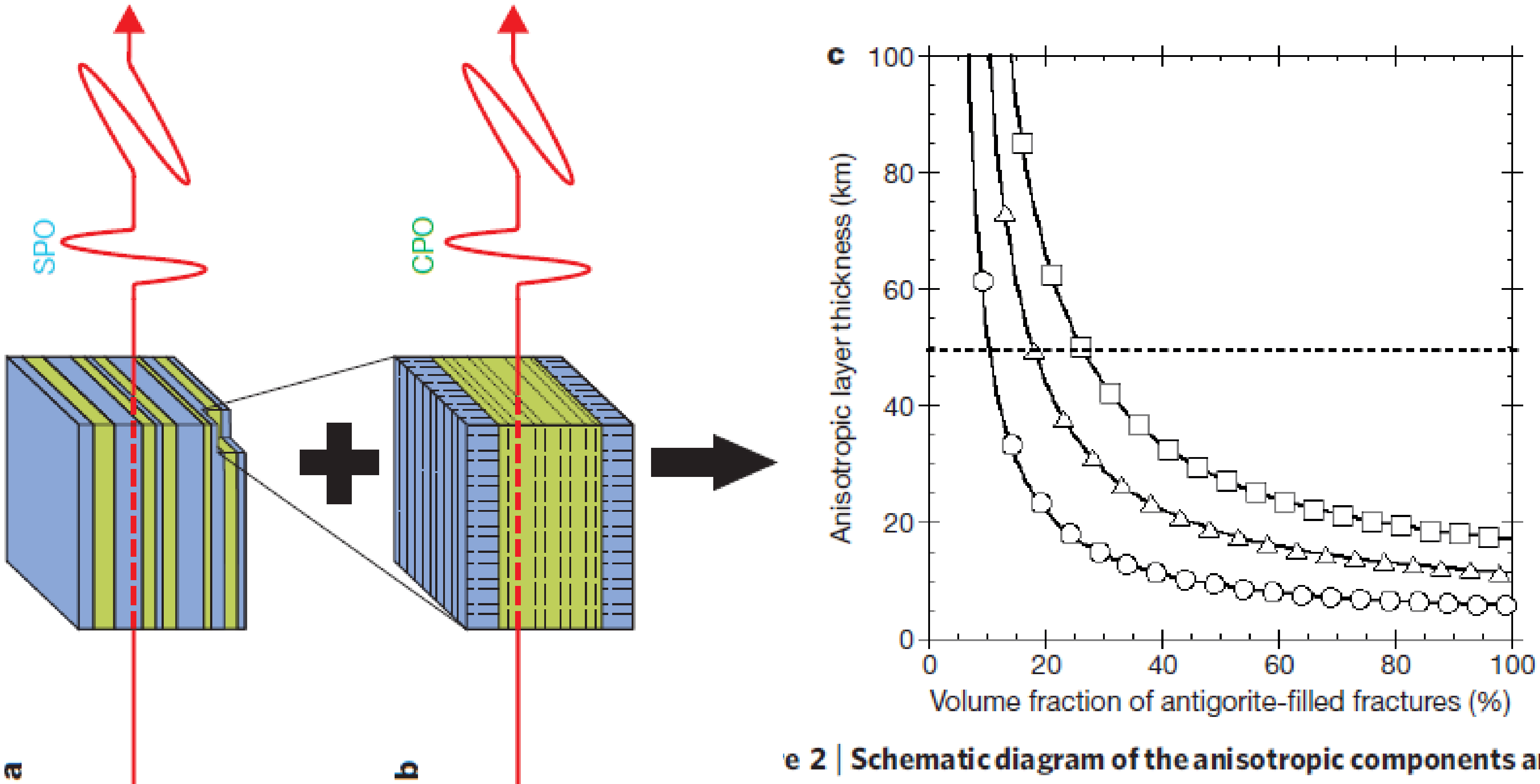

e 2 | **Schematic diagram of the anisotropic components and estimates**
e delay time. a, Thin layering of dry (blue) and hydrated (green) mantle
ons results in an SPO-induced anisotropy for long-wavelength SKS
s. **b,** $CPO_{(hyd-ol)}$ formed by hydrated minerals parallel to the layering in the hydrated mantle and by perpendicular olivine and enstatite grains in the dry mantle (destructive interference). **c,** Contours of delay time for an anisotropic plate dipping at 30° with strong transverse isotropic antigorite, as a function of the volume fraction of antigorite-filled fractures and fault length, with a fracture aspect ratio of 100:1 (see Methods for details of the anisotropy model). Delay times: circles, 0.5 s; triangles, 1.0 s; squares, 1.5 s. The horizontal dashed line indicates a 50-km-thick antigorite layer.

Faccenda et al. (2008)

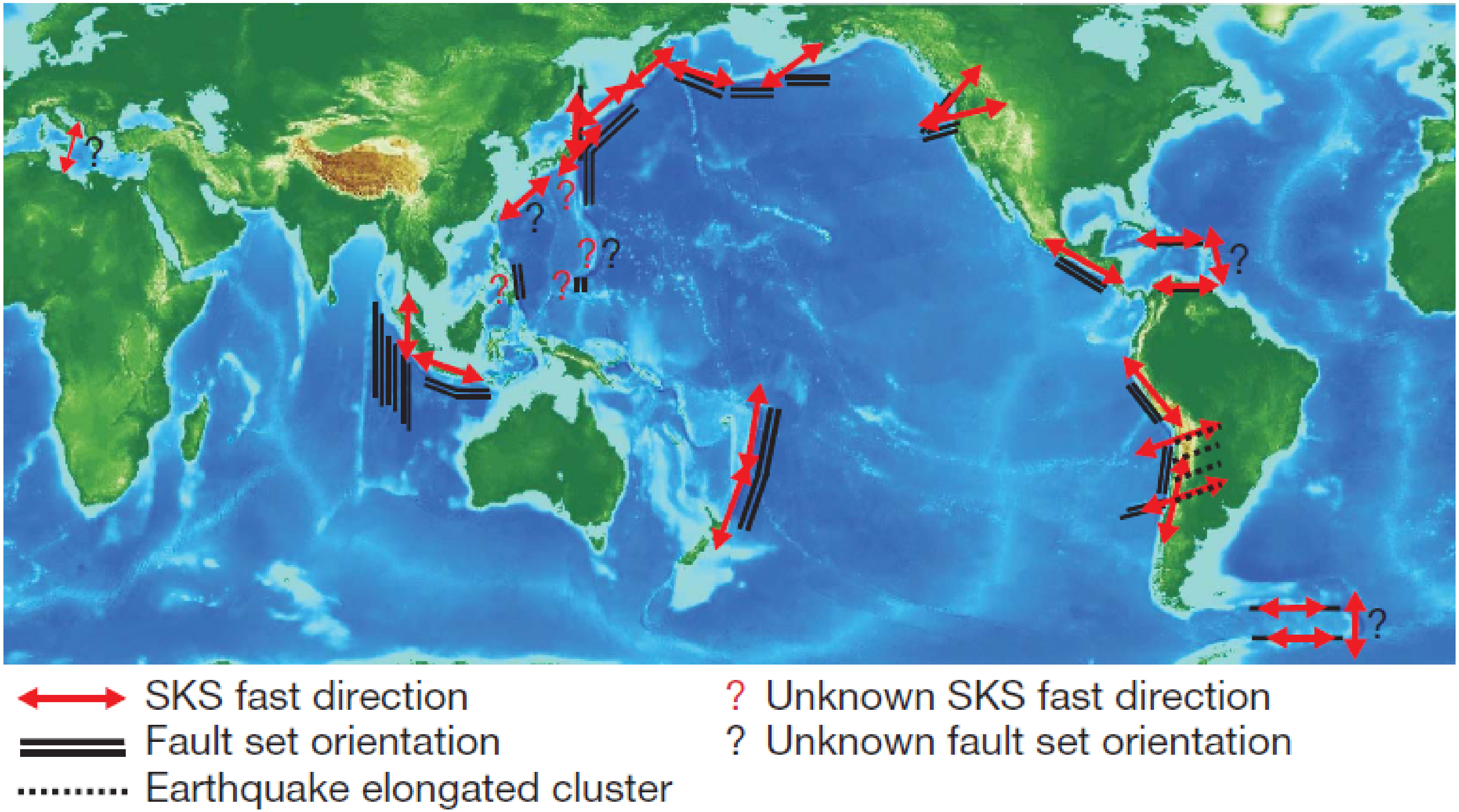

Figure 4 | Summary of SKS fast directions and fault set orientations. Question marks indicate that no data are available. See Methods for data sources.

Faccenda et al. (2008)

Hypotheses for formation of trench parallel anisotropy

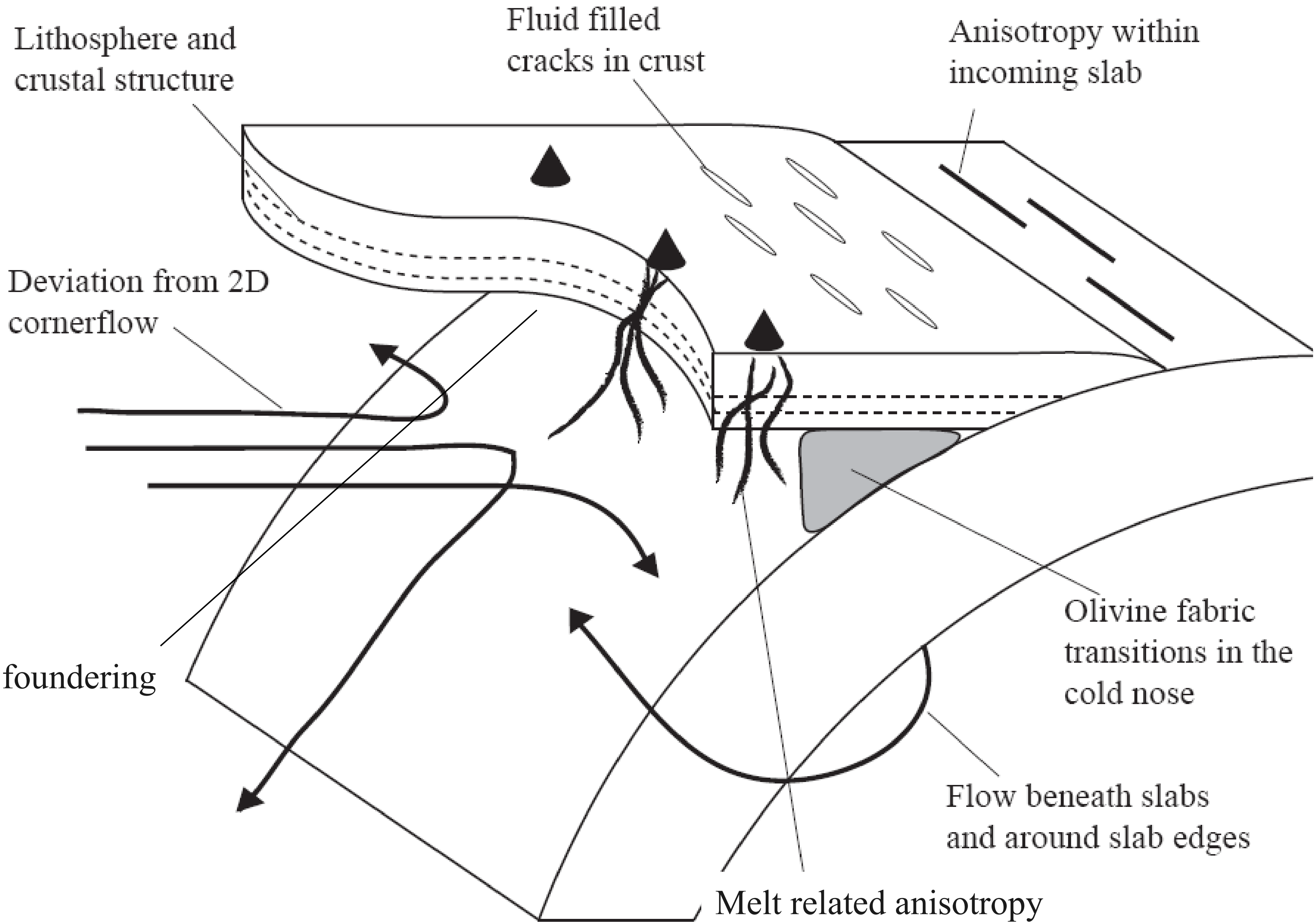

Slide courtesy of P. van Keken

The sub-slab splitting signal

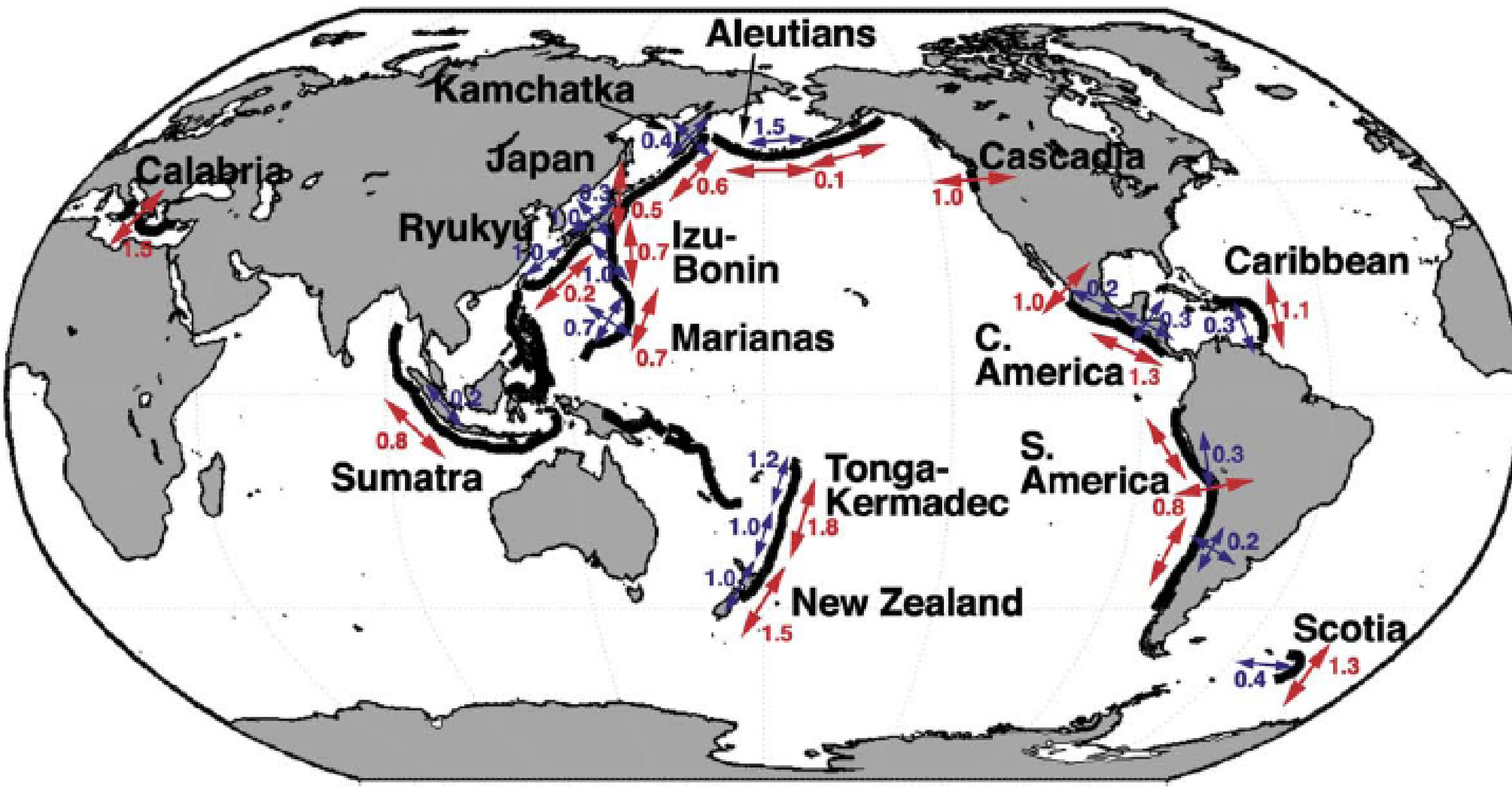

ig. 7. Sketch of constraints on subduction zone anisotropy from shear wave splitting measurements from the compilation of Long and Silver (2008, 2009b). The anisotropic signals f the wedge and sub-slab regions are shown separately. Red arrows indicate average fast directions for the sub-slab splitting signal from *SKS*, local *S*, and source-side teleseismic *S* plitting measurements. The associated average sub-slab delay times are shown in red. Blue arrows indicate average fast directions for wedge anisotropy from local *S* splitting. In egions where multiple fast directions are shown, splitting patterns exhibit a mix of trench-parallel, trench-perpendicular, and oblique fast directions.

Long and Becker (2010)

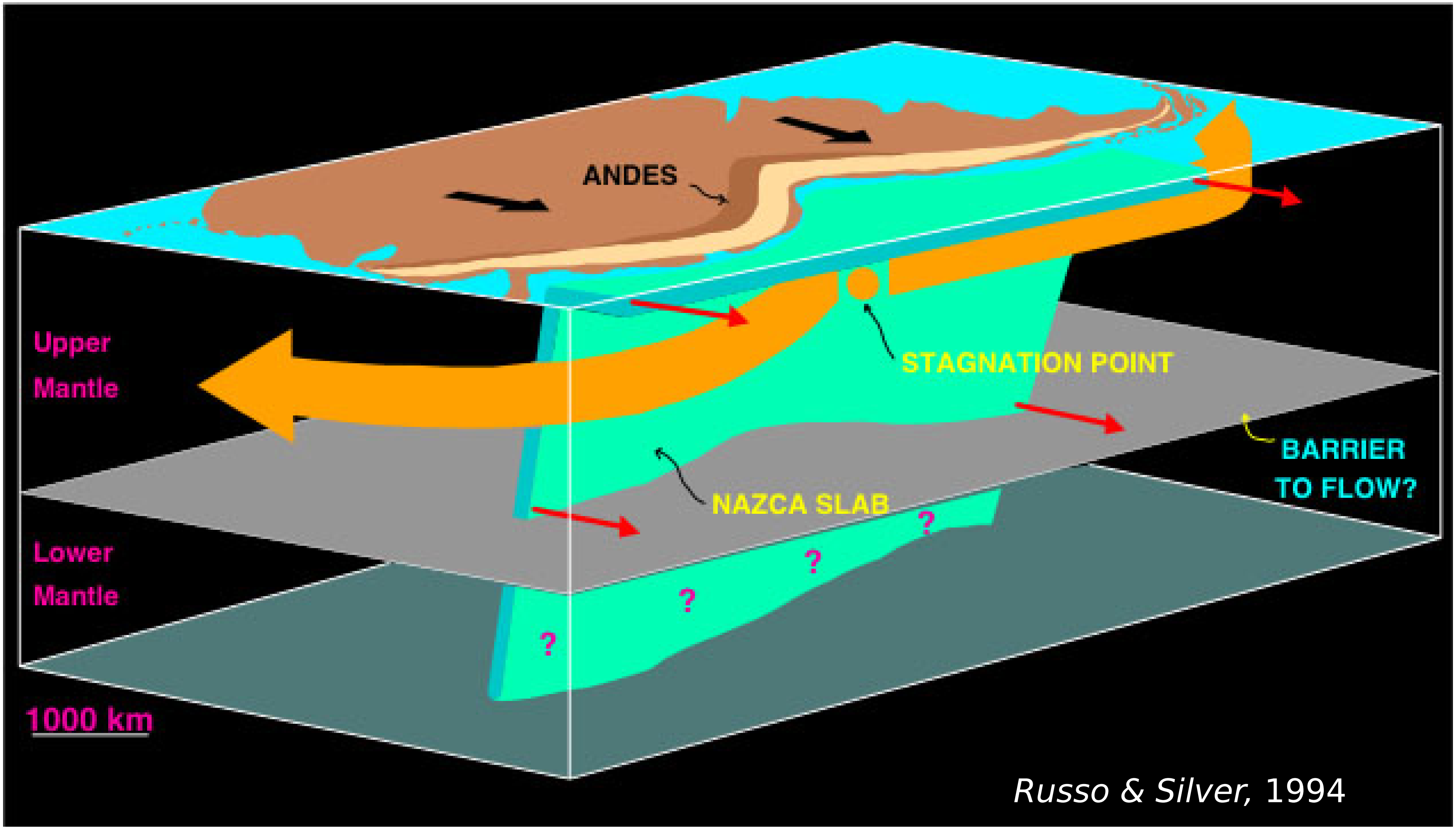
ANDES
Upper
Mantle
STAGNATION POINT
BARRIER
TO FLOW?
NAZCA SLAB
Lower
Mantle
?
?
?
?
1000 km
Russo & Silver, 1994

Long and Silver (Science, 2008)

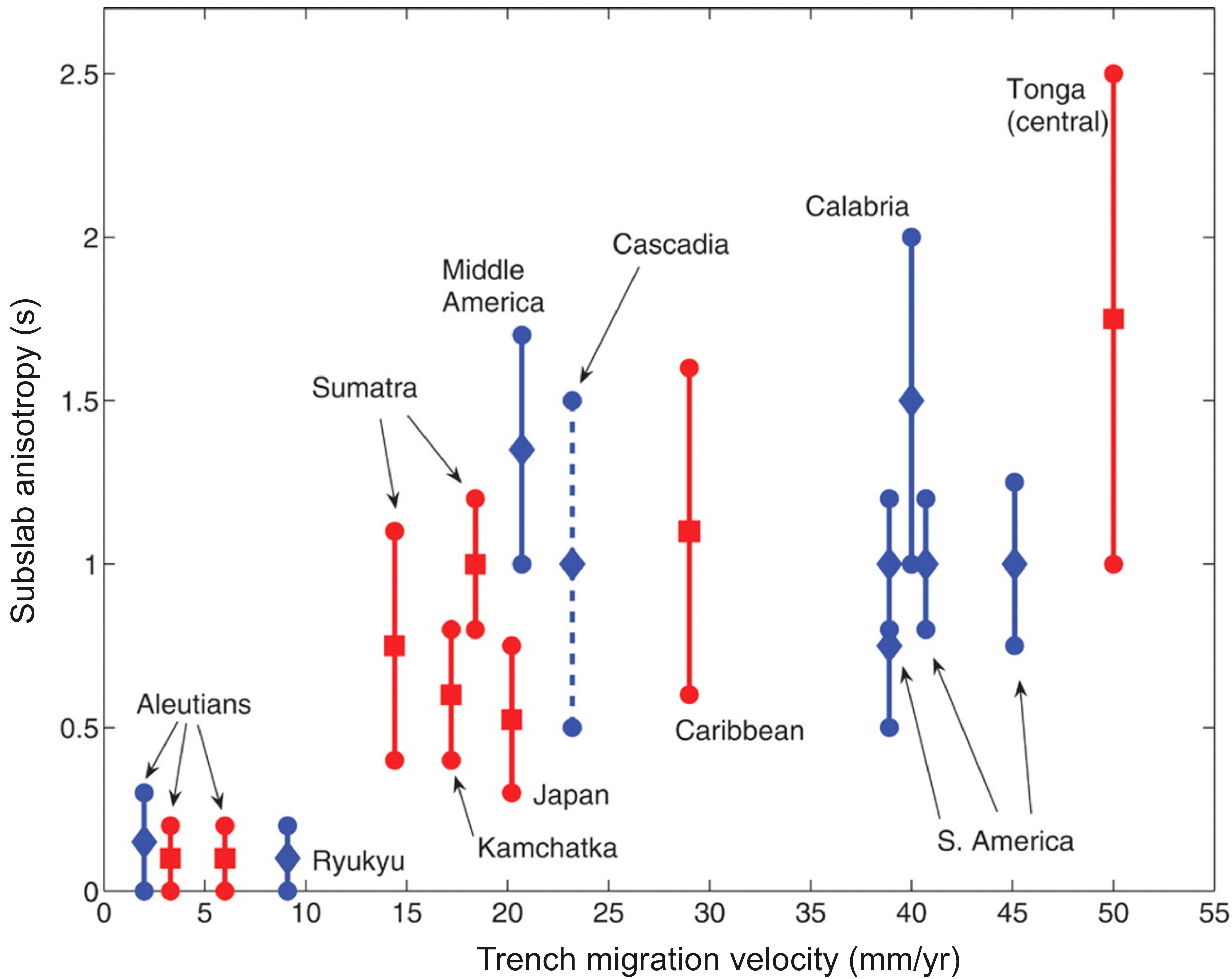

Some open questions

- Slab strength and "plate coupling"
- Interactions between continental and oceanic plates/slabs
  - Tectonics
  - Earth evolution
- Relationship between subduction, volatile transport, upper mantle, small-scale convection with tectonics and magmatism
- Long-term pass transport between upper and lower mantle